2019

Automotive Driveline Backlash State and Size Estimator Design for Anti-Jerk Control

Kaushal Kumar Darokar
Michigan Technological University, kdarokar@mtu.edu

AUTOMOTIVE DRIVELINE BACKLASH STATE AND SIZE ESTIMATOR DESIGN FOR ANTI-JERK CONTROL

By

Kaushal Kumar Darokar

A THESIS

Submitted in partial fulfillment of the requirements for the degree of

MASTER OF SCIENCE

In Mechanical Engineering

MICHIGAN TECHNOLOGICAL UNIVERSITY

2019

This thesis has been approved in partial fulfillment of the requirements for the Degree of MASTER OF SCIENCE in Mechanical Engineering.

Department of Mechanical Engineering - Engineering Mechanics

Thesis Co-advisor: *Dr. Mahdi Shahbakhti*

Thesis Co-advisor: *Dr. Darrell L. Robinette*

Committee Member: *Dr. Jason R. Blough*

Department Chair: *Dr. William W. Predenbon*

Contents

List of Figures

List of Tables

Acknowledgments

I would like to thank Dr. Mahdi Shahbakhti and Dr. Darrell Robinette for their continuous guidance and feedback during the project. Without their guidance and feedback, this work would not have been possible. Throughout the project, I learned a lot of invaluable lessons, on the subject matter and otherwise, which I shall try to implement throughout my life. I am also thankful to Dr. Jason Blough for his feedback during our meetings with the sponsor organization and for agreeing to be a member of my defense committee.

I would also like to thank Dr. Maruthi Ravichandran and Dr. Jeffery Doering from Ford Motor Company. They have contributed a lot to my technical understanding of the subject matter and their timely feedback and critic have significantly improved the novelty of this work. I would also like to thank other members at Ford Research and Advanced Engineering for their support in collecting and sharing vehicle data which has been used repeatedly in the project. A special thanks to Mary Farmer for instrumenting and collecting vehicle level data which has been used to validate the model developed in this work.

I would like to thank Jon Furlich, from the hardware team at Michigan Tech, for

conducting various vehicle measurements and graciously sharing with us the measurement data which has been used in this work to carry out different analysis.

I am also thankful to Prince Lakhani and Prithvi Reddy as their work has been the stepping stone for this work. Prince has always been a guide to me during and outside of this project. Prithvi has always supported me during this project and has contributed to this work. I would also like to thank my friends - Mohit Shah, Anupum Singh Solanki, Chetan Agarwal, Saurabh Bhasme, Akshat Sharma, Siddhant Nigam, Jinit Mistry and Palash Sharma for supporting me during this project.

Finally, I would like to thank my parents - Mr. Ganesh Kumar Darokar and Mrs. Sushma Darokar and my sister, Juhi Darokar, to whom I owe everything. Everything that I have accomplished in my life is because of their unconditional love, support and unwavering trust for me.

Nomenclature

α	Backlash angle $[deg.]$
θ_{ax}	Angular position of axle shaft $[rad]$
θ_b	Angular position of backlash $[rad]$
θ_d	Angular deflection of shaft $[rad]$
θ_e	Angular position of the engine $[rad]$
θ_s	Angular position of shaft $[rad]$
θ_{tr}	Angular position of transmission output shaft $[rad]$
θ_{ps}	Angular position of propeller shaft at final drive end $[rad]$
θ_{ti}	Angular position of tire $[rad]$
$\dot{\theta}_{ax}$	Angular speed of axle shaft at tire end $[rad/s]$
$\dot{\theta}_e$	Angular speed of the engine $[rad/s]$
$\dot{\theta}_{ps}$	Angular speed of propeller shaft at final drive end $[rad/s]$
$\dot{\theta}_{ti}$	Angular speed of tire $[rad/s]$
$\dot{\theta}_{tr}$	Angular speed of transmission output shaft $[rad/s]$
$\dot{\theta}_w$	Angular speed of wheel hub $[rad/s]$
$\ddot{\theta}_e$	Angular acceleration of the engine $[rad/s^2]$
c_{ax}	Damping of the axle shaft $[N.m/RPM]$
c_{ps}	Damping of the propeller shaft $[N.m/RPM]$

c_s	Damping of shaft $[N.m/RPM]$
c_{ti}	Damping of the tire $[N.m/RPM]$
D_x	Aerodynamic force in the longitudinal direction $[N]$
f	Frequency of oscillation $[Hz]$
F_{load}	Sum of aerodynamic, rolling resistance and slope forces acting on the vehicle $[N]$
g	Acceleration due to gravity $[m/s^2]$
i_{tr}	Gear ratio of current gear state of the transmission $[-]$
i_{fdr}	Gear ratio of the final drive$[-]$
J_e	Rotational inertia of the engine $[kg.m^2]$
J_w	Rotational inertia of the wheel hub $[kg.m^2]$
J_1	Lumped inertia of engine, torque converter clutch and transmission $[kg.m^2]$
J_2	Lumped inertia of propeller shaft and the differential $[kg.m^2]$
J_3	Lumped inertia of axle shaft, wheel hub assembly and tires $[kg.m^2]$
k_{ax}	Stiffness of the axle shaft $[N.m/deg]$
k_{ps}	Stiffness of the propeller shaft $[N.m/deg]$
k_s	Stiffness of shaft $[N.m/deg]$
k_{ti}	Stiffness of the tire $[N.m/deg]$
ϕ	phase delay $[radiasn]$
r_t	Radius of the tire $[m]$
R_x	Rolling resistance force $[N]$
t	Time $[sec]$

T_{ax}	Torque output from axle shaft $[N.m]$
T_{fdr}	Torque output from final drive $[N.m]$
$T_{gearloss}$	Torque loss inside the transmission $[N.m]$
T_{im}	Torque input at torque converter impeller $[N.m]$
T_{ps}	Torque output from propeller shaft $[N.m]$
T_{tr}	Torque output from transmission $[N.m]$
T_{tcc}	Torque through the torque converter lock-up clutch $[N.m]$
T_{ti}	Torque output at the tire $[N.m]$
T_{tu}	Torque output at torque converter turbine $[N.m]$
V	Velocity of the vehicle $[m/s]$

List of Abbreviations

2WD	Two Wheel Drive
4WD	Four Wheel Drive
AJC	Anti-Jerk Control
AT	Automatic Transmission
CAN	Controller Area Network
DKF	Discrete Kalman Filter
DSKSE	Discrete Switched Kalman State Estimator
ECU	Electronic Control Unit
EKF	Extended Kalman Filter
FOM	Full Order Model
IC	Internal Combustion
LO	Luenberger Observer
MHT	Modular Hybrid transmission
MPC	Model Predictive Controller
NVH	Noise Vibration and Harshness
OEM	Original Equipment Manufacturer
ROM	Reduced Order Model
SKF	Switched Kalman Filter

SP	Smith Predictor
TC	Torque Converter
TCC	Torque Converter Clutch
TKBSE	Triggered Kalman Backlash Size Estimator

Abstract

Vehicle drivability is an important factor which more and more customers have started assessing before buying a vehicle. Customers carry out this assessment based on both vehicle reviews/ratings and based on the test drives. One of common maneuver which a customers perform during the test drive is sudden accelerator pedal tip-in or tip-out to accelerate or coast the vehicle. Clunk and shuffle are the phenomena that usually occur during this scenario causing driver discomfort. The clunk and shuffle are caused by the backlash and compliance physical properties of the driveline. Consequently, control strategy needs to be developed which can provide a fast driveline response without clunk and shuffle. One major input to develop a control strategy is the knowledge of the vehicle states and parameters based on the available measurements, which is the major focus of this work.

This work begins with a discussion of various existing estimation strategies that have been used to estimate the states of vehicle along with their merits and demerits. Then a full order model, developed in the previous works, is validated for a locked torque converter case along with its reduced order model which is used for estimator development. The error in the simulated shuffle frequency for the full order model and reduced order model is less than 1%. The reduced order model is then used to develop an observable state space model to estimate the backlash state and size

of the model. The estimators developed are validated and the robustness analysis is done for different scenarios of torque inputs, delays and sampling times. It is found that the sampling time of the estimators and measurement inputs significantly effect the estimates of lash traversal time and backlash size with a mean error of 9% in lash traversal time estimate and 2% error in lash size for 10ms sampling time. Furthermore, the estimators are found to be more robust to the variations in the wheel speed measurements as compared to variations in the engine speed measurements.

Chapter 1

Introduction

1.1 Motivation

In the modern era, the value proposition of an automobile is not just to provide a means of transportation from one location to another, but to provide a unique experience to the customer. This unique experience is a combination of varying proportions of certain aspects of an automobile. The proportion of these aspects can be defined as the voice of the customer who are the potential buyer. Figure 1.1, refer [5], shows a list of some of the prominent aspects which a potential vehicle buyer considers. As a result of this, an automobile Original Equipment Manufacturer (OEM) also has to develop vehicles with attributes such that they can meet the

Figure 1.1: Customer's vehicle purchase criteria or Voice of customer

voice of the customer. Most of the OEMs, before the concept stage of the vehicle development, conduct market survey to gather data and also conduct bench-marking studies with vehicles of other OEMs. This is done so that they can define their targets (proportions) of these aspects the vehicle specifications can be derived.

The vehicle aspects shown in Figure 1.1 can be classified into 2 categories, quantitative and qualitative. Price and size aspects are straight forward quantitative aspects. For aspects such as fuel economy, emissions and safety, there exists standards and/or regulations which help provide quantitative assessment of these aspects for both the OEMs as well as the customers. But the other aspects are qualitative in nature, requiring subjective assessments in order to compare these aspects of different vehicles. The OEMs carry out jury trails or develop their internal standards to define criterion to assess these qualitative aspects. While the customers have to rely on test drives, word to mouth reviews or more recently on online reviews or ratings. Figure 1.2 shows one such overall ratings developed by the Edmunds [1] for a few of the vehicles.

Studies show these ratings are gaining traction among potential vehicle buyers. This can be seen in Figure 1.3 which shows the data collected by Deloitte [2] suggesting that 70% of the Gen Y (ref [6]) population are influenced by the independent reviews whereas 55% of the Gen X population are influenced by similar ratings. Thus, these ratings play a significant influence on the customer buying decisions

From the different aspects of the vehicle shown in Figure 1.1, one important aspect is the drivability of the vehicle. Drivability can be defined as driver's perception of how smoothly and consistently a vehicle's powertrain drives the vehicle in different operating conditions. Some of the operating conditions are discussed in references [5] and [7]. These scenarios are also shown in Figure 1.4, which are taken into consideration

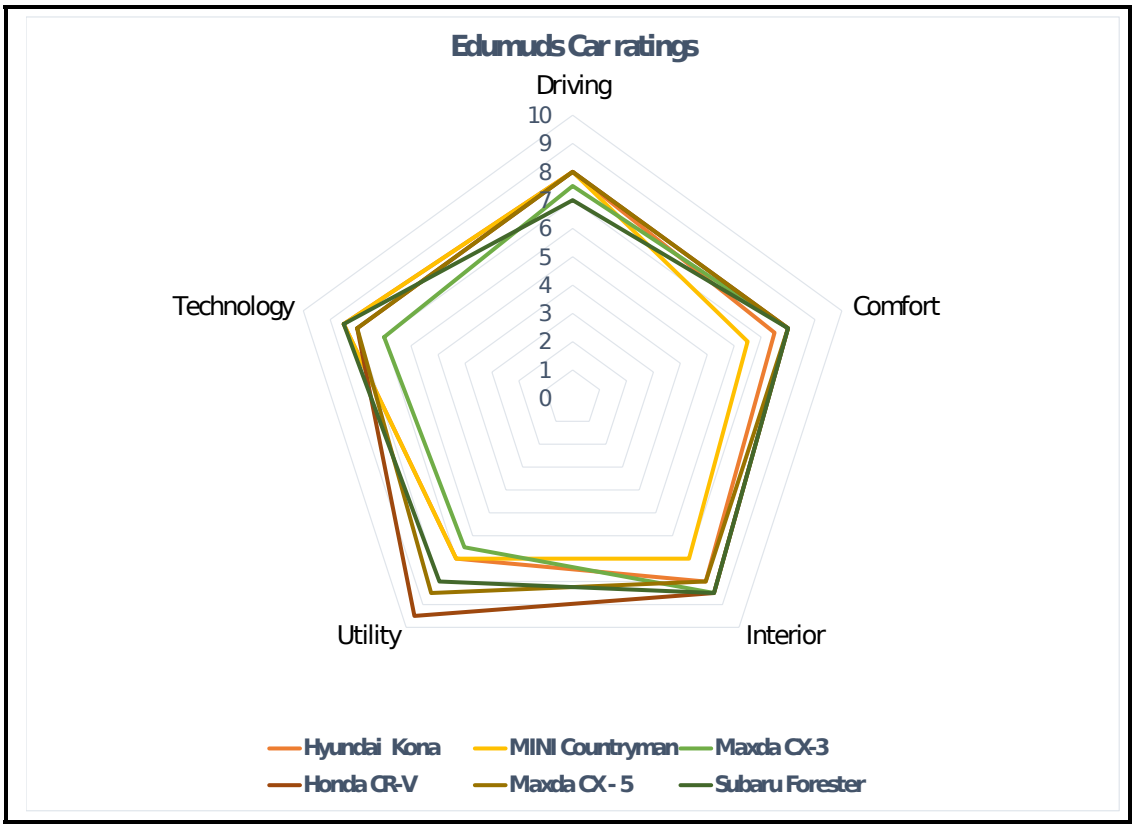

Figure 1.2: Edmunds overall ratings for a few vehicles, [1]

to assess the drivability of the vehicle. Study in [8] was one of the earliest papers to define drivability and effect of emission control strategies on the drivability of vehicle. The paper discusses measuring vehicle surge to objectively define drivability. More recent works such as [9], [5], [7], and [10] also aim to develop objective methods to assess drivability and its co-relation to subjective assessments. While a lot of work is going on in this field, it is mostly headed towards assisting the automotive development engineers to provide them with objective metrics to assess the drivability. This is important as they can thrive for continuous improvement in the drivability without the human error in subjective evaluation. Furthermore, these metrics also

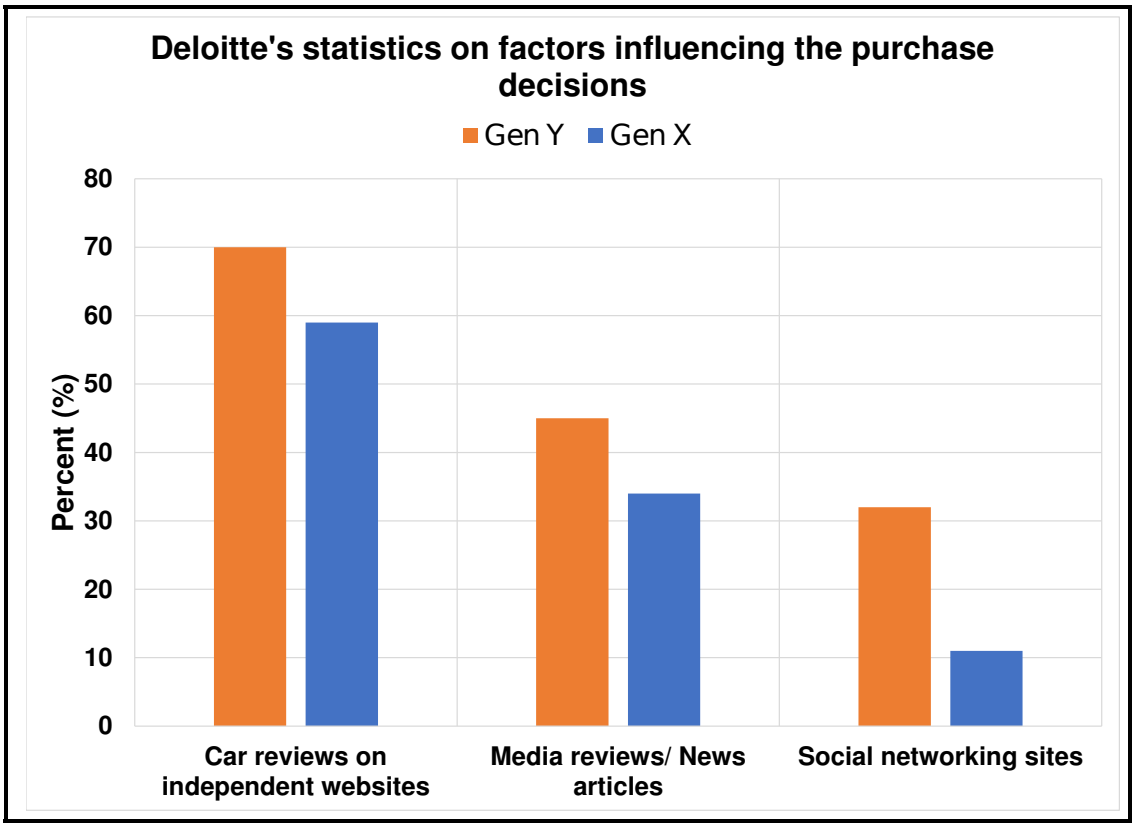

Figure 1.3: Results for the study conducted by Deloitte, [2]

provide them to objectively compare the performance of their vehicle with others. But from the customer point of view, online reviews provide ratings for drivability assessment based on their own developed criterion. This can be seen in Figure 1.5 were drivability ratings for a few of the vehicles is shown.

Thus, it can be seen that the drivability of the vehicle is an important voice of customer factor which needs to be considered while developing a vehicle. Out of the different scenarios which constitute the overall drivability assessment of a vehicle, Figure 1.4, this work focuses on vehicle driveline torque response during tip-in and

Figure 1.4: Criterion under drivability assessment of a vehicle

tip-out events. Next section of this chapter provides the background of tip-in/tip-out as well as how it affects the drivability as perceived by the customer.

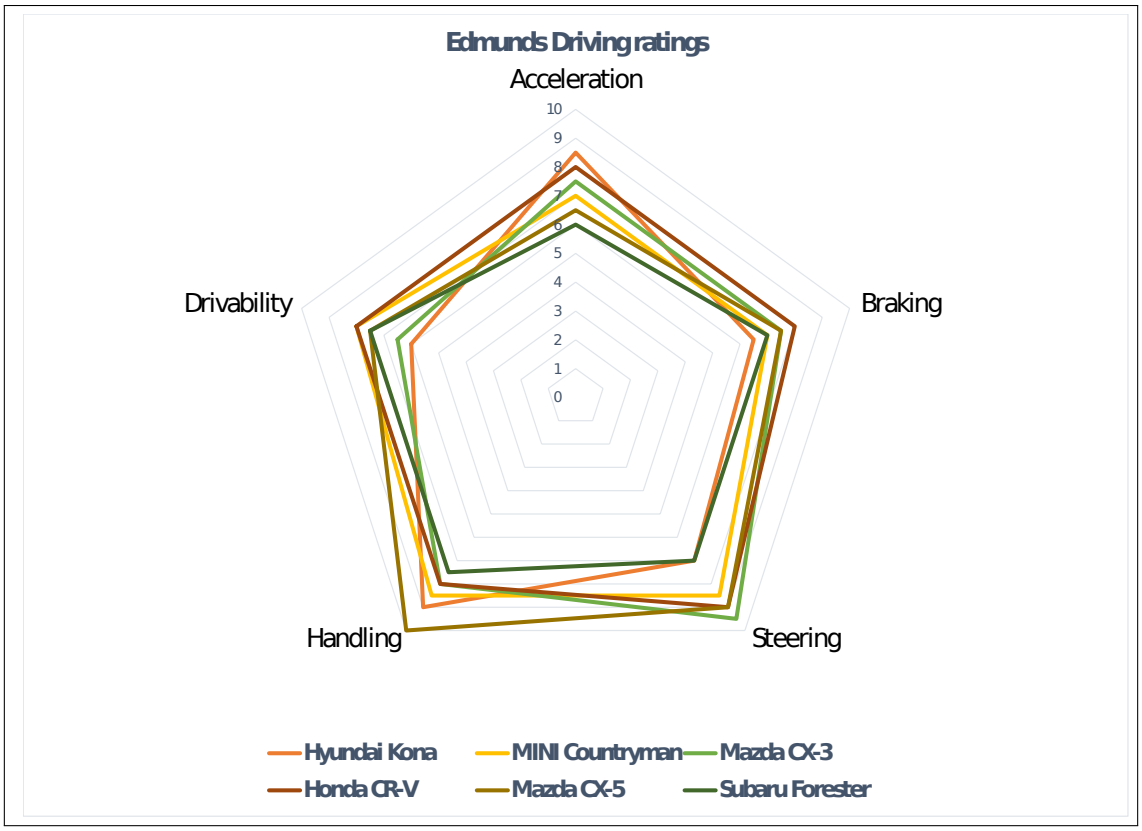

Figure 1.5: Edmunds overall ratings for a few vehicles, [1]

1.2 Technical terms used in this work

Some of the technical terms that have been frequently used in this work are discussed in this section and a background is provided to the reader to assist in understanding the objectives and findings of the this work.

An automotive driveline consists of a number of systems/components which makes the transfer of torque from the engine/propulsion device to the wheels possible. These

systems/components can be further classified into launch devices, gearbox and the axles/shafts. The launch devices decouple the propulsion system from the driveline via using either clutches or the torque converters. The gearbox is a set of gears, shafts and bearings (to name a few) constrained inside a housing with the purpose of reducing the speed and increasing the torque from the propulsion system. They can be further classified into transmission, transfer cases and differential for (North-South powertrain configuration) and, transaxles and Power Transfer units for (East-West powertrain configurations). The shafts/axles are defined as torsional interconnections among gears of the gearbox, among the gearbox and launch devices and among the differentials and the wheels.

All these systems and their constituting components have certain physical properties and certain constraints from the manufacturing, assembly or operation point of view. For example, the gear box has different mating gears to provide required gear reduction. But in order to make the assembly of those gears inside the gearbox possible certain amount of clearance needs to be provided between the mating gear teeth. The clearance also needs to be provided to avoid the gear biting into each other. The clearance also helps provide lubrication to the gear while transferring torque and finally, the clearance also occurs due to the limitation of manufacturing of the gear tooth profiles. Furthermore, the amount of clearance also depends of the type of gear geometry. For spur gears the clearance to be provided is lesser as compared to for gears with helical tooth profile. While the clearance is maximum for hypoid

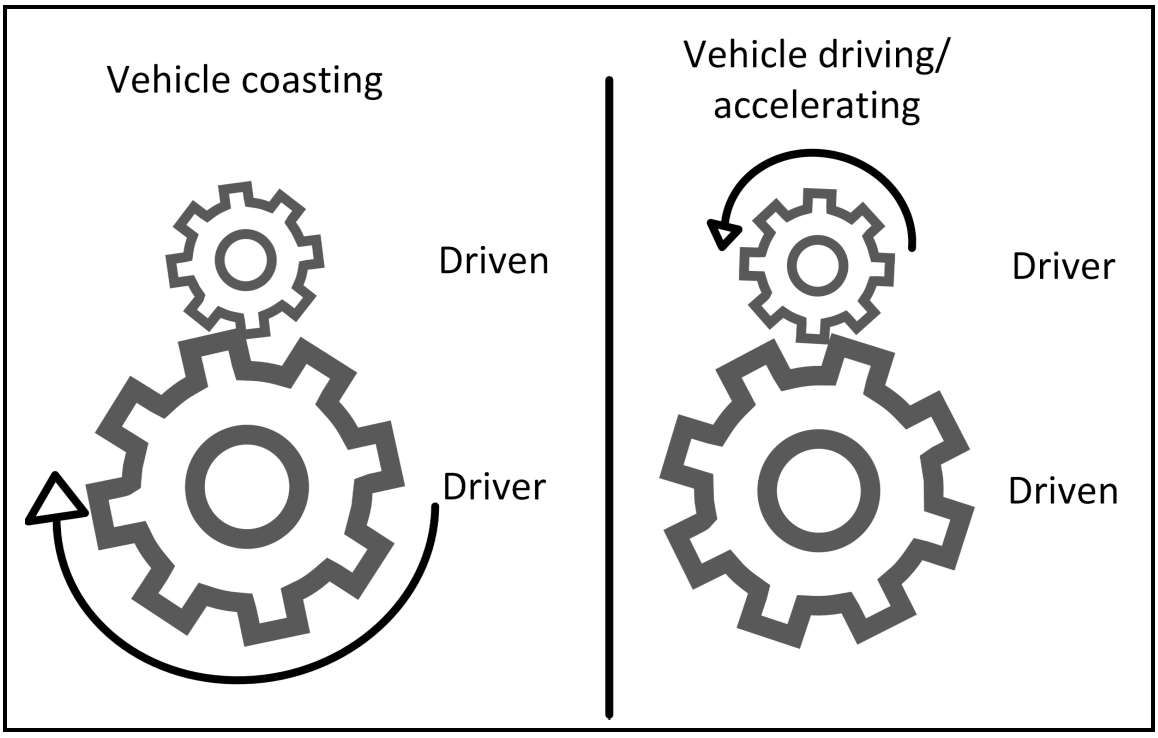

Figure 1.6: Backlash between mating gear teeth and change of tooth face from drive to coast

gear tooth profiles. This clearance is know as backlash. Even for shafts and axles to interface with the gears, splines are provided on the mating gear-shaft, gear-axle interface. These interfaces can also have a backlash associated with them which are typically smaller than the gear teeth meshing interface. Thus, the backlash inside the powertrain is distributed across the driveline. Figure 1.6 shows the clearance between the mating gear teeth i.e. the backlash.

Apart from backlash, the shaft and axles of the driveline have stiffness and damping physical properties associated with them. The stiffness causes the deflection of shaft when subjected to a torque input, and can lead to oscillation in the driveline. The

damping opposes the oscillation and tries to damp them out.

A combination of the two, the backlash and the compliance (stiffness and damping) of the driveline causes a response within the driveline when it is subjected to a sudden torque reversal, tip-in or tip-out. This is shown in Figure 1.7. A sudden torque reversal occurs when the magnitude of torque delivered by the engine/propulsion device suddenly changes its sign. This can be seen in subplot (a) where the delivered torque is initially negative and it suddenly changes to a positive torque value. This is referred to as the tip-in scenario in this work. The inverse of it can be referred to as the tip-out scenario where the torque suddenly changes from a positive value to a negative value. In the tip-in case, the vehicle is initially in coasting condition when the torque is negative. The coasting condition can be further defined as the wheels driving the engine because of vehicle's momentum. The vehicle driving/accelerating condition is when the engine delivered torque is positive. As it can be seen from Figure 1.6, if the vehicle transitions from coasting to driving or vice a verse, mating gears have to overcome backlash and the side of tooth face in contact changes. While traversing the backlash there is no torque transfer between the gears and thus the driver gear can accelerate during the lash traversal, causing an impact when it hits contact on the other side of lash. The impact can cause an audible noise which is referred to as clunk. Referring back to figure 1.7 the subplot (c) shows the traversal of the backlash from contact on the coast side, referred to as negative contact to contact towards the drive side, referred to as positive contact and the subplot (b) showing

the time of clunk in the propeller shaft torque. Finally, because of this impact an oscillation is caused in the propeller shaft trajectory because of its compliance. This is experienced by the driver in the form of longitudinal fore and aft oscillation with frequency between 2-10 Hz depending the current engaged gear of the vehicle.

The clunk and shuffle phenomena described above are critical as they affect the drive feel of the vehicle. Clunk affects in the form of audible noise generally causing irritation to the driver and the shuffle causes driver discomfort as the natural frequency of human organ lies within the frequency range of shuffle [11].

Jerk is defined as a sudden change in the acceleration. As can be seen that the shuffle causes fore and aft oscillation this gets reflected as longitudinal jerking of the vehicle. Furthermore, as both the backlash and the compliance are unavoidable, control strategies need to be developed which can shape the torque input to the driveline to mitigate the effects of clunk and shuffle. Such control strategies are known as Anti-Jerk control strategies.

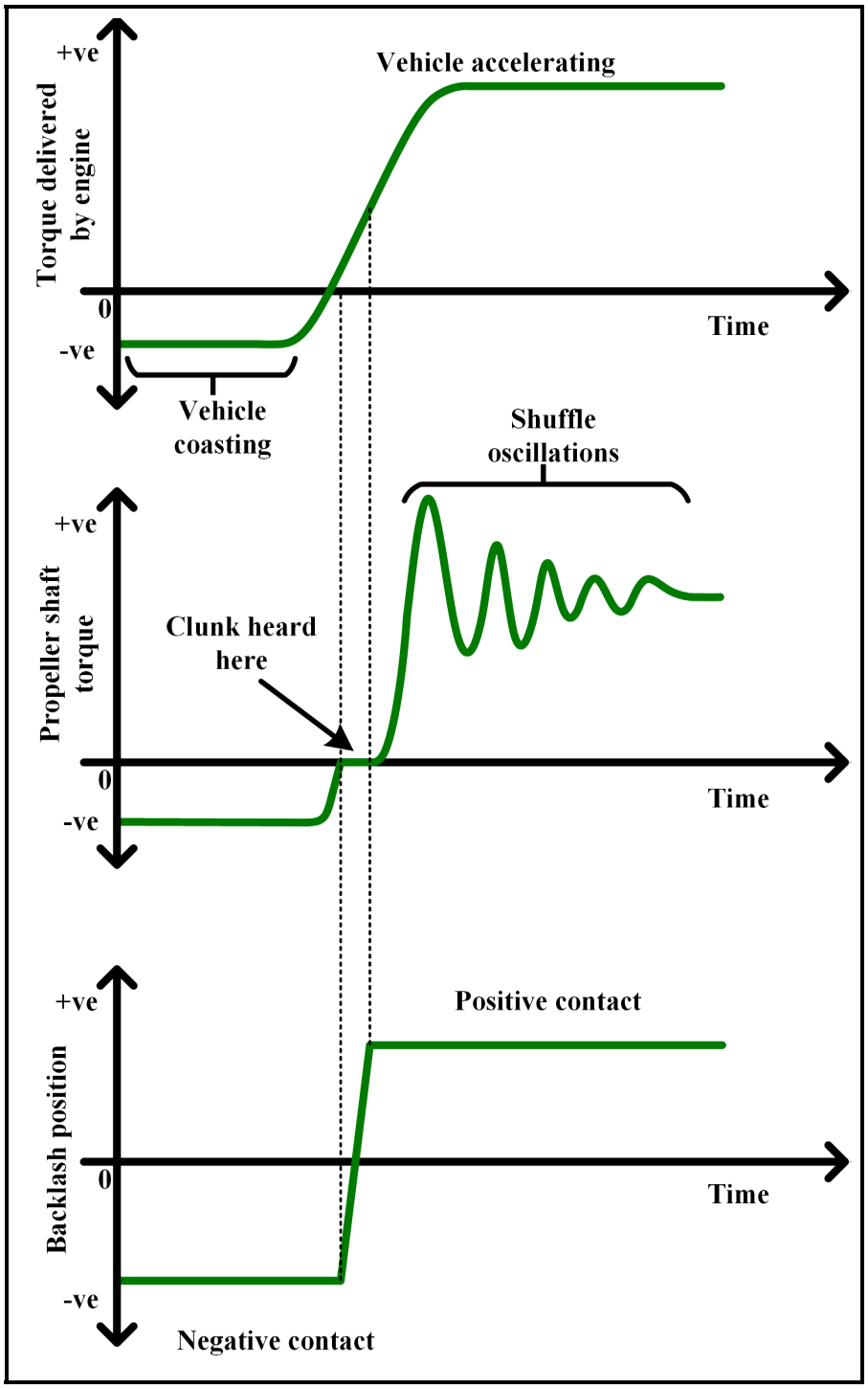

Figure 1.7: Representative output of driveline delivered torque indicating tip-in, propeller shaft torque indicating clunk and shuffle and driveline lumped backlash indicating backlash traversal

1.3 Literature review

Figure 1.8 shows the time-line of research in the field of driveline clunk and shuffle simulation, estimation and development of AJC control strategies to mitigate the effect of clunk and shuffle.

Estimating the response of vehicle during tip-in and tip-out scenarios and using that information to develop strategies to investigate and improve the vehicle performance started with simulating the driveline response during the tip-in and tip-out scenarios. The study in [12] was one of the earliest attempts to investigate the low frequency torsional oscillation of the driveline. The emphasis of the work is to simulate the low frequency (<30 Hz) driveline torsional oscillations during, tip-in/tip-out, due to engine firing pulsation and due to the self excited driveline oscillation.

The authors systematically define the tip-in jerk as clunk, which is defined as the abrupt change in the acceleration of the vehicle, the leading fore and aft oscillation of the driveline as shuffle and the characteristics of oscillation as frequency, amplitude and the tip-in overshoot. A simplified rear wheel drive driveline model is considered with engine torque input to the driveline, a torque converter with hydraulically or centrifugally controlled by-pass clutch, a one way clutch and a torsional damper, an option for a coast-unlock one way clutch, a lumped transmission inertia, stiffness and

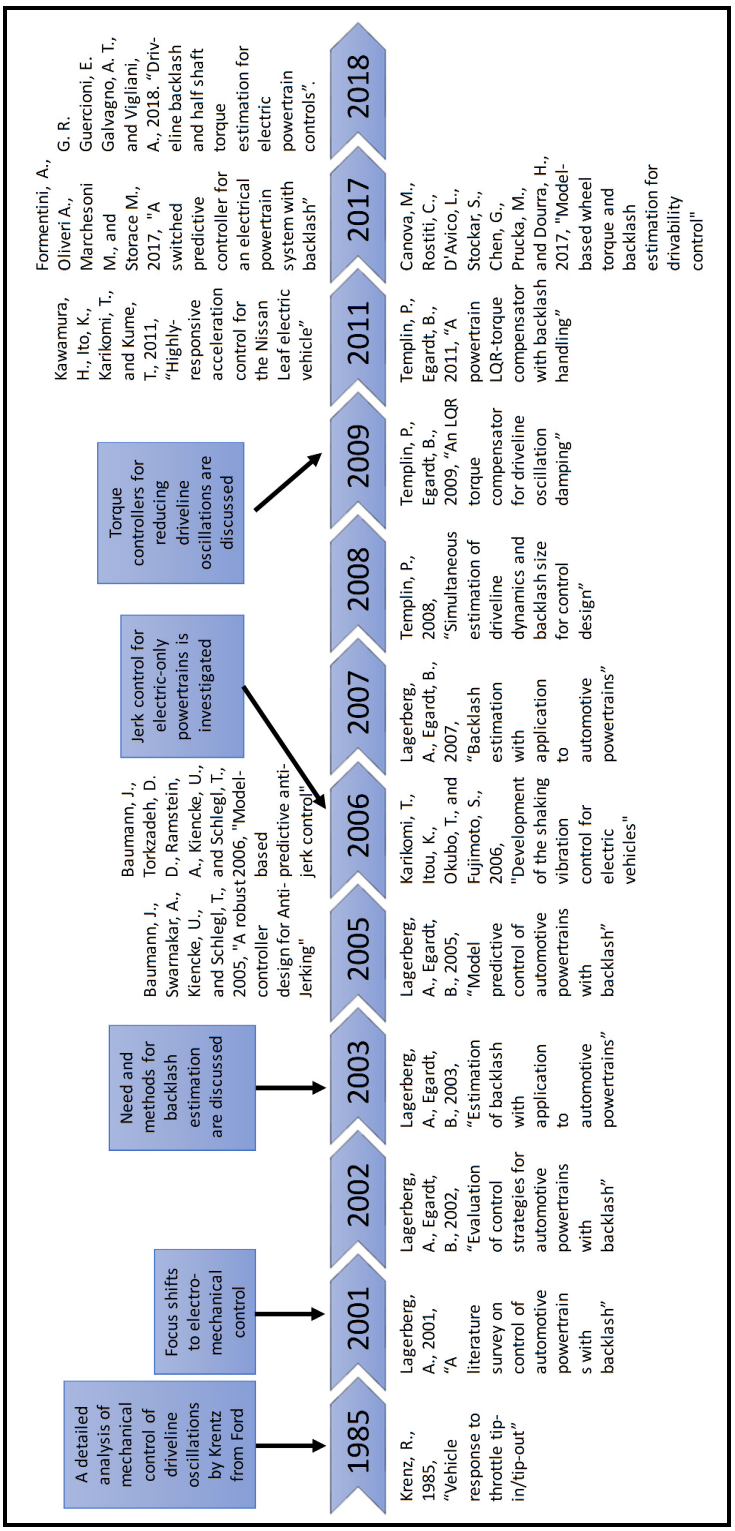

Figure 1.8: Progress of works in the field of AJC research [3]

damping, a lumped backlash for transmission and final drive gears, the axle shaft and tire stiffness and damping. The authors, as a part of their analysis, compared the clunk and shuffle observed in the driveline under various conditions such as a driveline with and without backlash, the effect of open and locked torque converter by-pass clutch, the effect of torsional damper properties on the response. An important study which was done as a part of this paper was the analysis of the driveline response with and without the coast down one way clutch. The authors also experimentally validated the model via vehicle level measurements and found the accuracy of the simulated frequency to be within 10%.

An experimental approach towards [12] is taken in [13] where the authors specifically focused on reduction of clunk and shuffle. Both clunk and shuffle have been described in detail using experimental data. Furthermore, the authors highlighted the major parameters affecting the clunk and shuffle as the engine torque rate, the driveline lash and the driveline compliance. The authors also discussed the experimental method to measure the lash in a driveline and highlighted major sources the driveline lash. Although significant progress has been and is being made in developing detail models capable of simulating the tip-in and tip-out response, works in the field of estimating the driveline states to control the engine torque during such scenarios started after the detailed models defining backlash were made.

Lagerberg in [14] discussed the various dynamical models which have been used to

represent the dynamics of the backlash in geared systems. All these models essentially have a non-linear structure categorizing the behaviour of the driveline into contact mode and backlash mode of operation which is based on the position of the shaft within the lash. Lagerberg and Egart also evaluated the performance of a number of control strategies in [15] and suggested that the controller with different compensations for contact mode and backlash mode provides better response as compared to controller which do not account for backlash. Thus, in order to develop a control strategy which can mitigate the effect of clunk and shuffle, the control input needs to be commanded based on the status of the driveline. This in turn requires the position of shaft within the lash needs to be known. Since the backlash in the driveline is distributed knowing the backlash position becomes difficult.

Various estimation methods have been used to estimate the backlash position and driveline parameters in the literature of anti-jerk control strategies. The need to estimate the parameter arises from the fact that, the properties of the driveline component changes over the life of vehicle because of usage. And in order for the controller to be effective, they should be updated as well.

Estimation methods generally use a dynamic model of the physical system with some of its states being measured via actual physical sensors. These measurements are used to correct the prediction made by the dynamical model resulting in the estimates of the system. The estimator developed so far can be classified into two categories.

The first classification can be made on the basis of the measurement signals that are used for the estimation of the backlash position. The study in [16] uses the actual position of the engine and wheel to determine. Other works such as [17] and [18] used the engine and the wheel speed measurements to estimate the position of backlash. The constraint with using angular positions as the measurement is that the angular position sensors are generally not used in production vehicles.

The other classification of estimator design can be made on the type of estimation strategy used to estimate the backlash position. Studies in referenes [19] and [16] uses two derivative of the Kalman filter estimation approach to estimate the size of backlash and position of backlash. In these works, for size estimation, a Switched Kalman Fiter (SKF) is developed while for backlash position estimation, an Extended Kalman Filter (EKF) approach is used.

The Kalman filter approach is applicable for linear dynamical models only. But if the non linear model of the dynamical system can be represented by a linear combination of multiple linear models , a SKF approach can be used to estimate the states of the system. The SKF applies the Kalman filter approach to the individual linear model or any linear combination of the models and use a switching variable to select the model to be used for estimation. As the backlash model of [19] and [16] can be represented by linear models of contact and backlash mode, this approach can be used to estimate the size of backlash. Apart from the contact and backlash modes a wait mode is also

used by the authors in [19] and [16].

The EKF approach uses the principle of linearization of a nonlinear state space model to apply the Kalman filter approach and estimate the states of the dynamic system. The model is linearized at each time step based on the mean value of last estimated state of the system. This method is widely used to estimate the states of non-linear models. The estimates of EKF are no longer optimal when compared to a Kalman filter estimates because of the linearization of the model. In the works of [19], [20] and [16], the non-linear backlash model is linearized and a switched EKF is developed.

When the driveline is in backlash mode, the engine and wheels are not directly connected to each other. As a result, the backlash model dynamics of the system are not observable. Consequently, the works in [21], [22] and [23] only estimate the states of the driveline in the contact mode but use the system dynamics to calculate the backlash position. The [21] and [23] used a standard Discrete Kalman filter approach for the state estimation while [22] uses Loop transfer recovery to estimate the states of the system.

A combined Simth Predictor and Luenberger based state observer approach is used to estimate the states of the driveline in [24]. The Smith predictor approach is generally used in control system with delay. In the case of driveline control, there is delay between the time torque is commanded by the engine to the time the command torque effects the wheel speeds and the wheel speed sensor data is received back by

the controller. The Luenberger observer is based on pole-placement to observe the states of the plant and is used in [24] to reduce the error between the simulated and measured engine speed.

These different estimation approaches that have been used in the literature to estimate the states and parameters of the driveline have their inherent pros and cons. The standard Kalman filter approach is optimal if the co-variances of the measurements and states are Gaussian in nature with zero mean. Any deviation from this affects the optimality. This same limitation is applicable to the case of SKF as well. The EKF approach is sub-optimal because of the state space linearization and consequently computationally demanding than the Luenberger Observer as well as the Kalman fitler. Furthermore, the Luenberger observer are not robust to model uncertainties and measurement noise.

Apart from the methods that have been discussed so far, a non-linear least square optimization-based approach is used to estimate the parameters of the driveline off-fline in [20]. It uses a cost function to minimize the error between the estimated and measured states to estimate the parameters of the system. A summary of the estimator used to estimate the states and the parameters of the driveline is shown in figure 1.9

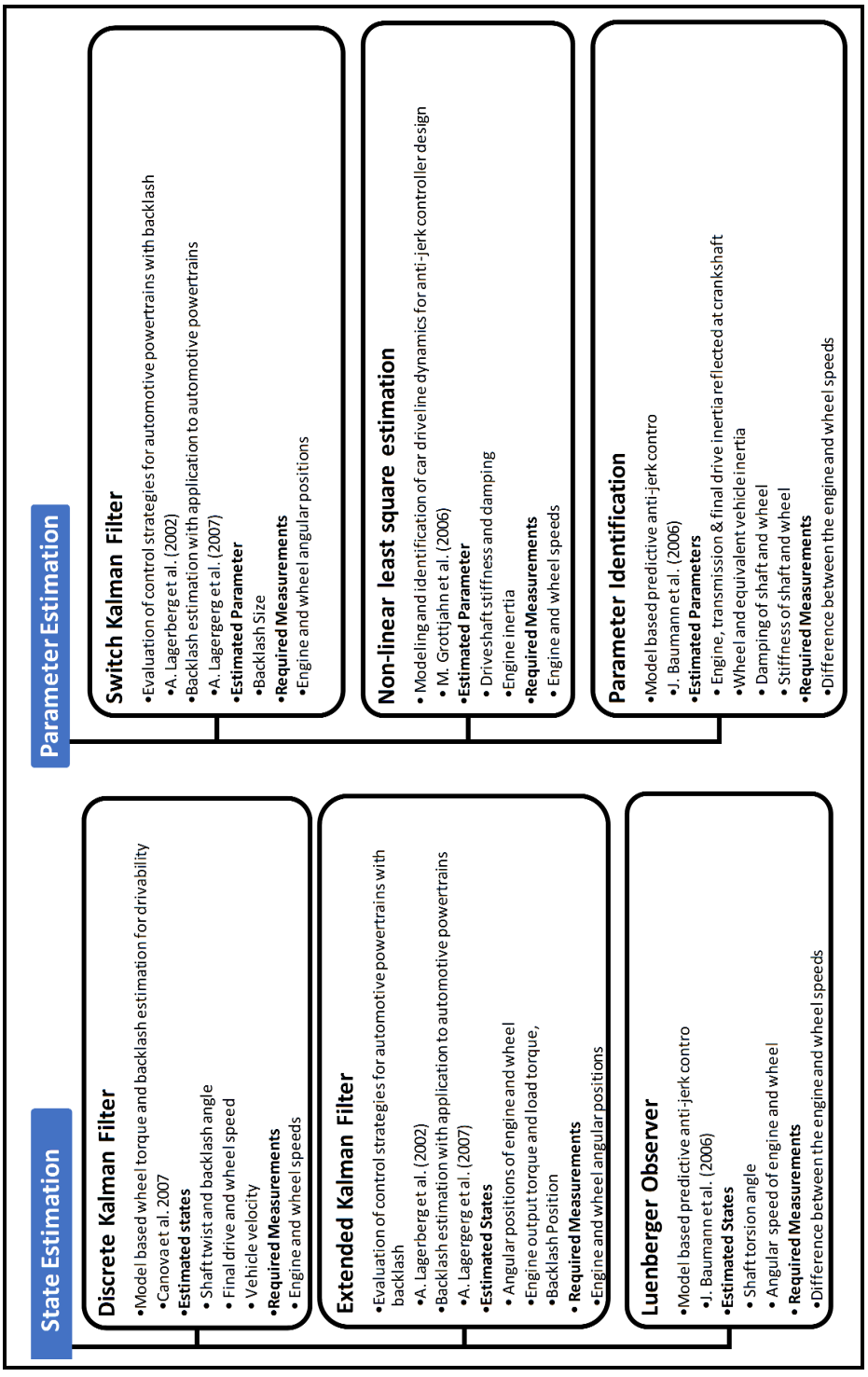

Figure 1.9: Summary of estimators used to estimate the states as well as the parameter of the driveline

1.4 Research scope and thesis organization

This work is in continuation to the work published in Prince [25] and Reddy [3] under aegis of the alliance project between Ford Motor Company and Michigan Technological University to develop estimation and control strategies for driveline jerk control. The previous works presented the development of a full order vehicle driveline model. This model is capable of simulating the driveline response of a vehicle during tip-in and tip-out scenarios. This work augments the previous works via validating their full order model (FOM). The validation is done for a use case of locked torque converter during tip-in and tip-out scenarios. As an intermediate step, this work further modifies the FOM to a control oriented reduced order model (ROM). The reason to transform the FOM to ROM is to develop an estimation strategy for backlash state and size, based on the ROM, so that necessary information about the state of the vehicle driveline is available. This available information is critical to achieve the final goal of controlling driveline jerk during tip-in and tip-out scenarios.

To estimate the backlash position of the driveline, [19] and [16] uses the angular position sensors to make the backlash model observable, while [22], [21] and [23] uses backlash mode simulation to predict the backlash position using the production speed measurements. This work uses a combination of the prediction and estimation to predict the backlash position of the driveline using production speed measurements

so that the error in the predicted backlash position can be reduced. Furthermore, the size estimation approach developed in this work uses commanded torque based trigger to estimate the backlash size as compared to backlash position based switching, as used [19] and [16], to estimate the size of the backlash. Finally, the performance of the estimators to production vehicle based measurement delays and signal jitters is also assessed this work.

Figure 1.10 shows the organizational layout of this thesis. The second chapter of the thesis discusses the validation of the full model, developed in the previous works, and the development of a reduced order model as well as its validation. The third chapter discusses the development of the backlash state estimator, its validation and the robustness analysis. Next, the fourth chapter discusses the development of backlash size estimator, its validation and its robustness analysis. Finally, the fifth chapter discusses the conclusion and future works that are planned based on the works of this thesis.

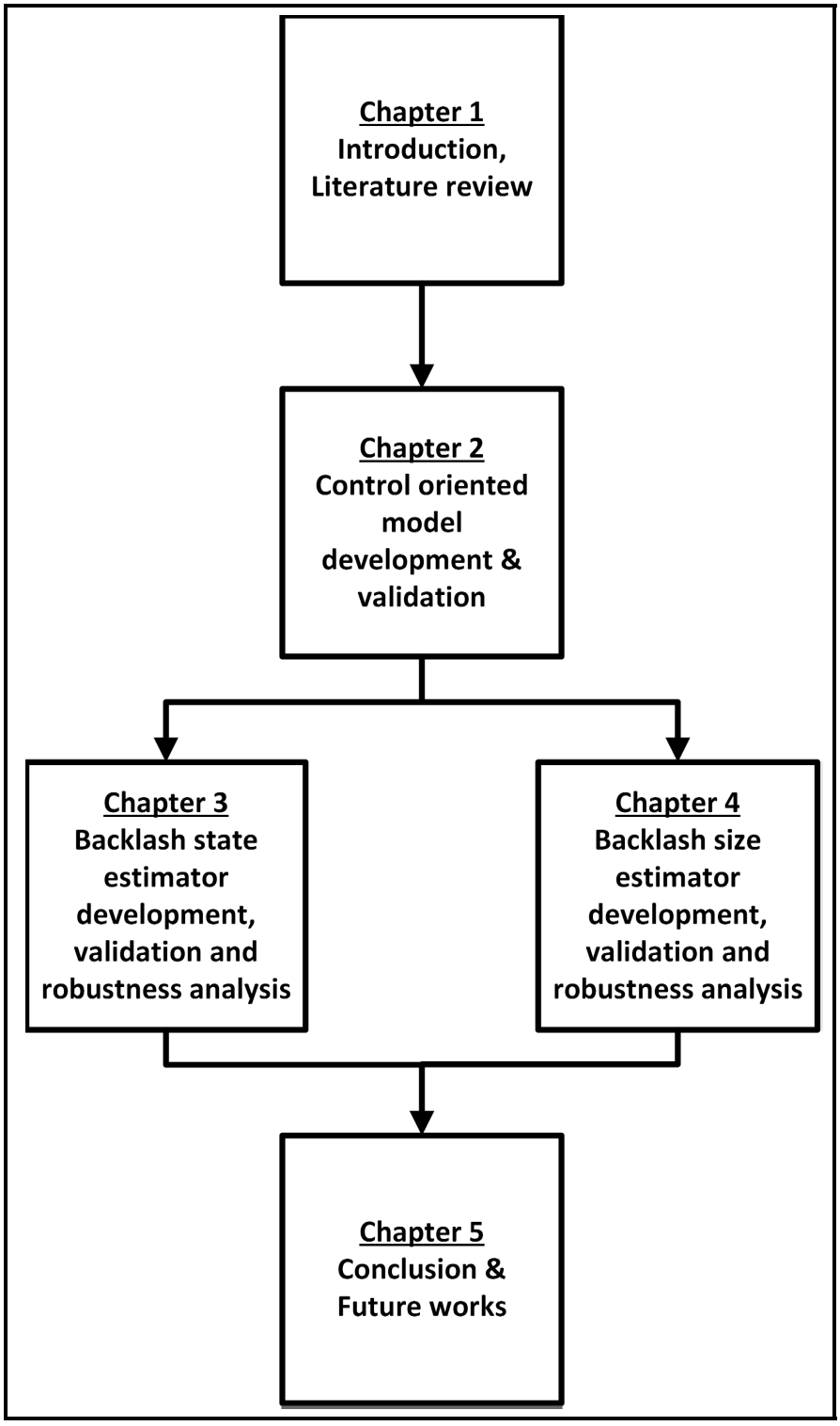

Figure 1.10: Thesis organization

Chapter 2

Control Oriented Driveline Model Development and Validation

This chapter starts with a brief discussion of the full order model (FOM) that has been developed by Lakhani [25] and Reddy [3]. An overview of the components of the model is discussed without the equations of the dynamics of these components. The model overview is followed by the discussion of the validation of the FOM based on the vehicle measurements data provided by the sponsor organization. Then, this chapter progresses towards the development and the validation of the reduced order model which will lay the ground for the development of state and size estimators discussed in the subsequent chapters.

2.1 Full order model (FOM)

2.1.1 Overview of Full order model

The FOM developed for this work is for a rear wheel driven vehicle with longitudinally mounted powertrain configuration. The model consists of a mean value engine model, a torque converter, a 10-speed automatic transmission, a propeller shaft, a final drive reduction, the axle shafts, and the tires. The engine is modeled to include the dynamics of the base path (air path) and the instantaneous path (spark path), refer [26]. The base path dynamics take into account the first order dynamics with a time delay. The instantaneous path dynamics take into account the effect of spark modulation to evaluate the torque delivered to the driveline. Uncertainty in the engine torque is also modeled to account for the error in the ECU estimated crankshaft torque as well as the error due to variation in production engines. The model for the engine dynamics, as a torque source, is developed in Simulink®.

The rest of the vehicle driveline is modeled in AMESim®. This is done so that the readily available driveline model library of AMESim® can be used with only changes in the value of model parameters. Refer [3] for the interface between Simulink® and AMESim®. In the driveline model, the torque converter is modeled using torque ratio

versus speed ratio, and capacity factor versus speed ratio look-up tables, a torsional damper and a torque converter clutch (TCC) is also considered in the model. When the TCC is engaged it locks up the impeller to the turbine establishing a mechanical connection between them. This leads to the torque flowing through the clutch path and not through the hydraulic path. As a result, the torque at the impeller and the torque at the turbine are the same. The 10-speed automatic transmission is modeled using 4 planetary gear sets with the node inertia for each of the planetary gear set and a lumped backlash for the transmission. The powertrain gear losses, which are a function of the currently engaged gear and the speed of the engine, are also modeled at the input to the transmission. The output of the transmission is connected to a propeller shaft which is modeled via a stiffness, and a damping element. The output of the propeller shaft is then connected to the differential via a backlash element to represent the backlash between the hypoid gear pair inside the differential. This hypoid accounts for the maximum backlash, in the wheel domain, for the powertrain. The differential is modeled as a gear reduction and its output is connected to the two axle shafts. The axle shafts, similar to propeller shaft are modeled via stiffness and the damping elements. The axle shafts finally drive the tires through the wheel hubs and the suspension stiffness elements modeled to account for the effect of suspension on the torsional oscillation. The wheel hubs, tires and vehicle longitudinal forces (aerodynamic and rolling resistance) are modeled via a simple vehicle model in the AMESim® using the inertia of wheels, the stiffness and damping of the tires. The

values of the parameters used in the model were provided by the sponsor organization. Figure 2.1 shows the AMESim® model that has been developed to represent the driveline model. Similarly, Figure 2.2 shows the layout and interactions between the different components involved in the full order driveline model.

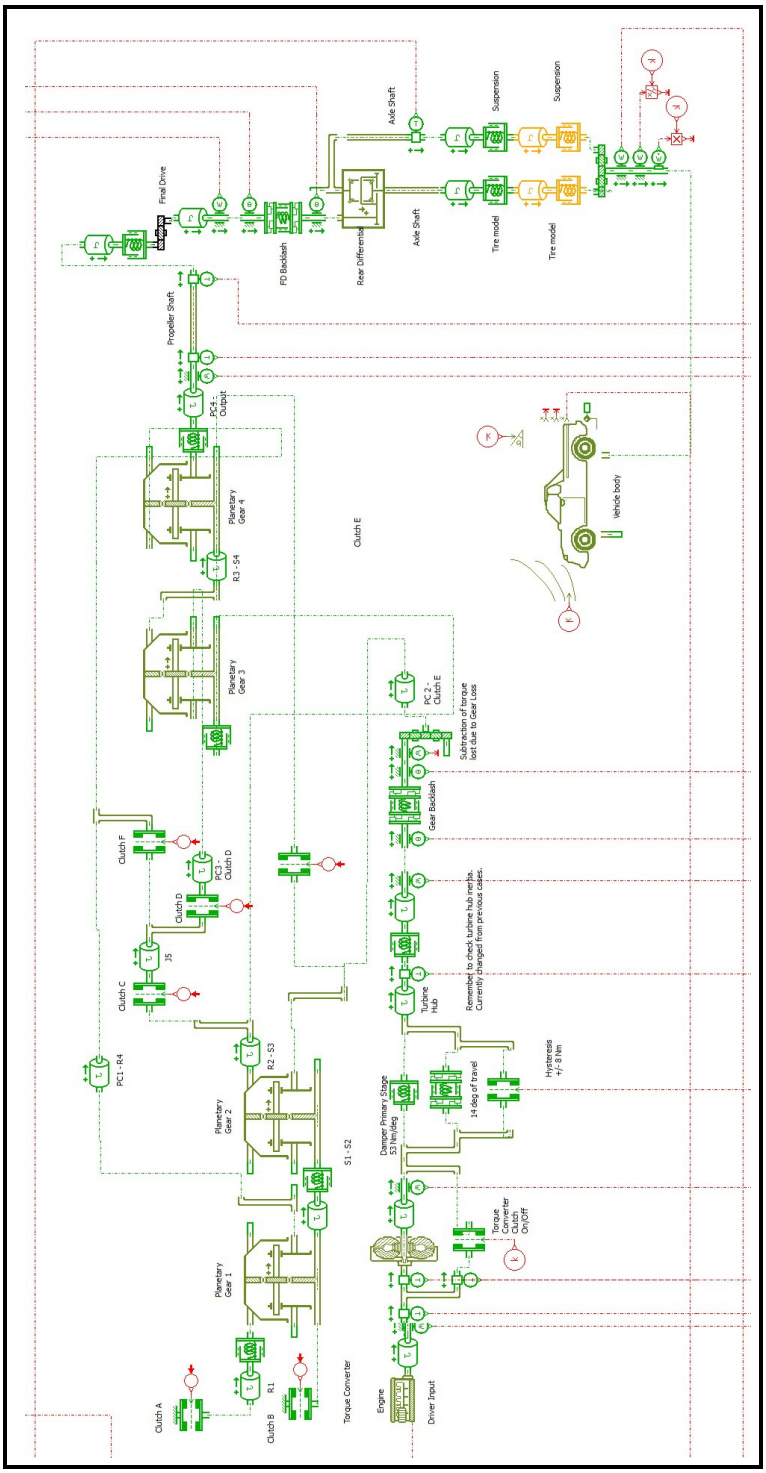

Figure 2.1: AMESim® Full Order Plant Model

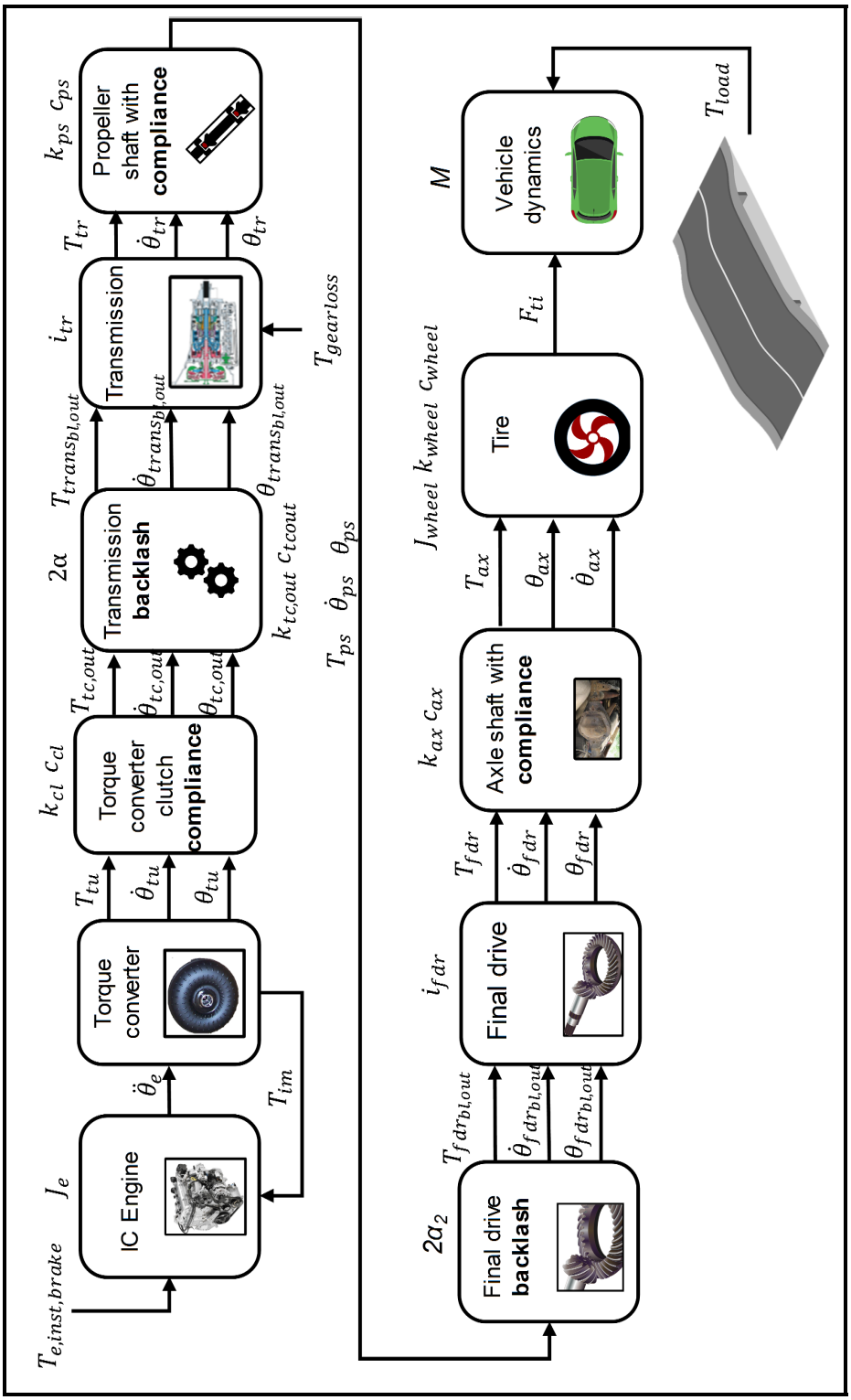

Figure 2.2: Layout of the components of the full order model [4]

2.1.2 Assumptions of full-order model

Certain assumptions have been made while developing the full order model of the vehicle to simulate the clunk and shuffle response. One of the major assumptions is that the model has been developed only to simulate straight line vehicle driving i.e. the affect of cornering is not considered. This assumption is valid as the longitudinal acceleration experienced by the driver during straight-line driving would be maximum. During cornering, the lateral acceleration will also affect the magnitude of shuffle as perceived by the driver. The second assumption is that the clunk and shuffle are simulated for a constant gear torque reversal scenario and not during the gear shift transients. This assumption is made because the control action to mitigate clunk and shuffle during constant gear tip-ins and tip-outs are managed via the torque actuators, while in the case of gear shifts, the transmission clutch pack actuators will also influence the resulting clunk and shuffle. Finally, a locked torque converter case is considered as this will lead to the maximum amount of clunk and shuffle as studied in [12] show that with open and slipping torque converter, the fluid path would act as a damper reducing the observed clunk and shuffle.

2.1.3 Validation of full order model

The primary motivation for the development of the full order model is to capture the dynamics of the driveline during the torque reversal (tip-in and tip-out) scenarios, thus vehicle level measurements were done by the sponsor organization to simulate torque reversal scenarios in the vehicle and data was provided to validate the full order model.

2.1.3.1 Vehicle measurements

In order to provide the data which can be used to validate the model, the sponsor organization conducted vehicle level measurements.A test vehicle was instrumented with a torque measurement sensor (torque meter) on the propeller shaft, a driver seat track accelerometer, and a differential case accelerometer. Although, the effect of shuffle is maximum on the axle shaft, because of the highest torque value due to the gear reduction and the compliance of the axle shaft, it is difficult to measure the torque on the axle shaft as it is enclosed inside the Banjo beam or the Salisbury axle (based on the construction of the rear axle). Consequently, the propeller shaft, which is easily accessible, was instrumented to measure the torque delivered to the vehicle. Furthermore, jerk is defined as a change in acceleration, thus in order to measure the

shuffle response as perceived by the driver, an accelerometer was placed at the driver seat track. Finally, since the maximum lash traversal takes place in the final drive, an accelerometer was placed on the differential housing to measure the acceleration response during the clunk event. Figure 2.3 shows a layout of the locations of sensors in the vehicle.

Apart from these additionally placed sensors, vehicle data on CAN such as the engine speed, the wheel speed, the vehicle speed, the ECU estimated crankshaft torque, the slip across the torque converter, the current gear position and the accelerator pedal position were also recorded in sync with the measured data. This was done to simulate the full order model with the same conditions as that of the test vehicle. Finally, the existing control strategy to shape the torque during torque reversal scenarios was also calibrated off so that the driveline can be excited and the clunk and shuffle response can be generated in the driveline and measured via instrumented sensors.

The vehicle data measured and provided by the sponsor organization was analyzed to identify intercepts of the data which can be used to validate the FOM. It was observed that the vehicle tip-in and tip-out trails were done in 5^{th} and 6^{th} gears. Out of this data, an intercept of 5^{th} gear data was taken out to validate the model which had sufficient steady state time before and after the tip-in maneuver. Additionally, feedback was received from the sponsor organization that even though the torque shaping strategy was calibrated off during the tip-in and tip-out scenarios, torque

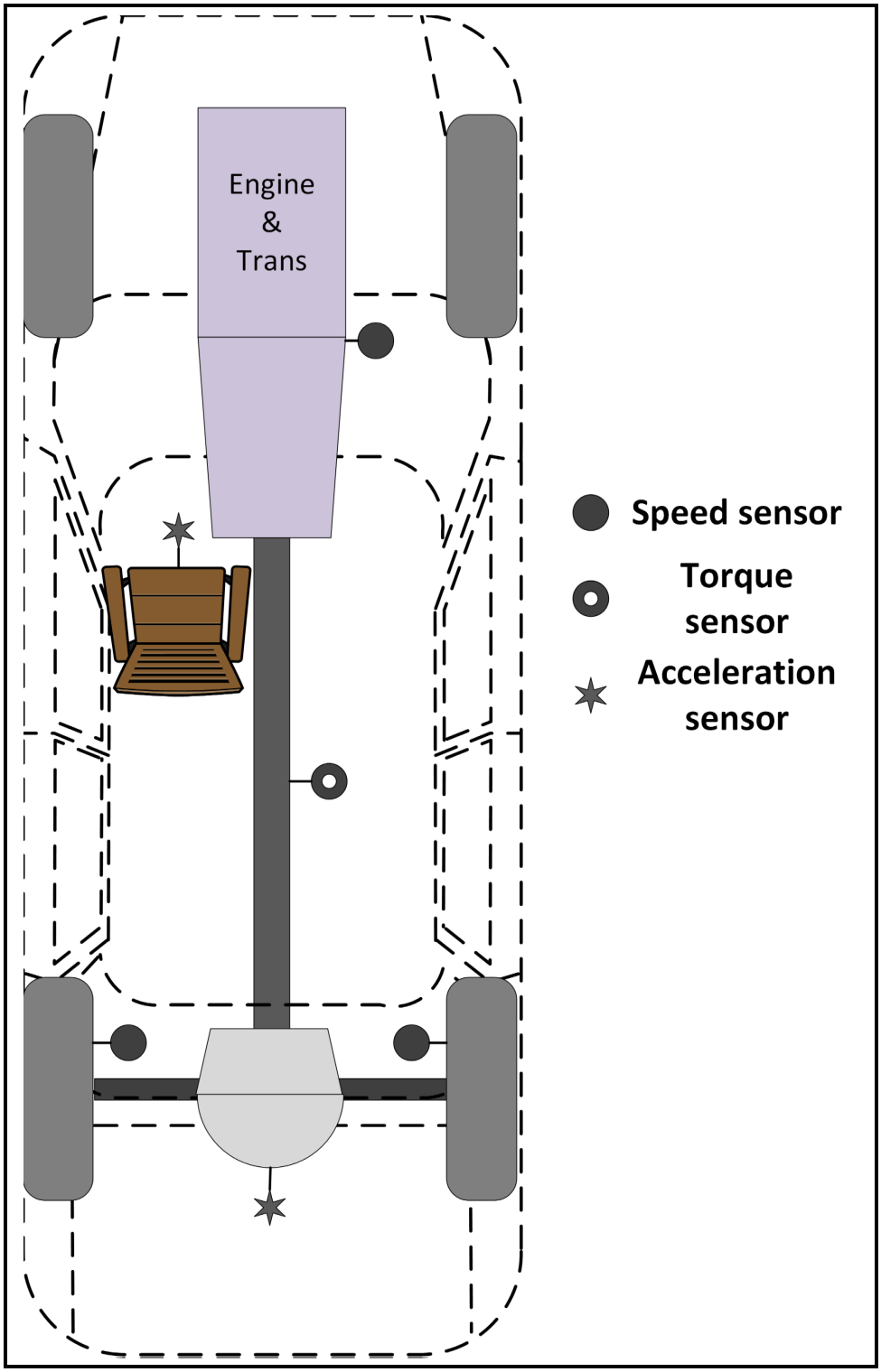

Figure 2.3: Layout of sensors on the instrumented vehicle

shaping still shaped during the tip-out event because of other controllers. Thus, model validation has been carried out only for tip-in scenarios.

Figure 2.4 shows the intercept of the vehicle measured data that is used to validate the FOM. Figure 2.4 (a) shows the CAN estimated crankshaft torque input to the driveline. The sudden rise in the crankshaft torque can be seen as an indicator of the tip-in scenario. Figure 2.4 (b), the left axis shows the variation of the engine speed caused by the sudden change in the crankshaft torque. It can be seen that the RPM of the engine has an oscillatory behavior which is representative of shuffle. The right-hand axis of the Figure 2.4 (b) shows the variation of vehicle speed during the event. It can be seen that the vehicle speed increases with slight oscillation in its trajectory. The reduced nature of oscillation in the vehicle speed can be explained by higher tire damping. Figure 2.4 (c) shows the variation of propeller shaft (alternatively referred to as driveshaft) torque during the event. It can be seen that before the tip-in, the torque at the propeller shaft is negative an indicative of the coasting torque due to the engine friction. As the crankshaft torque increases, the propeller shaft torque rises to a near-zero value, stays there for some time and shoots up with an oscillatory response. The zero torque is held by the propeller shaft until the backlash traversal in the driveline takes place as during lash traversal there is no resistance from the wheels on the shaft. This also leads to the acceleration of the propeller shaft leading to an impact at the end of backlash traversal. This impact causes a sudden rise in the propeller shaft torque twisting it to the drive side followed by untwisting and twisting

shuffle oscillations. The frequency of this shuffle oscillation, based on the measured propeller shaft, is found to be 5.84 Hz. Finally, Figure 2.4 (d) shows the variation of seat track acceleration in the longitudinal direction. The jerk i.e. a sudden change in the magnitude of the acceleration can be seen in the trajectory of the acceleration during the event. As all the signals plotted in Figure 2.4, except the ECU calculated crankshaft torque are actual measured data, these signals are considered from here on to validate the FOM as well as the ROM.

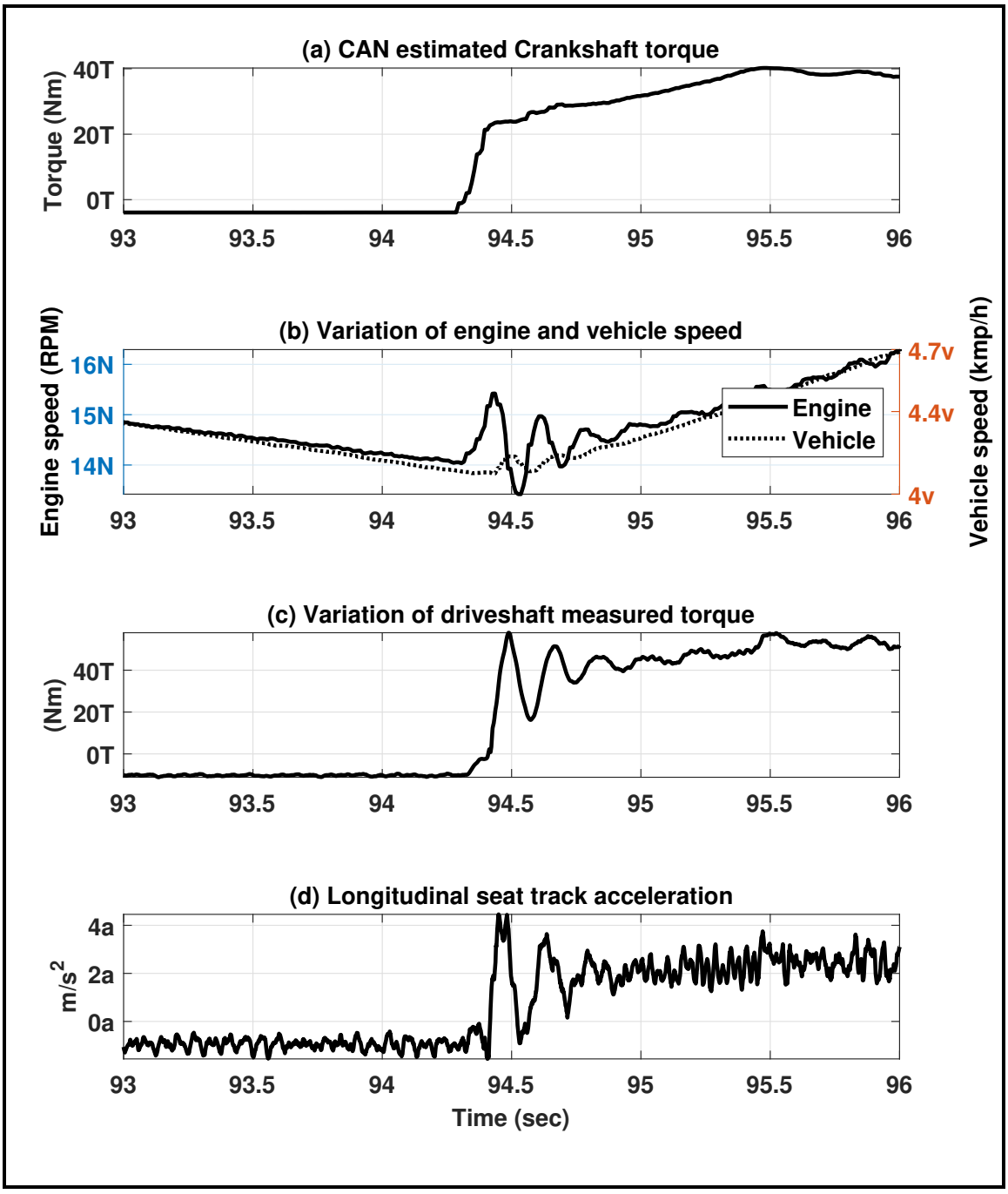

Figure 2.4: Sample vehicle measured data

2.1.3.2 Model validation results with baseline parameters

The FOM developed in Section 2.1.1 was simulated with ECU estimated crankshaft torque along with torque uncertainty as an input to the AMESim® driveline model. This was done so that the powertrain losses and the accessory load, which were not modeled in the engine dynamics, can be taken into account. Figure 2.5 shows the response of the FOM with the baseline model parameters. Figure 2.5 (a) shows the effect of the engine torque uncertainty causing a difference between the input crankshaft torque and the simulated crankshaft torque. Figure 2.5 (b) shows the variation of the simulated engine and vehicle speed with respect to the measured engine and vehicle speeds. The comparison of engine speeds suggest that although the plant model is capable of simulating the driveline dynamics, there is a significant error in the amplitude as well as the frequency of the simulated engine speed. In contrast to the engine speed, the error in the vehicle speed is less, this can be seen on the right axis of Figure 2.5 (b). This is because during the tip-in scenario, the vehicle speed does not change significantly due to the higher vehicle inertia as well as the higher damping of the tires. From Table 2.1 it can be seen that the error in the frequency of the shuffle oscillation is 22.26% while the maximum and average error in the simulated engine is 13.90% and 1.25%, respectively. Figure 2.5 (c) shows the comparison of the simulated and measured propeller shaft torque. It can be seen that the simulated frequency of the shuffle oscillation as well as the magnitude of the

Table 2.1
Summary of simulation results with baseline vehicle parameters

Description	Value	Unit
Measured frequency of shuffle	5.84	Hz
Simulated frequency of shuffle	7.14	Hz
Error in shuffle frequency	22.26	%
Max error in engine speed	13.90	%
Average error in engine speed	1.25	%
Max error in propeller torque	35.24	%
Average error in propeller torque	8.41	%

propeller shaft torque are different as compared to the measured shuffle frequency and torque amplitudes. The maximum and average errors in the simulated value of the propeller torque, from Table 2.1, are 35.24% and 8.41% respectively. Apart from the differences in amplitude and frequency, it can be seen that there is a phase lag in the measured propeller shaft torque as compared to the simulated propeller shaft torque. Finally, Figure 2.5 (d) shows the comparison of the simulated and the measured seat track acceleration were the effect of measurement noise can be seen in the measured acceleration. Ignoring the measurement noise in the seat track acceleration and taking into account the consistent difference in the frequency of oscillation, as observed in the engine and the propeller shaft trajectories, the simulated vehicle acceleration is higher than the mean values of the measured acceleration.

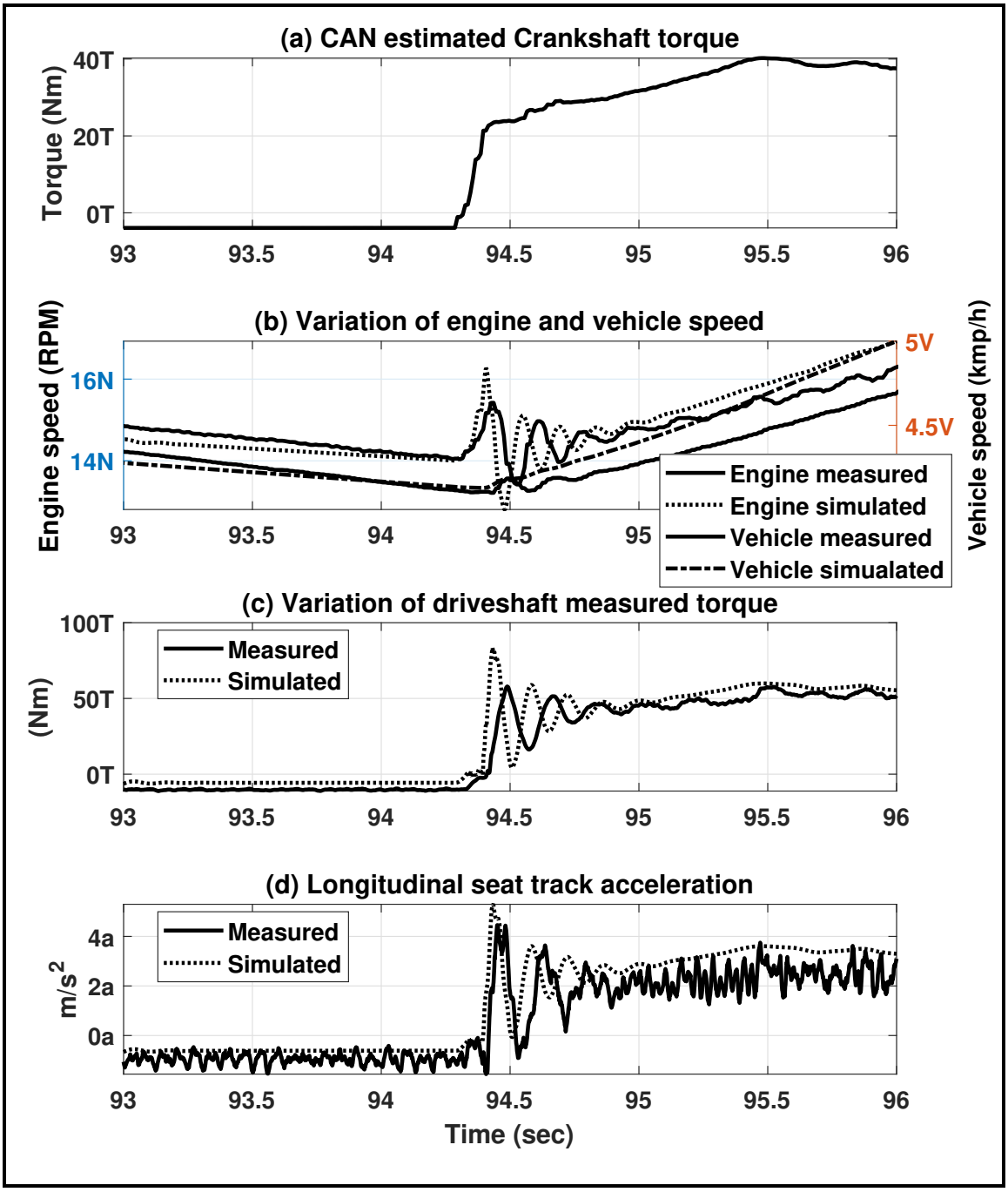

Figure 2.5: Comparison of measured data and simulation results based on baseline vehicle parameters

2.1.3.3 Full order plant model with modified parameters

The differences in the simulated and the measured engine speeds, wheel speeds, propeller shaft torques, and vehicle accelerations, refer Section 2.1.3.2, can be attributed to different sources in the vehicle FOM. A step by step approach to eliminate those differences, via updating the vehicle parameters, based on discussions with sponsor organization has been discussed in this section.

For a shaft with moment of inertia J, subjected to an input torque T_1 at one end and a load torque T_2 at the other end, the rate of change of angular speed of the shaft, $\frac{d\omega}{dt}$ is given by :-

$$T_1 - T_2 = J\frac{d\omega}{dt} \tag{2.1}$$

For a shaft with stiffness K and polar moment of inertia J, the natural frequency of oscillation, ω_n, is given by:

$$\omega_n = \sqrt{\frac{K}{J}} \tag{2.2}$$

† From Equation 2.1, it can be seen that the speed as well as the acceleration of the shaft, for a given input torque, is a function of the load torque. The load torque, for the FOM, is the sum of the aerodynamic drag and the rolling resistance force. The rolling resistance of the vehicle is a function of the coefficient of the rolling

resistance and the vertical load on the wheels which is a function of the mass of the vehicle. For the baseline model, the vehicle weight was taken as the un-loaded mass of the vehicle. This was changed to take into consideration the weight of passengers and the instrumentation when the vehicle test was carried out. Apart from the vehicle weight, the coefficient of rolling resistance was also modified. The coefficient of rolling resistance depends on factors such as the tire temperature, tire inflation pressure, vehicle velocity, tire material and design and tire slip, and based on studies in references [27], [28], [29], the value of the coefficient of rolling resistance was also modified from 0.02 to 0.01.

† From Equation 2.1 and Equation 2.2 it can be seen that the moment of inertia of the driveline components also plays a major role in the determination of the engine speed, vehicle speeds and the frequency of the driveline oscillations. Thus, in order to reduce the simulation error in speeds and the frequency, the values of driveline inertia should be a representative of the actual vehicle. Based on the discussion with the sponsor organization, it was found that the test vehicle had a 4WD configuration i.e. it was installed with a transfer case. Adding the transfer case would increase the inertia of the vehicle reducing the frequency of shuffle oscillation (refer Equation 2.2) inline with the desired frequency change (refer Table 2.1). Additionally, the engine was also equipped with a dual mass flywheel, which would increase the inertia at the crankshaft. Since the exact values of inertia were not available for the transfer case and the

dual mass flywheel, it was decided that a 25% increase in the inertia of engine, torque converter and the transmission would account for the effect of the dual mass flywheel and the transfer case.

† Equation 2.2 also suggests that the natural frequency of oscillation of the driveline is directly proportional to the square root of the stiffness of the driveline. Since the suspension was modeled to be a stiff element in the FOM, based on the discussions with sponsor organization the suspension element was eliminated and after a number of iteration to tune the model, the stiffness of the axle and propeller shaft were reduced by 25%.

† Finally, based on the discussion with the sponsor organization, it was identified that the supplier for the torque meter i.e. propeller torque measurement sensor, has installed a low pass filter with stopband frequency of 30 Hz to attenuate the high-frequency noise in the torque measurement of the propeller shaft. This can cause a phase lag between the measured and the simulated values of the propeller shaft torque. Thus, a Chebyshev low pass filter was designed based on the parameters shown in Table 2.2 and applied to the simulated propeller shaft torque to understand the effect of the low pass filter.

The changes discussed in the model parameters for the FOM are summarized in Table 2.3 and the result of the simulation is shown in Figure 2.6. A summary and comparison of results with baseline plant parameters and modified parameters for the

Table 2.2
propeller torque meter low pass filter design parameters

Description	**Value**
Filter Response type	Low pass
Filter Design method	IIR - Chebyshev Type II
Sampling Frequency	1000 Hz
Pass band frequency	27 Hz
Stop band frequency	30 Hz
Pass band ripple	1 dB
Stop band ripple	80 dB

Table 2.3
Comparison of baseline and modified full order plant parameters

Description	**Baseline parameter**	**Modified parameter**
Mass of vehicle	M kg	$M + 334$ kg
Coefficient of rolling resistance	0.02	0.01
Engine inertia	J_e	$1.25J_e$
Torque conveter inertia	J_{tc}	$1.25J_{tc}$
Transmission inertia	J_t	$1.25J_t$
Axle shaft stiffness	K_a	$0.75K_a$
propeller stiffness	K_d	$0.75K_d$
propeller torque meter low pass filter	No	Yes

full order model in Table 2.4.

It is evident from the comparison of Table 2.4 that error in the maximum as well as the average values of the simulated engine speed and the propeller shaft torque with respect to the measured values has significantly reduced with modified parameters as compared to the baseline parameters. It can also be seen that the frequency of shuffle oscillation with the modified parameters has less than 1% error with the vehicle measured frequency (refer Table 2.1 and 2.4). This can also be seen in Figure 2.6

Table 2.4
Validation summary results with baseline and modified plant parameters

Description	**Baseline parameter**	**Modified parameter**	**Units**
Simulated frequency of shuffle	7.14	5.88	Hz
Error in frequency of shuffle	22.26	0.68	%
Max error in engine speed	13.9	6.92	%
Average error in engine speed	1.25	0.86	%
Max error in propeller torque	35.24	32.4	%
Average error in propeller torque	8.41	0.6	%

(c) where the period of shuffle oscillation for the measured and simulated propeller shaft torques are significantly close as compared to the period of shuffle oscillation in Figure 2.5 (c). A comparison of of Figure 2.5 (c) and Figure 2.6 (c) also reveals that due to the implementation of the low pass filter (refer Table 2.2) there is no lag in the measured propeller torque with respect to the simulated propeller shaft torque. This can be further explained with the help of Figure 2.7 and Equation 2.3:

$$\phi = 2\pi \ f \triangle \ t \tag{2.3}$$

where ϕ represents the phase delay in radians, f represent the frequency of oscillation in Hz and $\triangle \ t$ represents the time delay in seconds.

Figure 2.7 shows the frequency response of the low pass filter represented by parameters in Table 2.2. From the phase response curve, shown by the dashed line, it can be seen that at approximately a frequency of 5.88 Hz, the phase delay caused by the

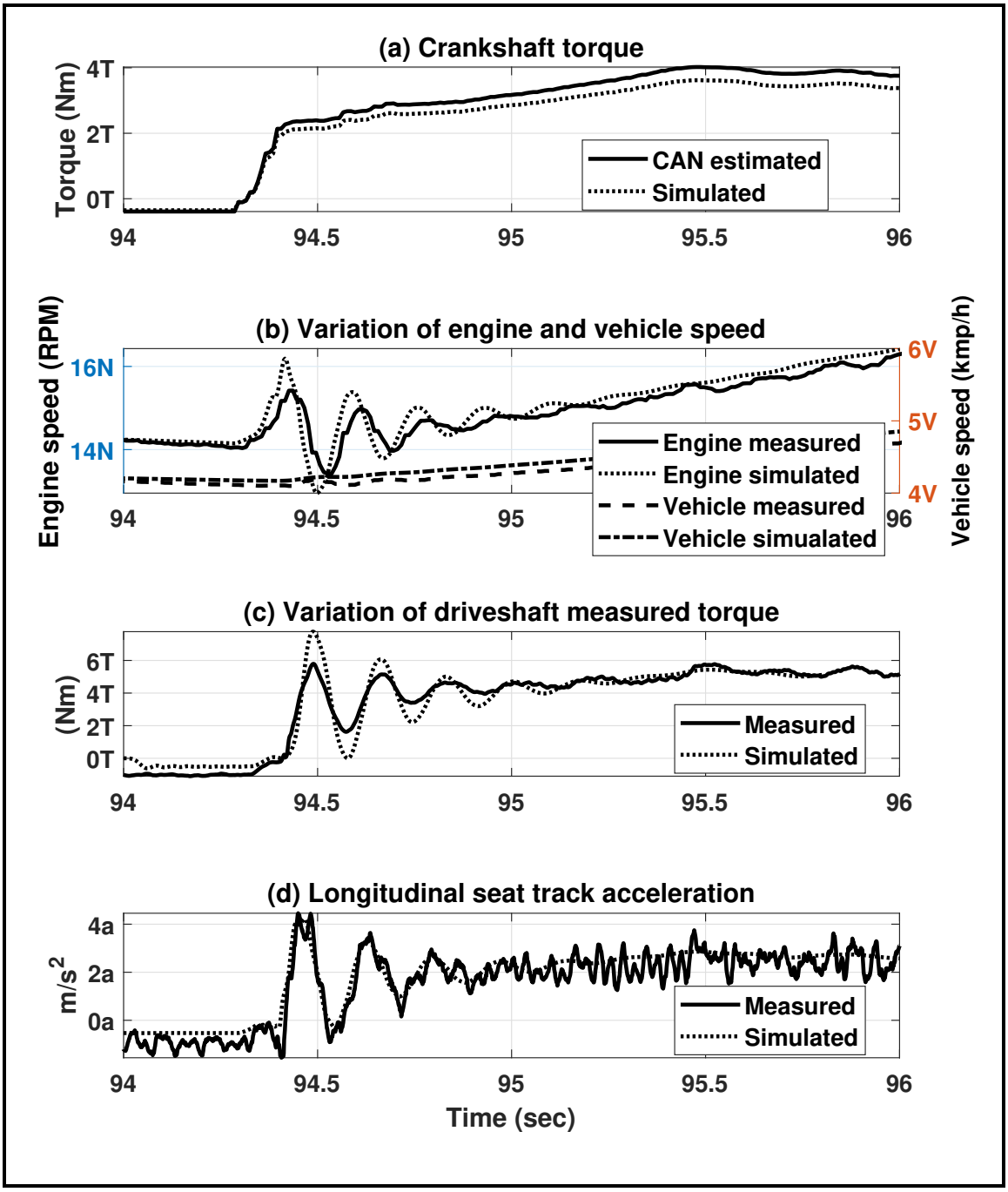

Figure 2.6: Comparison of measured data and simulation results based on modified vehicle parameters

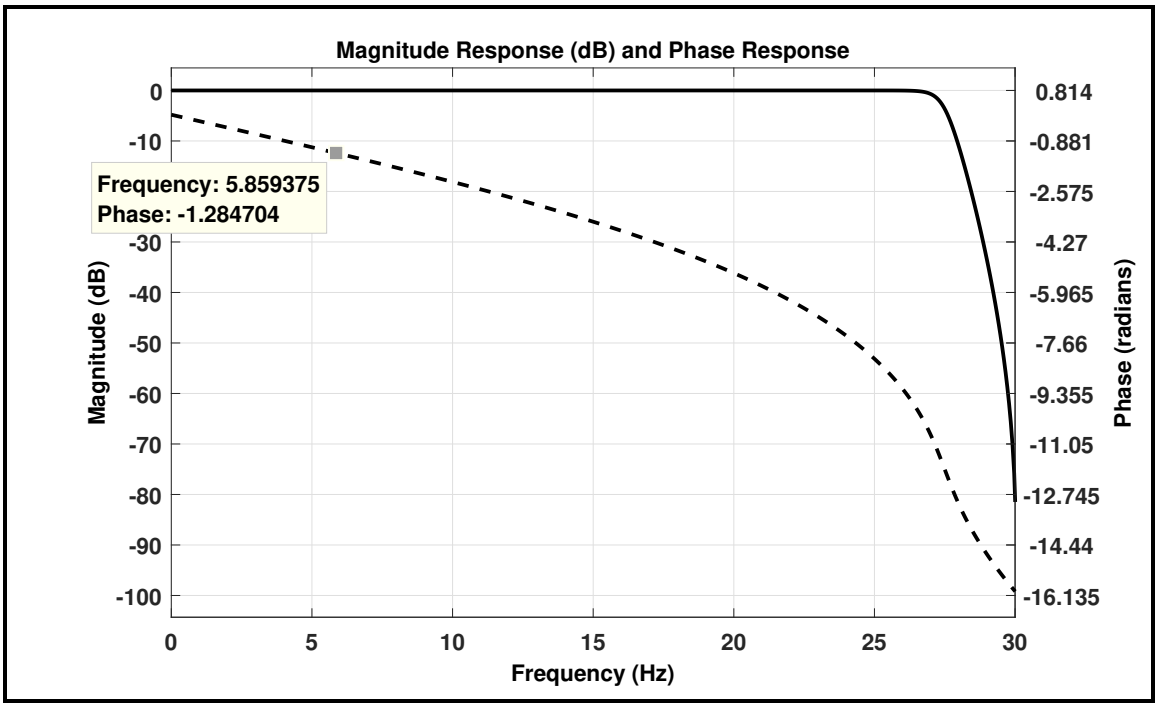

Figure 2.7: Frequency response of propeller torque meter bandpass filter, solid line shows the Magnitude response and dashed line shows the Phase response

filter would be -1.28 radians. Using Equation 2.3 with a phase value of 1.28 radians and frequency of 5.88 Hz, we get a time advance of 34.67 ms. A closer look to Figure 2.4 (c) reveals that the simulated values of shaft torque is approximately 37 ms advance of the measured value which is close to the advance calculated based on the frequency response of the low pass filter validating our filter design. The is also evident from the comparison of the simulated and measured propeller shaft torques in Figure 2.6 where the peaks and valleys of the trajectories are aligned with almost no delay. With these changes and discussions with the sponsor organization, the FOM was considered to be validated.

2.2 Reduced order model

Model order reduction is a process of representing a detailed dynamic model in a way that it is capable of capturing the important features of the full order model quickly, with a reasonable amount of accuracy and reliability. Usually, model order reduction involves simplifying a dynamic model so that either the number of equations or the number of variables or both can be reduced. This can be useful either via reducing the amount of calculations to be done or via reducing the number of variables to be stored. This is applicable for both offline or online systems were behavioral predictions are made. Refer [30] for further details. For instance, the current offline full order driveline model developed for this project, discussed in section 2.1.1 and Reddy [3], involves 47 AMESim® explicit states and 3 Simulink® states, 4 1-D tables and 10 2-D tables. Solving these requires considerable computation power in terms of solving the resulting state equations, carrying out the numerical iterations, as well as storing the output results, [31]. If such a computationally expensive model is used to control a real-time dynamic model of the system, there is a significant probability that the dynamics of interest would over by the time the detailed model is able to predict the behavior of the system. Thus, model order reduction becomes necessary in order to develop a control system which, with reasonable accuracy and within an acceptable time frame, can predict/estimate the behavior of the system to be controlled. Thus, for the FOM developed for this project, a reduced order model was developed so that

a backlash state estimator can be designed which can provide state information to the anti-jerk controller to mitigate clunk and shuffle with a reduced amount of complexity and acceptable accuracy.

As discussed in [32] and [33], a dynamic system with backlash is modeled using two inertia connected via a shaft and a nonlinear backlash element. The two inertia represent the driver and the driven components of the system while the shaft represents the stiffness and damping within the system. The shaft traverses the backlash with no torque transmission to the driven components while the traversal takes place. As a result of this model representation, in a significant number of literary studies of automotive driveline modeling with backlash, the driveline is modeled via 2 mass model along with the gear reduction of the transmission and the final drive. This is shown in [34], [14], [15], [16], [18], [35] and [23]. In this model type for the driveline, the first mass or the driver components represents the lumped inertia of the engine/propulsion system, the torque converters/clutch, the transmission and the propeller shaft, whereas the second mass or the driven components represents the lumped inertia of the final drive, the axle shafts, wheels and the vehicle inertia. The shaft represents the lumped stiffness and damping of the propeller shaft, the axle shafts, and the tires. Finally, the backlash represents the lumped backlash of the transmission assembly and the final drive assembly.

The validation of the full order driveline model has been discussed in [21] and [36].

[36] also discusses the development of a two mass and a three mass reduced order model referred to as 2 degrees of freedom (2DOF) and 3 degrees of freedom model (3DOF) respectively, based on the number of inertia elements present in the model. Their findings suggest that the errors in the simulated acceleration of the vehicle are lower for a 3DOF model as compared to that of 2DOF model. An important assumption of their model is that the backlash has been traversed. A similar study with a 3 inertia and 4 inertia model of the driveline was also done in [37] for a front wheel drive vehicle. Their simulations suggest that better results are obtained for a 4 mass model and a specific set of vehicle conditions, while performing tip-in and tip-out in 3^{rd} and 4^{th} gears. Thus, it was considered essential to evaluate both the configurations 2DOF model (2 mass model) and the 3DOF model (3 mass model) and increase the complexity based on the results of simulations, if required.

2.2.1 ROM I - 2DOF

In this section of the chapter, the development of the 2DOF ROM model is discussed along with the equations representing the dynamics of the model. The simulation results of the ROM model are then compared to that of the FOM to see if the model is able to capture the dynamics with acceptable accuracy.

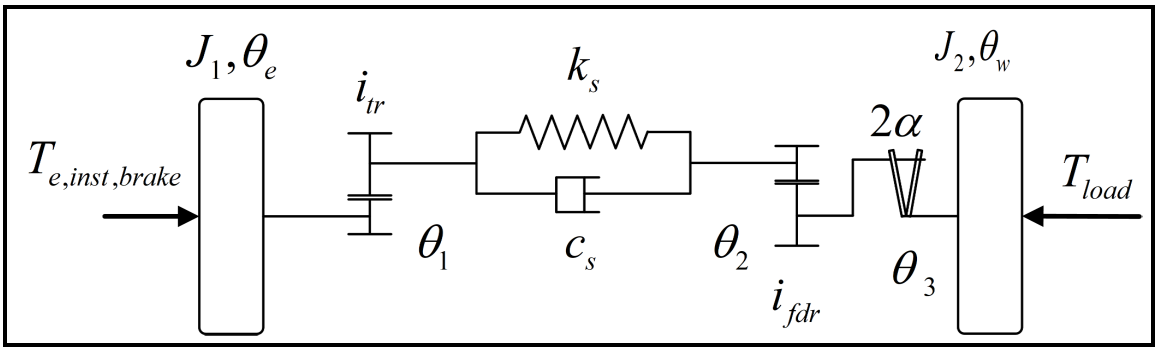

Figure 2.8: 2DOF reduced order model

2.2.1.1 Model development

This section discusses the 2DOF ROM model that has been developed based on the full order model developed in [3]. Figure 2.8 shows the layout of the reduced order model. The elements of the model are discussed below:

† $T_{e,inst,brake}$ and T_{load} [Nm] represent the input torque from the engine to the driveline model and the road load torque experienced by the vehicle respectively. The $T_{e,inst,brake}$ for the 2DOF model is the crankshaft torque with the gear losses taken into account. While the T_{load} is the result of the aerodynamic force, the rolling resistance, road gradient force, and toe load force, if any, acting on the wheels of the vehicle.

† J_1 [kgm^2] represents in the lumped inertia of the engine, the torque converter, the transmission, and the propeller shaft.

† θ_e and θ_w [radians] represent the angular position of the engine crankshaft and the wheels respectively.

† i_{tr} and i_{fdr} represent the transmission gear ratio and the final drive ratio respectively. For our study, the transmission gear is fixed as 5^{th} gear.

† θ_1, θ_2 and θ_3 [radians] represent respectively the angular position of the compliant shaft at the output of the transmission, at the input to the backlash element and at the output of backlash element.

† k_s Nm/rad and c_s [Nm/(rads/s)] represent respectively the lumped stiffness and the lumped damping of the propeller, axle shafts and the tires.

† J_2 [kgm^2] represents the lumped inertia of the axle shafts, the wheel hubs, and the tires.

† 2α [radians] represents the total driveline lumped backlash.

The governing equations for the 2DOF ROM model are -

$$J_1\ddot{\theta}_e = T_{e,inst,brake} + \frac{T_s}{i_{tr}} \tag{2.4}$$

here, T_s represents the shaft torque (torque on the compliant element)

$$\theta_d = \theta_1 - \theta_3 \tag{2.5}$$

$$\theta_b = \theta_2 - \theta_3 \tag{2.6}$$

here, θ_d and θ_b represent the shaft deflection angle and the backlash angle respectively and the derivative of the backlash angle is given by:

$$\dot{\theta}_b = \begin{cases} \max\{0, \dot{\theta}_d + \frac{k_s}{c_s}(\theta_d - \theta_b)\} & \text{if } \theta_b = -\alpha \\ \dot{\theta}_d + \frac{k_s}{c_s}(\theta_d - \theta_b) & \text{if } |\theta_b| < \alpha \\ \min\{0, \dot{\theta}_d + \frac{k_s}{c_s}(\theta_d - \theta_b)\} & \text{if } \theta_b = \alpha \end{cases} \tag{2.7}$$

$$T_s = k_s(\theta_d - \theta_b) + c_s(\dot{\theta}_d - \dot{\theta}_b) \tag{2.8}$$

Refer [15] for details of backlash element modeling.

$$J_2\ddot{\theta}_w = T_s i_{fdr} - T_{load} \tag{2.9}$$

$$M\ddot{\theta}_w r_t = \frac{T_{load}}{r_t} - D_x - R_x, \tag{2.10}$$

where M [Kg] represents the mass of the vehicle, r_t [m] represents the radius of the tires, D_x [N] represents the aerodynamic drag force at the tires and R_x [N] represents the rolling resistance force at the tires.

2.2.1.2 Model Validation

Based on the equations developed in section 2.2.1.1 for 2DOF ROM model, an AMESim® model of the ROM was developed and the input to the AMESim® model was given based on the measured crankshaft torque input. An additional modification was required to be made to account for the gear-train losses which were considered in the FOM at the input to the transmission [3]. This was done via subtracting the gear-train losses directly from the crankshaft torque in the Simulink® environment and then sending it to the AMESim®.

A comparison of the outputs of the 2DOF ROM with the outputs of the FOM (refer Section 2.1.3.3) is shown in Figure 2.9. Figure 2.9 (a) shows a comparison of the crankshaft torque for both the FOM and the ROM and it can be seen that the input to both the models is the same. Figure 2.9 (b) shows the comparison of the engine and the wheel speeds brought in the engine domain. Although the mean of the engine speed simulated by the ROM model is close to the mean of engine speed simulated by the FOM, the ROM model response is significantly under-damped. This is evident from the sustained oscillation in the ROM simulated engine speed. Another observation which can be made from the simulated engine speeds of the ROM and FOM is that the frequency of shuffle oscillation is also different for the ROM. Similar observations, i.e. an under-damped system with a lower frequency of

Table 2.5
Comparison of error in shuffle frequency for 2DOF-ROM with FOM and measured vehicle data

Model type	Shuffle frequency (Hz)	Error with vehicle measurement (%)	Error with FOM (%)
Measured	5.84	-	-
FOM	5.88	0.68	-
ROM - 2DOF	4.39	24.83	25.34

shuffle oscillations, can be made from the trajectories of the propeller shaft torque as well as the vehicle acceleration which are plotted in Figure 2.9 (c) and Figure 2.9 (d). Table 2.5 shows the error in the shuffle frequency for the ROM with 2DOF.

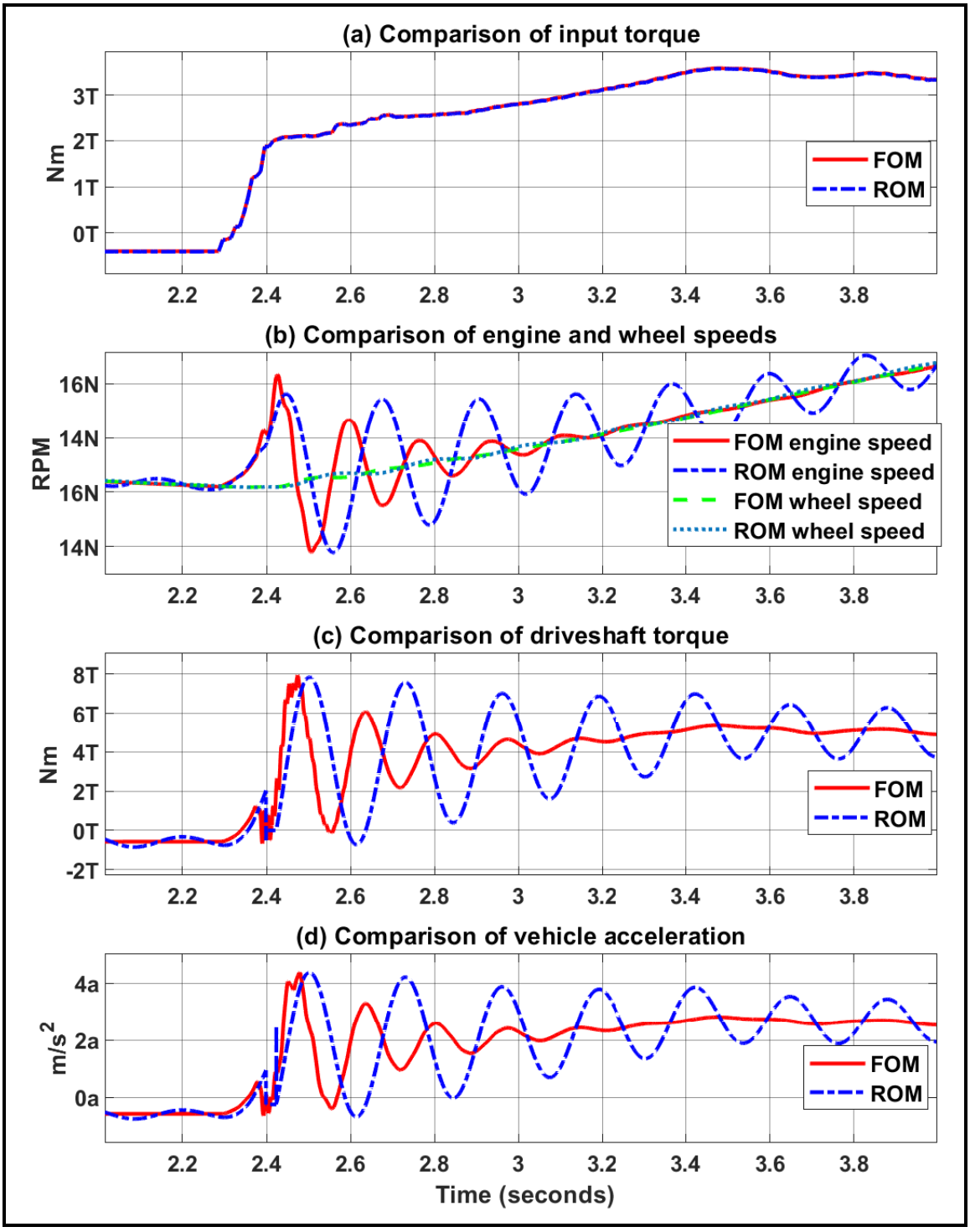

Figure 2.9: Validation result for 2DOF ROM model with FOM model

2.2.2 ROM II - 3DOF lumped backlash

Based on the observations made in the validation section of 2DOF ROM (section 2.2.1.2, it can be seen that the 2DOF model is not able to capture the dynamics of the driveline. Thus, 3DOF ROM was developed as shown in Figure 2.10. The changes in the model based on Figure 2.10 and the system dynamics are discussed in the next section.

2.2.2.1 Model development

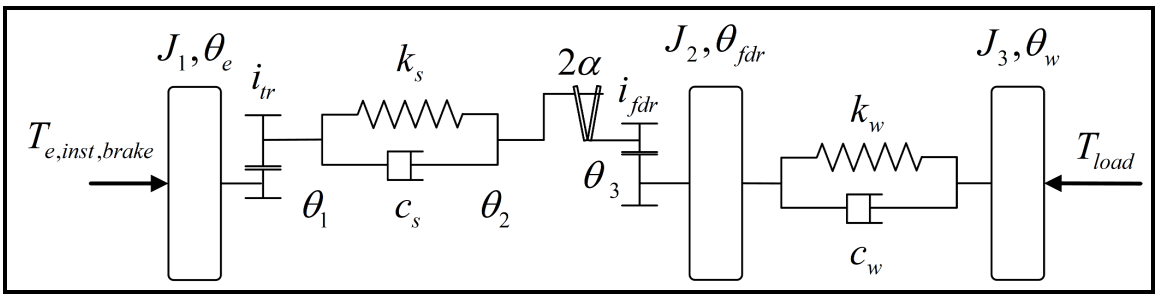

Figure 2.10: 3DOF reduced order model with lumped backlash element

For the 3DOF ROM, the axle shaft and the wheel inertia were lumped together in an intermediate inertia. The tire stiffness and compliance were modeled separately with a compliant element instead of lumping them inside the vehicle dynamics model. The modified dynamic equations are given below:

† $T_{e,inst,brake}$ and T_{load} [Nm] represent the input torque from the engine to the driveline model and the road load torque experienced by the vehicle at the wheels respectively.

† J_1 [kgm^2] represents the lumped inertia of the engine, the torque converter, the transmission and the propeller, whereas J_2 [kgm^2] represents the inertia of the axle shaft and the wheel assembly and J_3 [kgm^2] represents the inertia of the tires.

† θ_e, θ_{fdr} and θ_w [radians] represent the angular positions of the engine, the final drive and the wheel respectively.

† i_{tr} and i_{fdr} represent the gear ratios of the transmission and the final drive reduction respectively.

† θ_1, θ_2 and θ_3 [radians] represent the angular positions of the transmission output shaft, the angular position of the propeller shaft before backlash and the angular position at the input to the final drive reduction respectively.

† k_s and k_w [Nm/rads] respectively represent the stiffness of the propeller and the lumped stiffness of the axle shafts and the wheels.

† c_s and c_w [Nm/(rad/s)] represent the damping of the propeller shaft and the lumped axle shafts and the wheels respectively.

† 2α [radians]represents the total driveline lumped backlash.

The system dynamics are represented by below equations:

$$J_1\ddot{\theta}_e = T_{e,inst,brake} + \frac{T_s}{i_{tr}} \tag{2.11}$$

here, T_s represents the shaft torque (torque on the compliant element)

$$\theta_d = \theta_1 - \theta_3 \tag{2.12}$$

$$\theta_b = \theta_2 - \theta_3 \tag{2.13}$$

here, θ_d and θ_b represents the shaft deflection angle and the backlash angle respectively.

$$T_s = k_s(\theta_d - \theta_b) + c_s(\dot{\theta}_d - \dot{\theta}_b) \tag{2.14}$$

where the derivative of backlash angle $\dot{\theta}_b$ if given by: -

$$\dot{\theta}_b = \begin{cases} \max\{0, \dot{\theta}_d + \frac{k_s}{c_s}(\theta_d - \theta_b)\} & \text{if } \theta_b = -\alpha \\ \dot{\theta}_d + \frac{k_s}{c_s}(\theta_d - \theta_b) & \text{if } |\theta_b| < \alpha \\ \min\{0, \dot{\theta}_d + \frac{k_s}{c_s}(\theta_d - \theta_b)\} & \text{if } \theta_b = \alpha \end{cases} \tag{2.15}$$

$$\theta_1 = \frac{\theta_e}{i_{tr}} \tag{2.16}$$

$$\theta_{fdr} = \frac{\theta_3}{i_{fdr}} \tag{2.17}$$

$$T_{fdr} = T_s i_{fdr} \tag{2.18}$$

$$J_2 \ddot{\theta}_{fdr} = T_{fdr} - T_w \tag{2.19}$$

$$T_w = k_w(\theta_{fdr} - \theta_w) + c_w(\dot{\theta}_{fdr} - \dot{\theta}_w) \tag{2.20}$$

$$J_3 \ddot{\theta}_w = T_w - T_{load} \tag{2.21}$$

$$M\ddot{\theta}_w r_t = \frac{T_{load}}{r_t} - D_x - R_x, \tag{2.22}$$

where M [Kg] represents the mass of the vehicle, r_t [m] represents the radius of the tires, D_x [N] represents the aerodynamic drag force at the tires and R_x [N] represents the rolling resistance force at the tires.

Based on the equations developed for the 3DOF ROM system, an AMESim® model was developed with similar input torque, the difference of the crankshaft torque and the gear-train losses, from Simulink® sent to the AMESim® model.

2.2.2.2 Model Validation

This section compares the simulation results of the 3DOF ROM model, namely the engine speed, the wheel speed, the propeller shaft torque and the vehicle acceleration, with that of the FOM model. A comparison of the transmission and the final drive lash traversal of the FOM is also made with the lumped lash traversal of the 3DOF

Table 2.6
Comparison of error in shuffle frequency for 2DOF-ROM and 3DOF-ROM with FOM and measured vehicle data

Model type	Shuffle frequency (Hz)	Error with vehicle measurement (%)	Error with FOM (%)
Measured	5.84	-	-
FOM	5.88	0.68	-
ROM - 2DOF	4.39	24.83	25.34
ROM - 3DOF	5.85	0.14	0.54

ROM. Finally, a comparison of the 3DOF ROM simulated output is made with the vehicle measurements to validate the model with respect to vehicle measurements.

Figure 2.11 shows the comparison of the simulated FOM and 3DOF ROM. Figure 2.11 (a) shows the comparison of the input torque to the driveline. This same for both the cases so that the model can be validated. Figure 2.11 (b) compares the engine and wheel speeds for the FOM and the 3DOF ROM when brought in the engine domain. When compared to the outputs of the 2DOF ROM, refer Figure 2.9, it can be seen that the outputs with 3DOF ROM overlaps with the FOM. The error in the frequency of shuffle has reduced from 25% to 0.5% with respect to the FOM, refer Table 2.6. Similar trends can be seen in Figure 2.11 (c) and Figure 2.11 (d) for the propeller shaft torque and the vehicle acceleration were the amplitude of oscillation as well as the shuffle frequency is close to the FOM simulated amplitude and the frequency.

A critical parameter for the ROM is the simulated lumped backlash traversal. Error

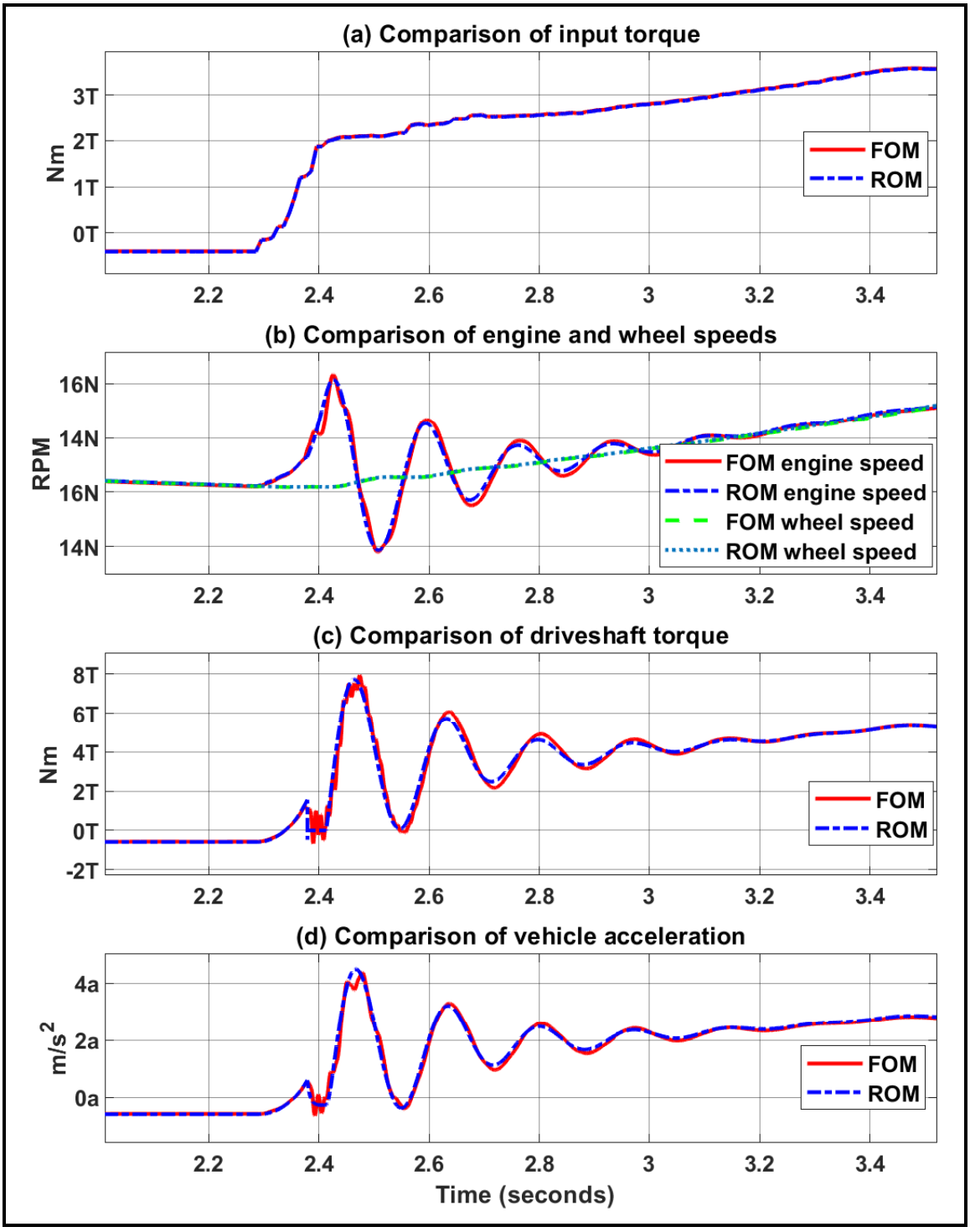

Figure 2.11: Validation of 3DOF with lumped backlash ROM with FOM

in the simulation of backlash traversal would affect the estimator's accuracy which is based on the ROM model developed. This would consequently affect the controller performance as backlash state estimation is an important aspect of controlling jerk during lash traversal scenarios (refer [16]). Figure 2.12 shows the comparison of lash traversal for the FOM and the 3DOF ROM. Figure 2.12 (a) shows the comparison of the FOM's final drive reduction and the transmission backlash traversal, brought at the input to the final drive domain, with the lumped backlash traversal of the 3DOF ROM. It can be seen that the ROM lash traversal starts when the FOM transmission backlash starts to traverse and ends when the final drive lash traversal ends. Figure 2.12 (b) shows the comparison of ROM lash traversal and the lash traversal of FOM when the final drive and the transmission lash are lumped together. It can be seen that the ROM is able to track the FOM lash traversal closely.

A comparison of the 3DOF ROM simulation outputs is also made with the vehicle measurements which is shown in Figure 2.13. An overview of Figure 2.13 for the ROM's comparison with vehicle measurements shows similarities with Figure 2.6 for the FOM's comparison with the vehicle measurements. There is a difference in the input torque for the vehicle and the ROM, Figure 2.13 (a), which is because of the gear-train losses being accounted at the input to the ROM as compared to the input to transmission in case of the FOM. The engine speeds and the wheel speeds have the same frequency of shuffle oscillation with a difference in the magnitude of the oscillations which can be seen in Figure 2.13 (b). We also see a delay in the vehicle

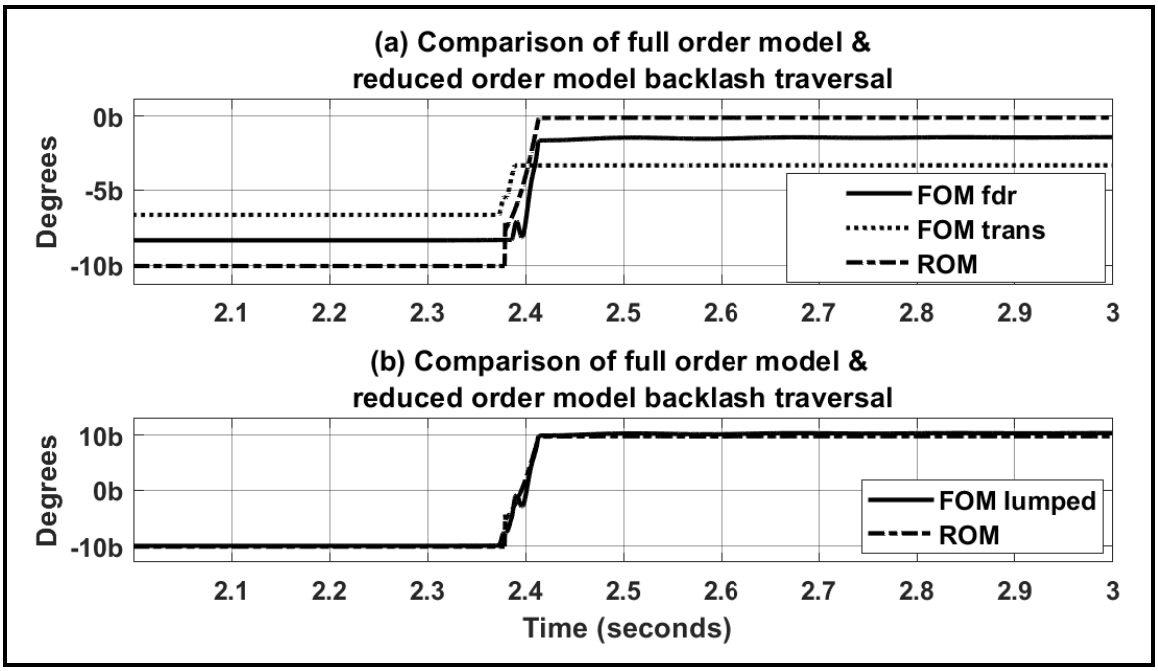

Figure 2.12: Comparison of backlash traversal for 3DOF lumped backlash ROM with FOM

measured propeller shaft torque as compared to the ROM simulated torque in Figure 2.13 (c) as the low pass filter was not modeled for the ROM. Finally, Figure 2.13 (d) shows the comparison of the vehicle acceleration and the ROM simulated acceleration and it can be seen that they align with each other.

As a final step in the development of ROM, the effect of lumping the backlash was also studied via having two backlash elements in the 3DOF-ROM. A layout of the 3DOF ROM with two backlash elements is shown in Figure 2.14 where the lumped backlash 2α in 2DOF ROM and 3DOF-ROM is split into two backlashes, one at the input to the transmission, $2\alpha_1$ and one at the input to the final drive reduction,$2\alpha_2$. Rest of the structure of the ROM is similar to 3DOF model. With the inclusion of the

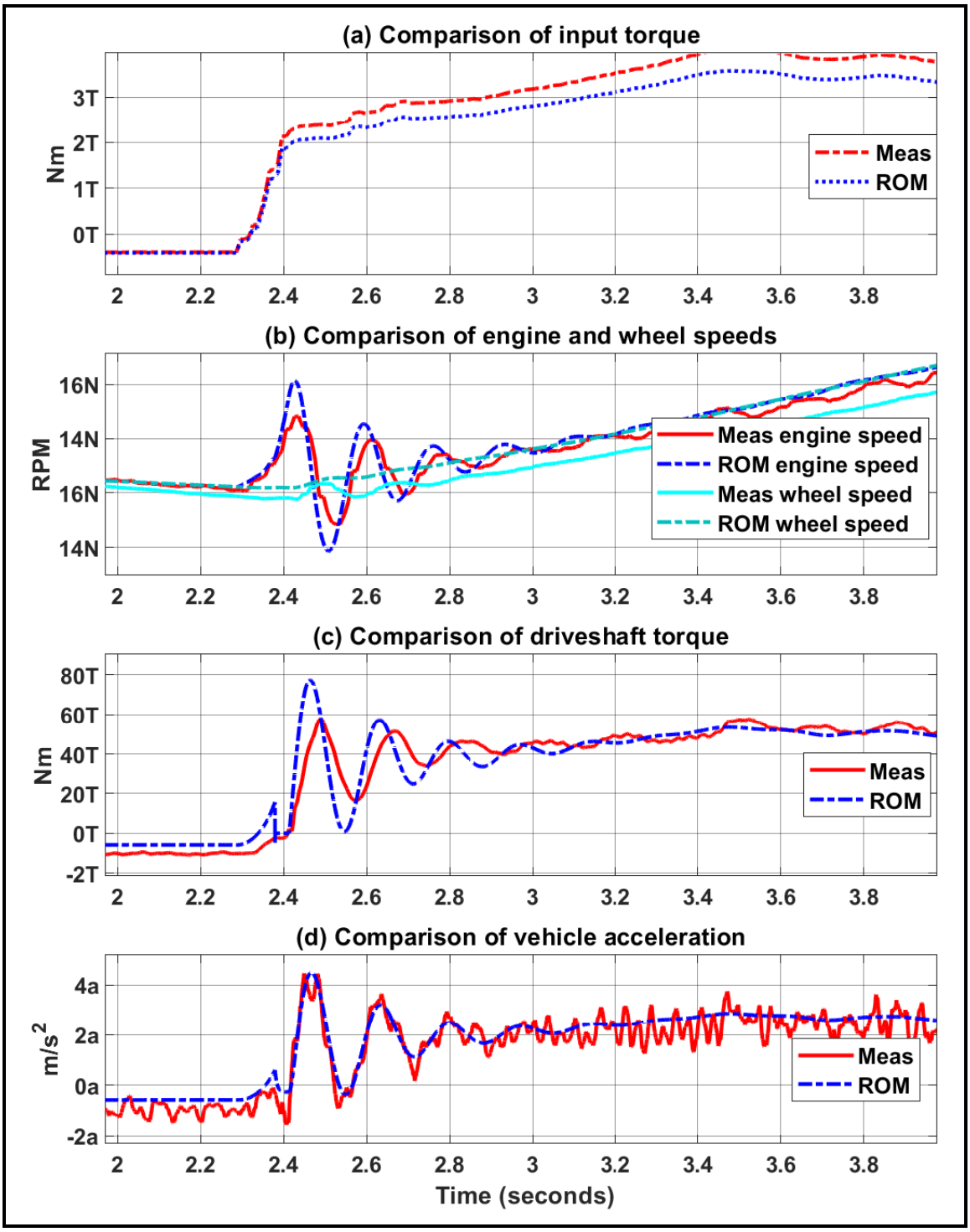

Figure 2.13: Validation of 3DOF lumped backlash ROM with vehicle measurements

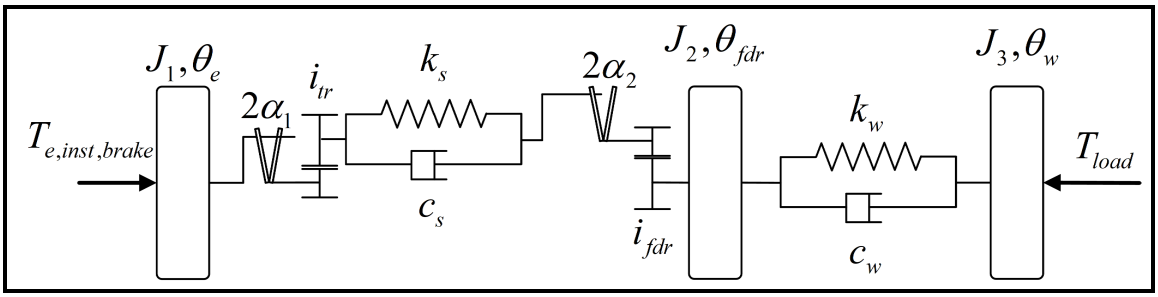

Figure 2.14: 3DOF reduced order model with 2 backlash elements

2 backlashes, the response of the ROM with respect to the FOM is shown in Figure 2.15

If Figure 2.11 for the 3DOF lumped backlash validation results is compared with Figure 2.15 for the 3DOF split backlash validation results, it can be seen that the results are similar and there no significant difference in outputs. Thus, a 3DOF-ROM model with lumped backlash is able to simulate the dynamics of the system with less than 1% error in the shuffle frequency and can be used for representing the vehicle driveline model in locked TCC and for 5^{th} gear with lower order as compared to the spilt backlash 3DOF-ROM model.

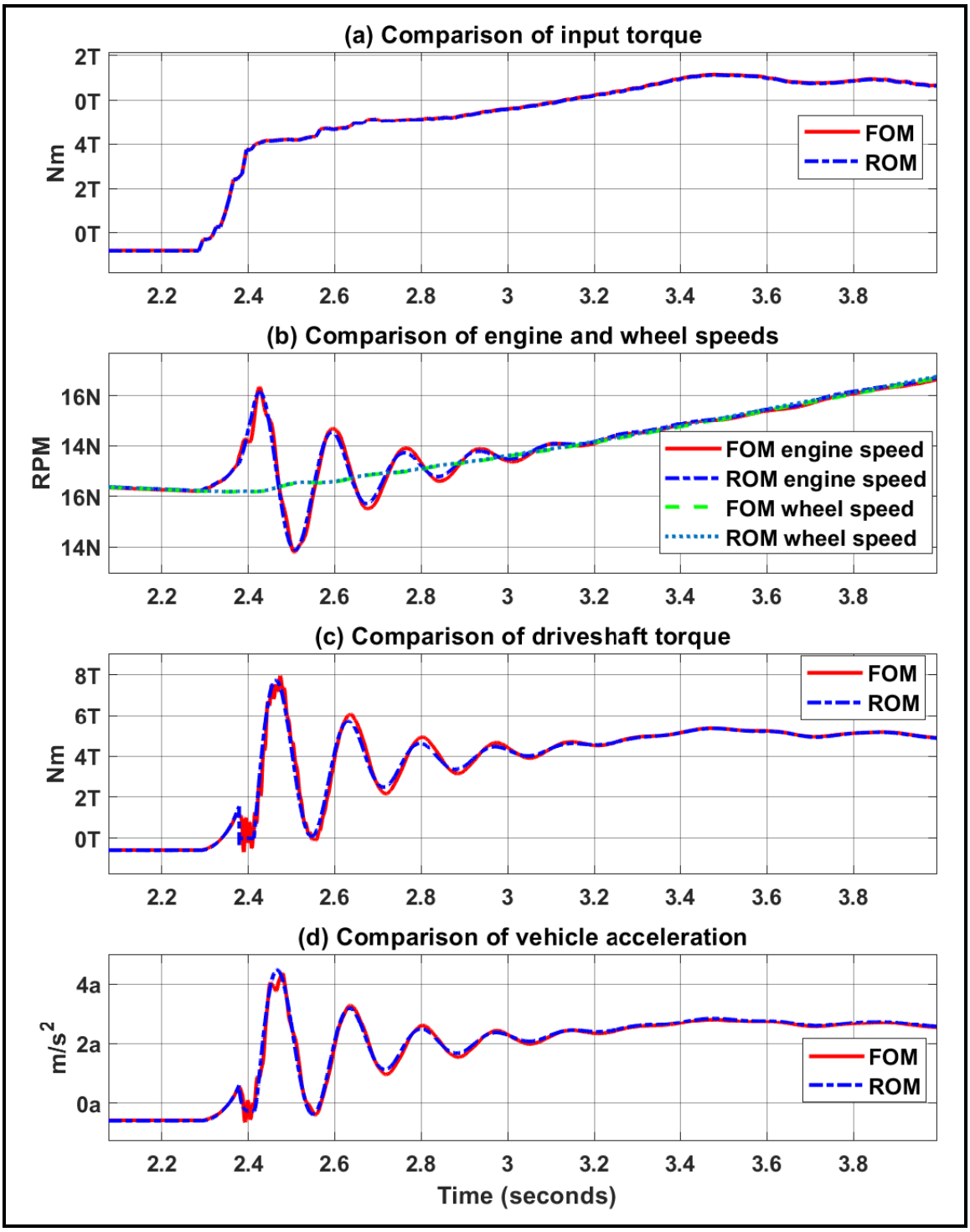

Figure 2.15: Validation of 3DOF ROM with split backlash with FOM model

2.2.3 Assessment of model order reduction

Table 2.7 shows the system configuration which was used to evaluate the run time for the various models that have been discussed in this chapter. Table 2.8 shows a summary of the number of AMESim® explicit states, the run time and the ratio of run time to simulation time for the two ROM models well as the FOM model. It can be seen that with model order reduction, the number of explicit states in the driveline model reduces from 47 for FOM to 10 for 3DOF ROM and the simulation time also reduces from 37.54 to 15.42 seconds which is 59% reduction in time. It is also evident from table 2.8 the reduction in states, as well as run time, is more for the ROM with 2DOF as compared with that of the 3DOF model, but as the 2DOF model is not able to satisfactorily represent the dynamics of the system it cannot be used.

Table 2.7
System configuration used for model performance assessment

System details	**Description**
Processor	Intel® Core™ i7-7700K CPU @4.20GHz
RAM	32 GB
System type	64 - bit Operating System - x64 based processor

Table 2.8
Comparison of simulation time and number of AMESim® explicit states for the ROM and FOM models

Description	ROM-2DOF	ROM-3DOF	FOM	Units
AMESim Explicit states	8	10	47	-
Run time	13.64	15.42	37.54	s
run/sim time ratio	3.41	3.85	9.38	-

Chapter 3

Backlash State Estimator

State of a dynamic system is considered as the memory of the system (refer [38] and [39]). It is a critical resource as the system's current state and the future inputs define the future output/state of the system. Thus, knowing the current state provides an opportunity to manipulate the future input to the dynamic system such that a desired future output/state can be achieved, which is the control objective for a feedback control system.

One approach towards knowing the states of a physical system is to measure them continuously using sensors. With the available measurement of the states and knowing the input to be given, the physical system can be controlled to achieve the desired behavior. But, all the states of interest cannot be always measured. This can be

because of the physical limitations of the measuring sensors or due to the inherent nature of the model. Another approach towards knowing the states of a system is via developing a mathematical model representing the physical system using a set of ordinay differential equations. These equations represent the dynamics of the system. The limitation of this approach lies in the fact that the actual physical system is never known completely due to model uncertainty. Thus, the model developed can deviate from the actual physical system, resulting in the controller receiving information of the system which is not true and affecting the performance of the controller.

A third approach can be referred to as a combination of the above two approaches, wherein a few of the system states are measured and the dynamic model of the system is also developed. This dynamic model uses those measurements to correct the predictions made by the dynamic model by analyzing the error in the predicted states and the measured states. Various methods have been developed in the controls theory to develop such a system, refer [40] and [41].

The current goal of mitigating clunk and shuffle poses a similar problem, wherein the engine torque needs to be cautiously shaped so that the desired driveline response can be achieved. In this case, certain measurements of the vehicle such as the speeds of the engine and the wheels are available but the position of the shaft within the lash cannot be measured. This is primarily because the backlash inside the driveline is distributed at multiple locations of gear and spline mesh interfaces within the

driveline. If it is aimed to measure the overall backlash, from one end of the driveline to the another end, two position sensors would be required to determine the exact position of the shafts, which is expensive in terms of a commercially saleable vehicle. Thus, a state observer/estimator needs to be developed which can use the available measurements and can estimate the backlash position state of the driveline.

The rest of the chapter is categorized into three sections. The first section discusses the development of a state estimator model which builds upon the 3DOF model validated in the previous chapter and uses the available measurements of the engine and the wheel speeds to estimate the backlash position. The second section discusses the validation of the state estimator with respect to the 3DOF plant model as well as the FOM. The third section of this chapter discusses the robustness of the developed state estimator to various changes in the system inputs and measurements.

3.1 Model development

As discussed, the estimator design is a two-step process. The first step involves the development of a state space model, representative of the dynamic system, having some of its states that are available measurements. The second step involves using an estimation method on the state space model and the measurements to estimate the rest of the states of the system. As a result, the estimator model development

is divided into 2 sections where the first section discusses the state space model development and the second section discusses the application of estimation strategy on the state space model. Furthermore, the state space model development section discusses two state space models - one with shaft angular positions as the states of the system and its drawbacks and the other with shaft twist angles as the states to overcome those drawbacks.

3.1.1 State Space models

The state space model to be developed for the estimation of the backlash position is based on the 3DOF ROM that has been developed and validated in the previous chapter and represented using Equation 2.13 to Equation 2.22. An analysis of Equation 2.15 for the derivative of the backlash position suggests a non-linear behavior where the derivative of the backlash angle is zero when the lash is at either positive contact or at negative contact ($|\theta_b| = \alpha$) and non-zero ($|\theta_b| < \alpha$) during the lash traversal. As a result of the non-linear nature of the backlash, the shaft torque, represented by Equation 2.14, also has a non-linear behavior where the shaft torque is zero during the backlash traversal and non-zero during either the positive contact or the negative contact. This can be seen via substituting, the value of $\dot{\theta}_b$ for the case of $|\theta_b| < \alpha$ from Equation 2.15 in Equation 2.14. If $T_{s_{bl}}$ is the shaft torque in the backlash mode,

then it is given by:

$$T_{s_{bl}} = 0 \tag{3.1}$$

and the shaft torque during the contact mode, $T_{s_{cm}}$, is given by:

$$T_{s_{cm}} = k_s(\theta_d - \theta_b) + c_s(\dot{\theta}_d - \dot{\theta}_b) \tag{3.2}$$

Thus, the model of the backlash and consequently the driveline model, by the nature of this dynamics, can be divided into two modes of operation - the contact mode and the backlash mode. This implies that the 3DOF ROM non-linear driveline model can be categorized into two linear state space models representing the dynamics in contact mode and backlash mode.

A general state space representation of a dynamic system is given by:

$$\dot{\mathbf{x}} = \mathbf{A}\mathbf{x} + \mathbf{B}\mathbf{u} \tag{3.3}$$

$$\mathbf{y} = \mathbf{C}\mathbf{x} + \mathbf{D}\mathbf{u} \tag{3.4}$$

where, $\mathbf{x} \in \mathbb{R}^n$ is the state vector

$\mathbf{u} \in \mathbb{R}^m$ is the input or control vector

$\mathbf{y} \in \mathbb{R}^p$ is the output vector.

$\mathbf{A} \in \mathbb{R}^{nxn}$ is the dynamic matrix

$\mathbf{B} \in \mathbb{R}^{nxm}$ is input matrix

$\mathbf{C} \in \mathbb{R}^{pxn}$ is the output matrix

$\mathbf{D} \in \mathbb{R}^{pxm}$ is the feedthrough matrix.

3.1.1.1 State Space Model I

Equation 2.13 to Equation 2.22 represent the dynamics of the system. To develop a state space representation of form Equation 3.3 and Equation 3.4, the states of the model need to be decided. Below are the rationales for choosing some of the states:

† Since the speed of the engine ($\dot{\theta}_e$) and the wheels ($\dot{\theta}_w$) are the measurements and are required to compare the error with estimates, they are considered as a part of the state vector.

† As the primary intention of the estimator is to determine the position of the backlash (θ_b) thus it is also considered as a state.

† In order to consider the speeds as the states and based on the reference [16] and [21], it can be seen that the positions of the inertia elements (Figure 2.14) also need to be considered as states of the state space model, thus the angular positions of the engine (θ_e), final drive (θ_{fdr}) and the wheel (θ_w), and their respective speeds ($\dot{\theta}_e$, $\dot{\theta}_{fdr}$ and $\dot{\theta}_w$) are considered as the states of the model.

The resulting state vector is given by:

$$\mathbf{x} = \begin{bmatrix} \theta_e & \dot{\theta}_e & \theta_{fdr} & \dot{\theta}_{fdr} & \theta_w & \dot{\theta}_w & \theta_b \end{bmatrix}^{\mathsf{T}} \tag{3.5}$$

The inputs in this case are the engine torque $T_{e,inst,base}$ and the road load to the system T_{load}. Thus, the inputs can be defined as:

$$\mathbf{u} = \begin{bmatrix} T_{e,inst,brake} & F_{load} \end{bmatrix} \tag{3.6}$$

Based on the above $\mathbf{x}$ and $\mathbf{u}$ and the discussion of two modes of driveline operation, the dynamic matrix, the input matrix, and the output matrix are given by:

$$\mathbf{A_{cm}} = \begin{bmatrix} 0 & 1 & 0 & 0 & 0 & 0 & 0 \\ -\frac{k_s}{J_1 {i_{tr}}^2} & -\frac{c_s}{J_1 i_{tr}^2} & \frac{k_s i_{fdr}}{J_1 i_{tr}} & \frac{c_s i_{fdr}}{J_1 i_{tr}} & 0 & 0 & \frac{k_s}{J_1 i_{tr}} \\ 0 & 0 & 0 & 1 & 0 & 0 & 0 \\ \frac{k_s i_{fdr}}{J_2 i_{tr}} & \frac{c_s ifdr}{J_2 i_{tr}} & -\frac{k_s {i_{fdr}}^2 + k_w}{J_2} & -\frac{c_s {i_{fdr}}^2 + c_w}{J_2} & \frac{k_w}{J_2} & \frac{c_w}{J_2} & -\frac{k_s i_{fdr}}{J_2} \\ 0 & 0 & 0 & 0 & 0 & 1 & 0 \\ 0 & 0 & \frac{k_w}{M {r_w}^2 + J_3} & \frac{c_w}{M {r_w}^2 + J_3} & -\frac{k_w}{M {r_w}^2 + J_3} & -\frac{c_w}{M {r_w}^2 + J_3} & 0 \\ 0 & 0 & 0 & 0 & 0 & 0 & 0 \end{bmatrix} \tag{3.7}$$

$$\mathbf{A_{bl}} = \begin{bmatrix} 0 & 1 & 0 & 0 & 0 & 0 & 0 \\ 0 & 0 & 0 & 0 & 0 & 0 & 0 \\ 0 & 0 & 0 & 1 & 0 & 0 & 0 \\ 0 & 0 & -\frac{k_w}{J_2} & -\frac{c_w}{J_2} & \frac{k_w}{J_2} & \frac{c_w}{J_2} & 0 \\ 0 & 0 & 0 & 0 & 0 & 1 & 0 \\ 0 & 0 & \frac{k_w}{Mr_w{}^2+J_3} & \frac{c_w}{Mr_w{}^2+J_3} & -\frac{k_w}{Mr_w{}^2+J_3} & -\frac{c_w}{Mr_w{}^2+J_3} & 0 \\ \frac{k_s}{c_s i_{tr}} & \frac{1}{i_{tr}} & -\frac{k_s i_{fdr}}{c_s} & -i_{fdr} & 0 & 0 & -\frac{k_s}{c_s} \end{bmatrix} \tag{3.8}$$

$$\mathbf{B} = \mathbf{B_{cm}} = \mathbf{B_{bl}} = \begin{bmatrix} 0 & \frac{1}{J_1} & 0 & 0 & 0 & 0 & 0 \\ 0 & 0 & 0 & 0 & 0 & \frac{r_w}{Mr_w{}^2+J_3} & 0 \end{bmatrix}^{\mathsf{T}} \tag{3.9}$$

$$\mathbf{C} = \mathbf{C_{cm}} = \mathbf{C_{bl}} = \begin{bmatrix} 0 & 1 & 0 & 0 & 0 & 0 & 0 \\ 0 & 0 & 0 & 0 & 0 & 1 & 0 \end{bmatrix} \tag{3.10}$$

$$\mathbf{D} = \mathbf{D_{cm}} = \mathbf{D_{bl}} = [\mathbf{0}] \tag{3.11}$$

An important property of a state space system is its observability. Observability has to do with the interconnection between the states and the outputs. If a state space model is observable, this implies that using finite observations of the output, the initial state of the system can be identified. As for our case, since we need to identify the backlash position of the system based on the measurements of the engine and the wheel speeds, if the state space model developed is not observable, then the estimator will not be able to estimate the states of the system. References in [42], [40] and [43] discuss various methods to determine the observability of a state space

Table 3.1
Observability for the State Space model I

Mode	Matrix Pair	Number of states	Rank of Observability matrix	Observable
Contact mode	$(\mathbf{A}_{cm}, \mathbf{C})$	7	5	No
Backlash mode	$(\mathbf{A}_{bl}, \mathbf{C})$	7	4	No

model. For this work, we have calculated the observability matrix for the state space model which is given by:

$$\mathcal{O} = \begin{bmatrix} \mathbf{C} & \mathbf{CA} & \mathbf{CA^2} & \dots & \mathbf{CA^{n-1}} \end{bmatrix}^{\intercal} \tag{3.12}$$

A system is said to be completely observable if the rank of $\mathcal{O}$ is equal to n i.e. the number of states of the system. Since we have both the contact mode and the backlash mode, to determine the position of backlash, both the modes should be observable. This can be seen in Table 3.1, where both the contact mode as well as the backlash mode state space models are not observable. Thus, the state space models need to be modified so that the states can be observed.

3.1.1.2 State Space model II

The test of observability for the contact and the backlash modes of the state space model suggests that using the measurements of the engine and wheel speeds, we cannot determine the backlash position of the system, thus the model needs to be

modified.

A closer look at the physics of the contact mode model, i.e. when the backlash is either at the positive contact or at the negative contact and the entire driveline is rigidly connected, suggests that the measurements available are the speeds of either end of the driveline. These are the speeds of the engine lumped inertia and the wheel lumped inertia. With only the measurements of the speeds of the lumped inertia and not the positions, determining the actual position of the engine and wheels are not possible. This is because the initial conditions of the positions of either of the inertias are not known. Thus, if the difference of the positions of the engine, final drive and wheels are considered as the states of the system, then the initial conditions of the positions of the engine, final drive and wheels are not required as they get canceled out, making the system observable. Based on this rationale, the states of both the contact mode and backlash mode models were updated to:

$$\mathbf{x} = \begin{bmatrix} \frac{\theta_e}{i_{tr}} - \theta_{fdr} i_{fdr} & \dot{\theta}_e & \theta_{fdr} - \theta_w & \dot{\theta}_{fdr} & \dot{\theta}_w & \theta_b \end{bmatrix}^{\mathsf{T}} \tag{3.13}$$

where, $(\frac{\theta_e}{i_{tr}} - \theta_{fdr} i_{fdr})$ represents the twist angle of the lumped propeller shaft and $(\theta_{fdr} - \theta_w)$ represents the twist angle of lumped axle shaft, refer Figure 2.14 for the layout of the model. The inputs and the outputs remain the same and based on this, the modified state space model for the contact and the backlash mode is given by:

$$\mathbf{A_{cm}} = \begin{bmatrix} 0 & \frac{1}{i_{tr}} & 0 & -i_{fdr} & 0 & 0 \\ -\frac{k_s}{J_1 i_{tr}} & -\frac{c_s}{J_1 {i_{tr}}^2} & 0 & \frac{c_s i_{fdr}}{J_1 i_{tr}} & 0 & \frac{k_s}{J_1 i_{tr}} \\ 0 & 0 & 0 & 1 & -1 & 0 \\ \frac{k_s i_{fdr}}{J_2} & \frac{c_s i_{fdr}}{J_2 i_{tr}} & -\frac{k_w}{J_2} & -\frac{c_s {i_{fdr}}^2 + c_w}{J_2} & \frac{c_w}{J_2} & -\frac{k_s i_{fdr}}{J_2} \\ 0 & 0 & \frac{k_w}{M{r_{tr}}^2 + J_3} & \frac{c_w}{M{r_{tr}}^2 + J_3} & -\frac{c_w}{M{r_{tr}}^2 + J_3} & 0 \\ 0 & 0 & 0 & 0 & 0 & 0 \end{bmatrix} \tag{3.14}$$

$$\mathbf{A_{bl}} = \begin{bmatrix} 0 & \frac{1}{i_{tr}} & 0 & -i_{fdr} & 0 & 0 \\ 0 & 0 & 0 & 0 & 0 & 0 \\ 0 & 0 & 0 & 1 & -1 & 0 \\ 0 & 0 & -\frac{k_w}{J_2} & -\frac{c_w}{J_2} & \frac{c_w}{J_2} & 0 \\ 0 & 0 & \frac{k_w}{M{r_{tr}}^2 + J_3} & \frac{c_w}{M{r_{tr}}^2 + J_3} & -\frac{c_w}{M{r_{tr}}^2 + J_3} & 0 \\ \frac{k_s}{c_s} & \frac{1}{i_{tr}} & 0 & -i_{fdr} & 0 & -\frac{k_s}{c_s} \end{bmatrix} \tag{3.15}$$

$$\mathbf{B} = \begin{bmatrix} 0 & \frac{1}{J_1} & 0 & 0 & 0 & 0 \\ 0 & 0 & 0 & 0 & \frac{r_w}{M{r_w}^2 + J_3} & 0 \end{bmatrix}^{\mathsf{T}} \tag{3.16}$$

$$\mathbf{C} = \begin{bmatrix} 0 & 1 & 0 & 0 & 0 & 0 \\ 0 & 0 & 0 & 0 & 1 & 0 \end{bmatrix} \tag{3.17}$$

The analysis of observability for the modified state space model and the results are shown in Table 3.2.

Table 3.2
Observability for the State Space model II

Mode	Matrix Pair	Number of states	rank of Observability matrix	Observable
Contact mode	$(\mathbf{A}_{cm}, \mathbf{C})$	6	6	Yes
Backlash mode	$(\mathbf{A}_{bl}, \mathbf{C})$	6	4	No

From the results of Table 3.2, it can be seen that the state space model is observable in contact mode but not in the backlash mode. Looking at the physics of the backlash mode, it can be seen that, the driveline in the backlash mode is disconnected at the backlash element i.e. the input engine torque goes into accelerating the propeller shaft inside the lash zone without any torque being transferred to the wheels. Furthermore, since there is no resistance torque on the propeller shaft, the twisting of the shaft does not take place. Similarly, due to the coasting behavior of the vehicle, the momentum of the vehicle keeps driving the wheels and reducing the vehicle speed based on the road load acting on the wheels. Thus, the backlash mode system can be reduced to two smaller subsystems. The first subsystem is from the engine lumped mass to the backlash element and the second subsystem is from the final drive lumped mass to the wheels. The engine subsystem can be modeled as a shaft accelerating due to the input torque. The wheel subsystem can be modeled as two inertia elements connected via a compliant element, with the wheel inertia subjected to the road load. In this scenario, with the measurements of the engine and wheel speed, all the states of both the subsystems can be determined. The equations of the backlash subsystem (engine

subsystem and wheel subsystem) are given by:

$$\mathbf{x}_{red} = \begin{bmatrix} \dot{\theta}_e & \theta_{fdr} - \theta_w & \dot{\theta}_{fdr} & \dot{\theta}_w \end{bmatrix}^\intercal \tag{3.18}$$

$$\mathbf{A}_{bl_{red}} = \begin{bmatrix} 0 & 0 & 0 & 0 \\ 0 & 0 & 1 & -1 \\ 0 & -\frac{k_w}{J_2} & -\frac{c_w}{J_2} & \frac{c_w}{J_2} \\ 0 & \frac{k_w}{Mr_{tr}{}^2+J_3} & \frac{c_w}{Mr_{tr}^2+J_3} & -\frac{c_w}{Mr_{tr}^2+J_3} \end{bmatrix} \tag{3.19}$$

$$\mathbf{B}_{bl_{red}} = \begin{bmatrix} \frac{1}{J_1} & 0 \\ 0 & 0 \\ 0 & 0 \\ 0 & \frac{r_w}{Mr_w{}^2+J_3} \end{bmatrix} \tag{3.20}$$

$$\mathbf{C}_{bl_{red}} = \begin{bmatrix} 1 & 0 & 0 & 0 \\ 0 & 0 & 0 & 1 \end{bmatrix} \tag{3.21}$$

The test of observability for the reduced backlash model suggests that the rank of the observability matrix is 4 which is equal to the number of states of the reduced subsystem, as a result, all the states in Equation 3.18 are observable. It can be seen that the reduced system developed for the backlash mode does not contain the backlash position state, i.e. the backlash position cannot be estimated during the backlash traversal using the engine and wheel speed measurements. Whereas in the contact mode, all the states are observable and can be estimated.

3.1.2 Estimator design

As discussed, the model that has been developed is always an approximation of the actual physical system. So, to estimate the states of the system, some of the states need to be measured. With the help of the measured state and the approximate plant model, an estimation method needs to be used so that the rest of the states of the model can be determined. The estimation method should be capable of handling the errors caused by the approximation of the system, the noises in the measurements - measurement noise, as well as the noise due to the propagation of the uncertainty in estimated states - known as the process noise. Furthermore, the estimation method should also be able to weigh the accuracy of the measurements to the accuracy of the plant model to rely on either the measurement or the plant model to estimate the states of the system.

One such method for estimation for a linear dynamical model is known as the Kalman filter estimation method, refer [40] and [41]. This method uses the measurements, the plant model dynamics and the error co-variances of the process as well as the measurements to output an optimal estimate of the states of the system. Optimal results are obtained when the plant model perfectly matches the real physical system, the process and the measurement noises are uncorrelated and Gaussian in nature with zero-means (white noise) and the co-variances of the noise are exactly known. The

Kalman filter is optimal as it tries to minimize the square of the error between the prediction and the measurements and uses this information to estimate the states of the system, ref [40].

With an assumption that the process noise and the measurement noise co-variances of the driveline are zero-mean Gaussian in nature, a switched Kalman state estimator is designed based on the contact mode and the backlash mode state space models. (Refer 3.1.1.2, Equation 3.13 to Equation 3.21). Figure 3.1 shows the layout of the Switched Kalman State Estimator (SKSE) that has been developed to estimate the states of the model, with an interface to the plant model. The SKSE, developed in Simulink®, uses the measurements of the engine speed and the wheel speed from the FOM (plant model), developed in Simulink® and AMESim®. The engine speed ($\dot{\theta}_e$) and wheel speeds ($\dot{\theta}_w$) are the output of the FOM for a tip-in torque input, $T_{e,inst,brake}$. $T_{e,inst,brake}$ is also an input to the SKSE along with road load, F_{load}. The F_{load} is calculated based on the measured wheel speed and the parameters of the vehicle. The SKSE has two modes of operation, the contact mode and the backlash mode, defined by their respective state space models, $(A_{cm}, B_{cm}, C_{cm}, D_{cm})$ and $(A_{bl}, B_{bl}, C_{bl}, D_{bl})$ and their respective Kalman gains (K_{cm} and K_{bl}) used to estimate the states of the model. An initial condition, $\mathbf{x}_0$, is also given to the SKSE. The switching between the two modes takes place when the conditions for switching between the two modes are met, i.e. when $TC_{bl\rightarrow cm}$ is met, the SKSE switches from the backlash mode to the contact mode and when $TC_{cm\rightarrow bl}$ is met, the SKSE switches to the backlash mode

from the contact mode. The output of the SKSE are the estimated states of the driveline, $\hat{\mathbf{x}}$.

Based on the layout shown in Figure 3.1, the SKSE is discussed in further details in the next sections.

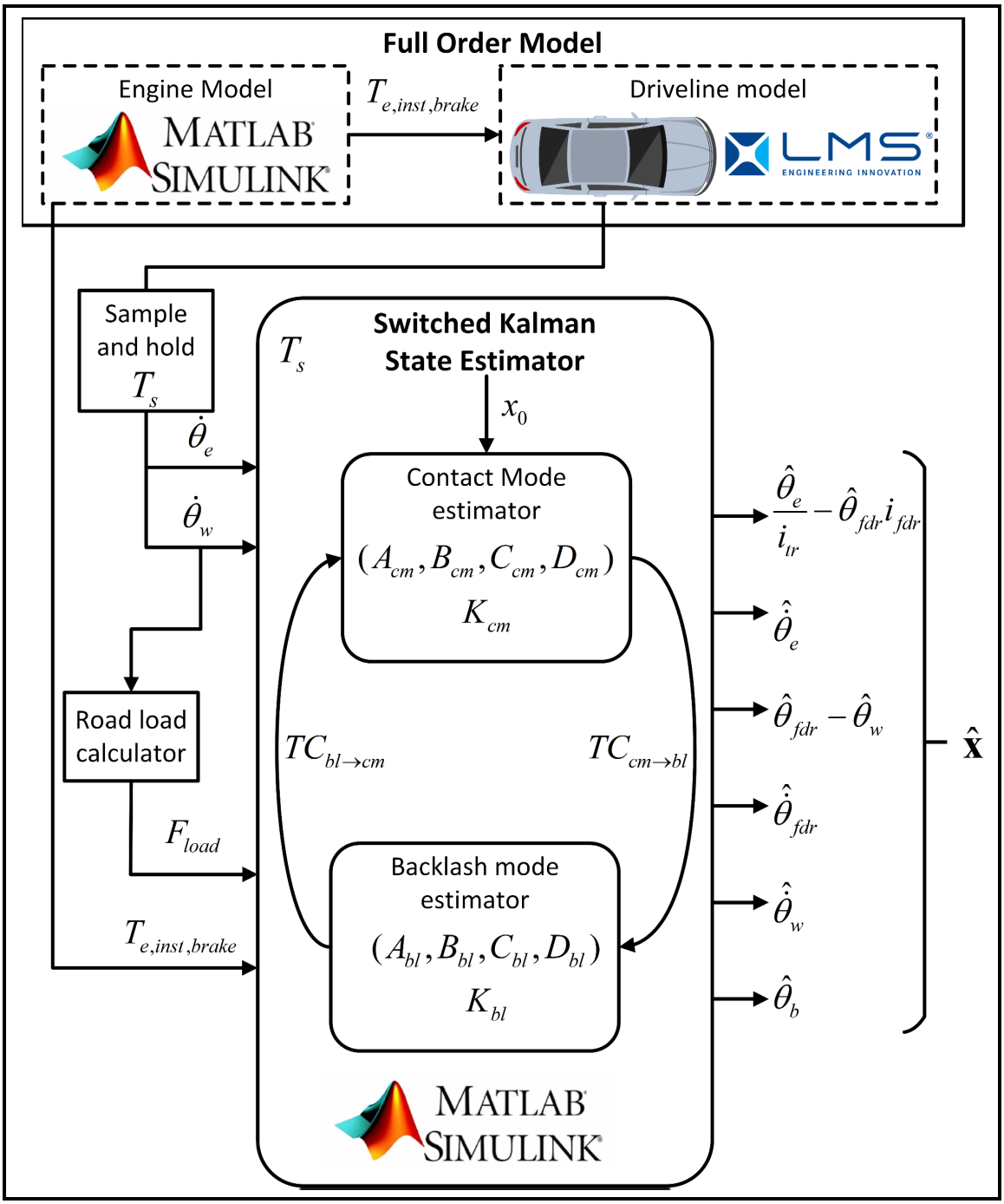

Figure 3.1: Layout of the designed backlash state estimator

3.1.2.1 Kalman estimator

The steps taken for the development of Kalman state estimator are listed below:

† As the FOM model was in the continuous time domain, to facilitate the integration of Simulink® and AMESim®, and as the estimator needs to be implemented in the vehicle ECU, a Discrete Switched Kalman State Estimator (DSKSE) was required.

† In order to implement the DSKES, both the contact mode and the backlash mode dynamics were discretized based on the sampling time of the engine and the wheel speeds available, T_s.

† The Kalman filter estimation is a two-step method, the prediction step, and the measurement-update or the innovation step. In the prediction step, the States and the Error co-variance of the system (either the contact mode or the backlash mode based on the current mode of driveline operation) are propagated based on the state dynamics, input dynamics, and output dynamics. This propagation predicts the states as well as the error co-variances. In the innovation step, the propagated error co-variance is used to evaluate the Kalman gains. This is based on the process noise and the measurement noise. The Kalman gains are then used to estimate the States as well as the Error co-variance. In addition, this cycle is repeated at every time step.

† **Prediction step -** Let, $\mathbf{x}$ be the States of the system, $\mathbf{P}$ the Error co-variance matrix, $\mathbf{A}$ the State dynamics matrix, $\mathbf{B}$ the input matrix, $\mathbf{C}$ the output matrix, $\mathbf{Q}$ the process noise co-variance matrix, $\mathbf{R}$ the measurement noise co-variance matrix, $\mathbf{Z}$ represents the measurements and k is the current time step, then the a-priori state and error co-variance estimates are given by:

A-priori state estimate:

$$\hat{\mathbf{x}}_{k+1}^{-} = \mathbf{A}\hat{\mathbf{x}}_k + \mathbf{B}\mathbf{u}_k \tag{3.22}$$

A-priori error co-variance estimate:

$$\mathbf{P}_{k+1}^{-} = \mathbf{A}\mathbf{P}_k\mathbf{A}^{\intercal} + \mathbf{Q} \tag{3.23}$$

† The above estimates are then compared with the measurement data to calculate the Kalman gain:

$$\mathbf{K}_{k+1} = (\mathbf{P}_{k+1}^{-}\mathbf{C}^{\intercal})(\mathbf{C}\mathbf{P}_{k+1}^{-}\mathbf{C}^{\intercal} + \mathbf{R})^{-1} \tag{3.24}$$

† **Measurement-update step** - Using the Kalman gain, Equation 3.24, the errors between the predicted and the measured states are propagated to the estimates of the states and the error co-variance.

A-posteriori state estimate:

$$\hat{\mathbf{x}}_{k+1} = \hat{\mathbf{x}}_{k+1}^{-} + \mathbf{K}_{k+1}(\mathbf{Z}_{k+1} - \mathbf{C}\hat{\mathbf{x}}_{k+1}^{-}) \tag{3.25}$$

A-posteriori error co-variance:

$$\mathbf{P}_{k+1} = (\mathbf{I} - \mathbf{K}_{k+1}\mathbf{C})\mathbf{P}^{-}_{k+1} \tag{3.26}$$

Depending on the mode of operation of the dynamics of the system, the **A**, **B** and **C** take the values of the contact mode dynamic or the backlash mode dynamics.

3.1.2.2 Backlash mode - Prediction and estimation updates

As discussed in the previous section, the Kalman filter estimates the states of the dynamical system via switching between the two modes of operation of the model, propagating the states based on the state equations of that model and finally updating the predictions based on the measurements. Referring to Section 3.1.1.2, it can be seen that for the backlash model, only the reduced backlash model is observable. The reduced backlash model can only update the $\dot{\theta}_e$, $(\theta_{fdr} - \theta_w)$, $\dot{\theta}_{fdr}$ and the $\dot{\theta}_w$ states and not the $(\frac{\theta_e}{i_{tr}} - \theta_{fdr} i_{fdr})$ and the θ_b states of the backlash model. This problem is mitigated via only carrying out the *a-priori* step of the Kalman filter for the $(\frac{\theta_e}{i_{tr}} - \theta_{fdr} i_{fdr})$ and θ_b states. This is done with the assumption that the measurement-based update of the remaining states would provide some information to drive these states to the actual outputs of the plant. Figure 3.2 shows the difference between the *a-priori* and *a-posteriori* estimates along with the states which are estimated, and are only predicted for both the contact mode as well as the backlash mode.

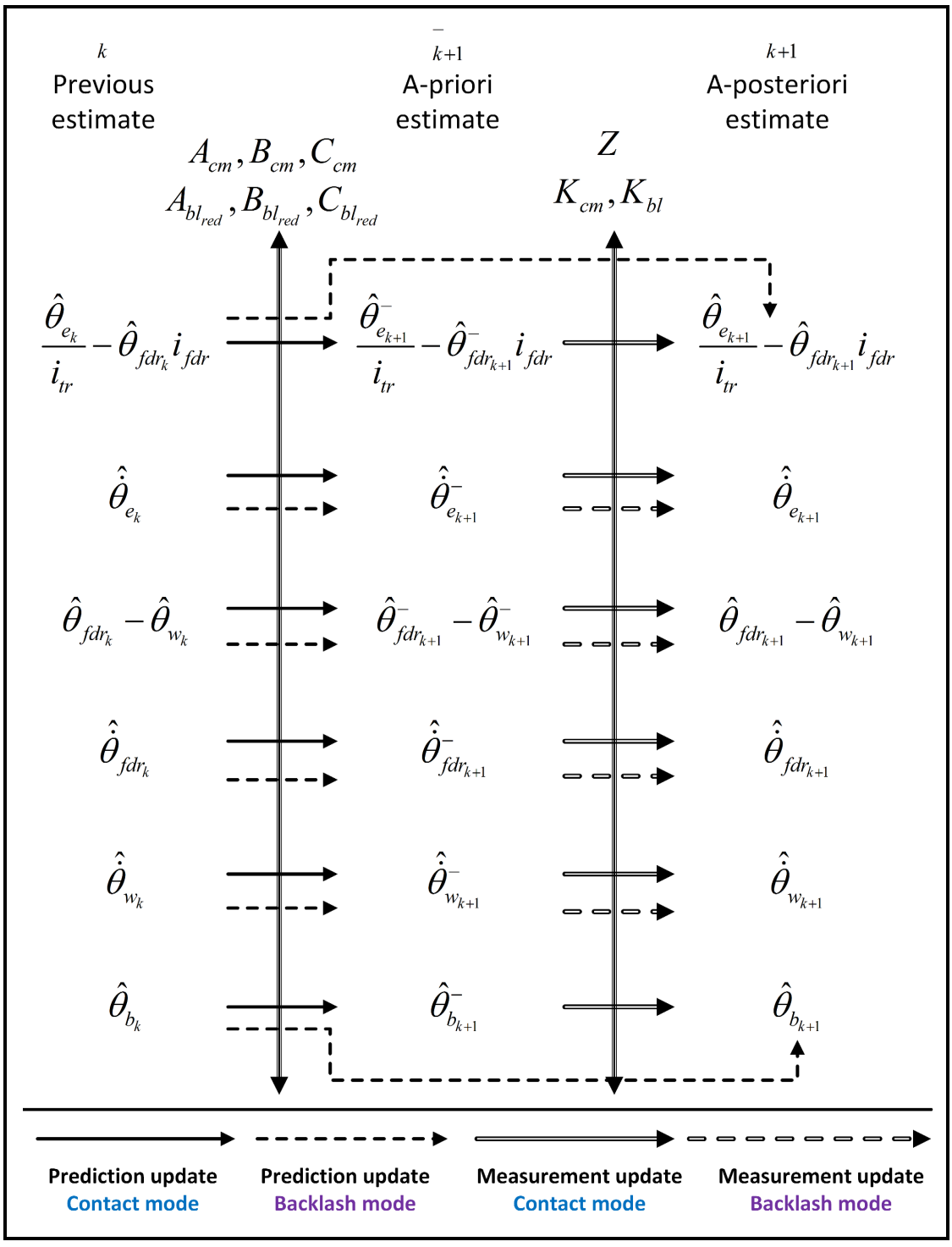

Figure 3.2: Discrete Switched Kalman State Estimator prediction and estimation steps for contact mode and backlash mode

3.1.2.3 DSKSE Transition conditions

Since the operation of the driveline model has been divided into the contact mode operation and backlash mode operation, the estimator needs to switch between those modes. One obvious choice for transition condition is, if the absolute value of backlash angle is less than the half lash size, $|\hat{\theta}_b| < \alpha$ then we know for a certainty that the driveline is in backlash mode. Another set of conditions to decide the mode of operation can be determined based on the derivative of the backlash angle.

From Equation 2.15 for the derivative of backlash angle, it can be seen that for negative contact

$$\dot{\theta}_b < 0 \text{ for } \theta_b = -\alpha \tag{3.27}$$

this implies:

$$\theta_b \dot{\theta}_b > 0 \tag{3.28}$$

Similarly, for positive contact,

$$\dot{\theta}_b > 0 \text{ for } \theta_b = \alpha \tag{3.29}$$

which also implies

$$\theta_b \dot{\theta}_b > 0 \tag{3.30}$$

Consequently, for backlash mode:

$$\theta_b \dot{\theta}_b \leqslant 0 \tag{3.31}$$

Thus, the transition from the contact mode to the backlash mode will take place when:

$$\hat{\theta}_b \hat{\dot{\theta}}_b \leqslant 0 \;||\; |\hat{\theta}_b| < \alpha \tag{3.32}$$

The transition from the backlash mode to the contact mode will take place when:

$$\hat{\theta}_b \hat{\dot{\theta}}_b > 0 \;\&\; |\hat{\theta}_b| = \alpha \tag{3.33}$$

3.1.2.4 Process noise and Measurement noise co-variance matrices

The DSKSE uses a Process noise co-variance matrix, $\mathbf{Q}$ in Equation 3.23 and the Measurement noise co-variance matrix, $\mathbf{R}$, in Equation 3.24 to evaluate the Kalman gains to propagate the error in the predictions with respect to the measurements to the states of the system. Here, $\mathbf{Q} \in \mathbb{R}^{nxn}$, represents the noise in the states due to the imperfect model of the system. The diagonal elements of $\mathbf{Q}$ represent the variance of each state variable, while the non-diagonal elements represent the co-variance between different states with respect to each other. On the other hand, $\mathbf{R} \in \mathbb{R}^{mxm}$ represents the noise in the measurements i.e. the sensor noise which needs to be considered to evaluate the Kalman gains. For the current estimator design, the diagonal elements

of **Q** were chosen as a calibration parameter to tune the estimator while the values of elements of **R** were decided based on the respective sensor accuracy data.

Figure 3.3 (b), (c) and (d) shows the estimates of DSKSE when subjected to an input ramp torque shown in Figure 3.3 (a). The DSKSE, in this case, is discretized at a sampling time of 10 ms and the engine and the wheel speed inputs to the DSKSE are also sampled at 10 ms. Figure 3.3 (b) shows the variation of the engine-side and the wheel-side twist angles. Both the twist angles are negative when the input engine torque is negative and as the torque reversal takes place, the twist angles become positive. The maximum change in twist angles takes place in the engine side twist angle. This is because the backlash has been modeled at the engine side (ref. Figure 2.8) so when the torque reversal takes place, the traversal of backlash also takes place and gets accounted in the engine side twist angle. Once the lash traversal has been completed, the positive torque deflects the shaft and twisting-untwisting take place due to the stiffness and the damping of the propeller shaft. This twisting-untwisting manifest in the form of shuffle oscillations. On the contrary, as the wheel side does not have a backlash element, the wheel side twist angle only represents the twisting and untwisting of the axle shaft.

Figure 3.3 (c) shows the estimates of the engine and the wheel speeds in the engine domain. The shuffle oscillations are significant in the engine speed and less significant in the wheel speed as discussed in the FOM validation section of this work. Finally,

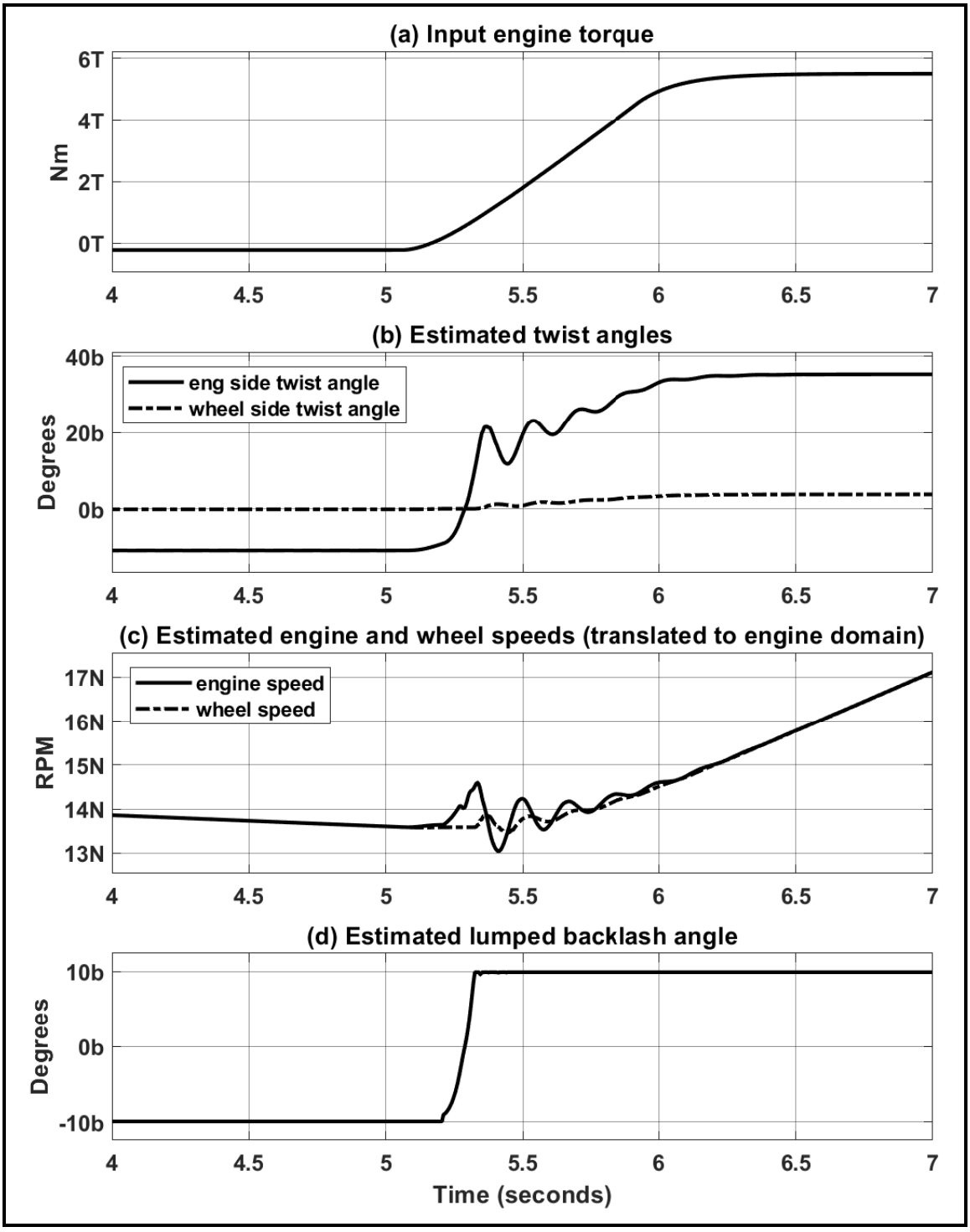

Figure 3.3: DSKSE estimated states

Figure 3.3 (d) shows the estimate of the lumped backlash traversal. It can be seen that the estimated lumped backlash traversal aligns with the twisting of the engine side twist angle.

3.2 Discrete Switched Kalman State Estimator - Validation

The DSKSE designed in the previous section is validated with respect to the FOM which has been discussed in Section. 2.1.3.3.

The DSKSE uses the engine and the wheel speeds as measurements to update the predictions of the model. Thus, the error between the estimated and measured engine and wheel speeds are considered as one of the primary assessment parameters for the DSKSE. Furthermore, one of the major inputs to the torque shaping controller is the backlash position of the driveline. As a result, the comparison of the lumped backlash position of the FOM and the estimated backlash position is also considered as a parameter to assess the performance of the DSKSE. Refer Figure 3.1 to see the interface of the FOM and the DSKSE.

Figure 3.4 shows the comparison of the outputs of the DSKSE and the FOM when the DSKSE is discretized at 10 ms sampling time and the engine and the wheel speeds

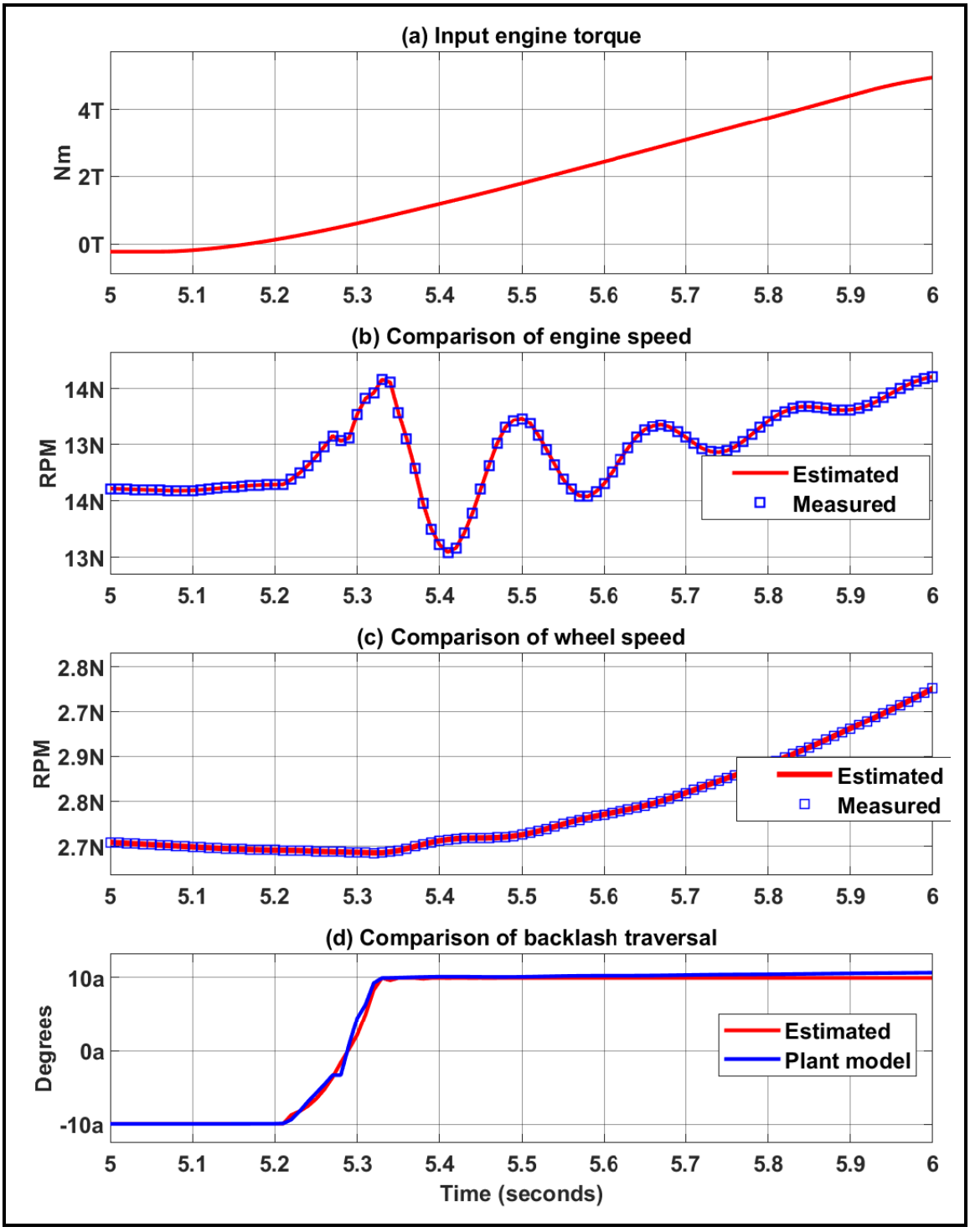

Figure 3.4: Validation of DSKSE with respect to FOM

are also sampled every 10 ms. Figure 3.4 (a) shows the input torque to the DSKSE and the FOM. Figure 3.4 (b) shows the comparison of the estimated engine speed with respect to the measured engine speed input to the estimator (output of the FOM). Similarly, Figure 3.4 (c) shows the comparison of the estimated wheel speed and the measured wheel speed input. It can be seen from Figure 3.4 (b) and (c) that the estimates overlap the measured inputs. Table 3.3 shows the maximum absolute errors in estimation of the engine and the wheel speeds. It can be seen that the errors in the speed estimates are significantly small. Figure 3.4 (d) shows the comparison of the FOM lumped lash traversal with respect to the estimated lash traversal. For the current torque ramp rate, the DSKSE starts to estimate the lash traversal later than the FOM lumped backlash traversal and the lash traversal ends close to the end of lash traversal of the FOM. This can be further seen in Figure 3.5 where the magnified view of the start of backlash traversal for the plant and the estimator are shown. It can be seen that the plant backlash slowly starts to traverse, and it takes the estimator 1-time-step (10 ms) to detect the change in the lash traversal. The error in the lash traversal time is 14.3%, refer Table 3.3, which is significantly higher than the errors in the estimates of the engine and the wheel speeds. The major reasons contributing to the difference in the estimation errors of the speeds and the backlash position are highlighted below:

† As has been discussed in the Section 3.1.2.2 the engine side twist angle and the backlash position in the backlash mode are not updated with the Kalman

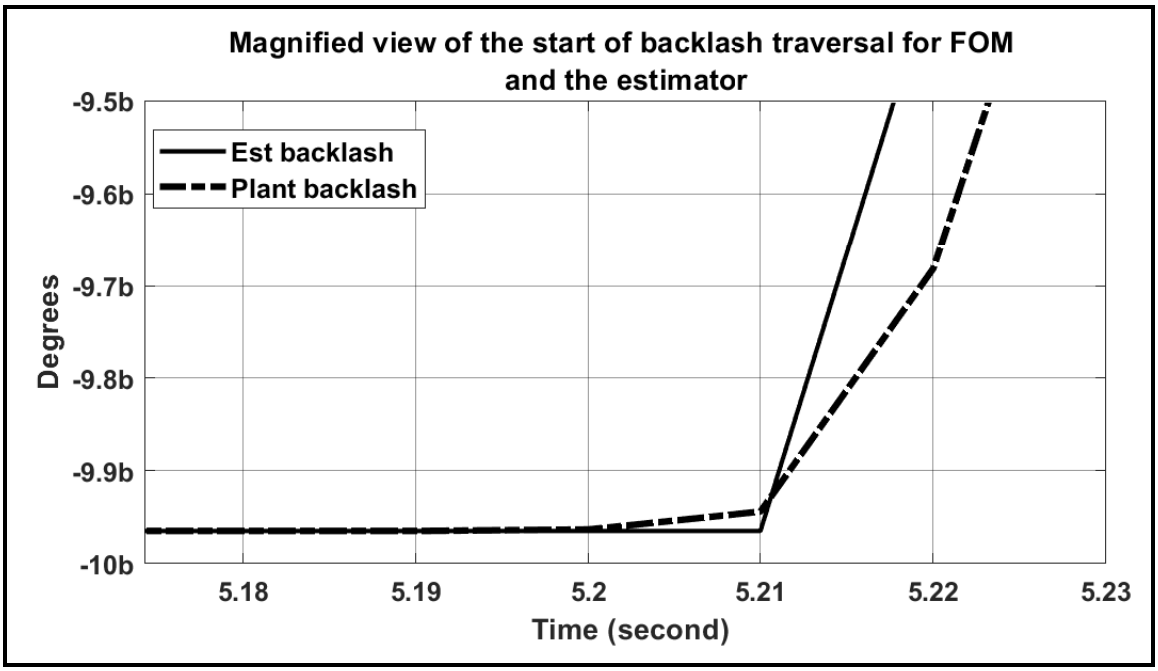

Figure 3.5: Comparison of start of backlash traversal for the FOM and the DSKSE

Table 3.3
Validation of DSKSE with FOM for a sampling time of 10 ms

Description	**Error (%)**
Engine speed estimate	2.50E-08
Wheel speed estimate	1.00E-05
Lash traversal time	14.29

gains based measurement correction and are only calculated using the prediction equations of the system. This limits the capability of the DSKSE to optimally estimate the backlash position leading to increased error as compared to the errors in the engine and the wheel speeds.

† The lash traversal time for the current torque input is 130 ms and the sampling time for the estimator is 10 ms. Even if the estimator takes 1 sample data to

detect the change in backlash position, this will lead to an error in the lash size estimate of approximately 7.5%. Thus, the sampling time of the estimator also affects the error in the estimated backlash position.

† It is important to note that the accuracy of the lash traversal time estimate would keep varying with the change in torque amplitude to which the estimator is subjected to. This is because, as the rate of change of the torque input increases, it reduces the lash traversal time. This would further amplify the effect of sampling time on the error in the estimated lash traversal time.

The current discretization time for the DSKSE and the sampling time for engine and wheel speeds were based on the sponsor organizations feedback of the sampling time for the engine speed and the wheel speed in the current production vehicles. Figure 3.6 shows the state estimates if the DSKSE is discretized at 1 ms and the engine and wheel speed samples are available every 1 ms. Figure 3.7 shows the comparison of the start of lash traversal with a sampling time of 10 ms and 1 ms. It can be seen that with 1ms sampling the DSKSE is able to estimate the start of lash traversal closer to the actual FOM's lash traversal when compared to the output with 10 ms sampling. This is in line with the effect of the sampling time on the percentage error in the lash traversal time estimate.

Table 3.4 shows a quantitative summary of the effect of sampling time on the errors in the estimates. It can be clearly seen that the error in the lash traversal time reduces

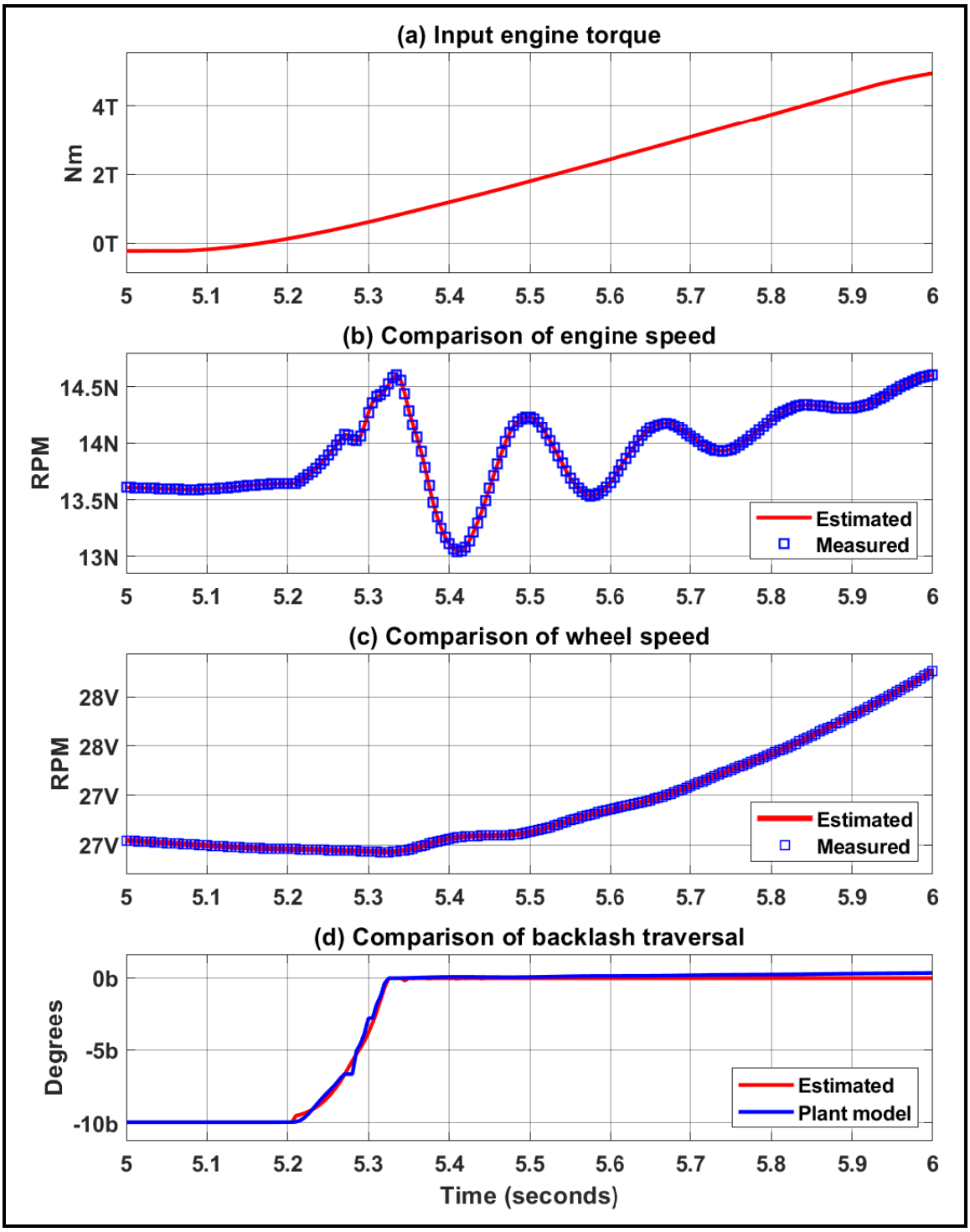

Figure 3.6: Validation of DSKSE with respect to FOM for a sampling time of 1 ms.

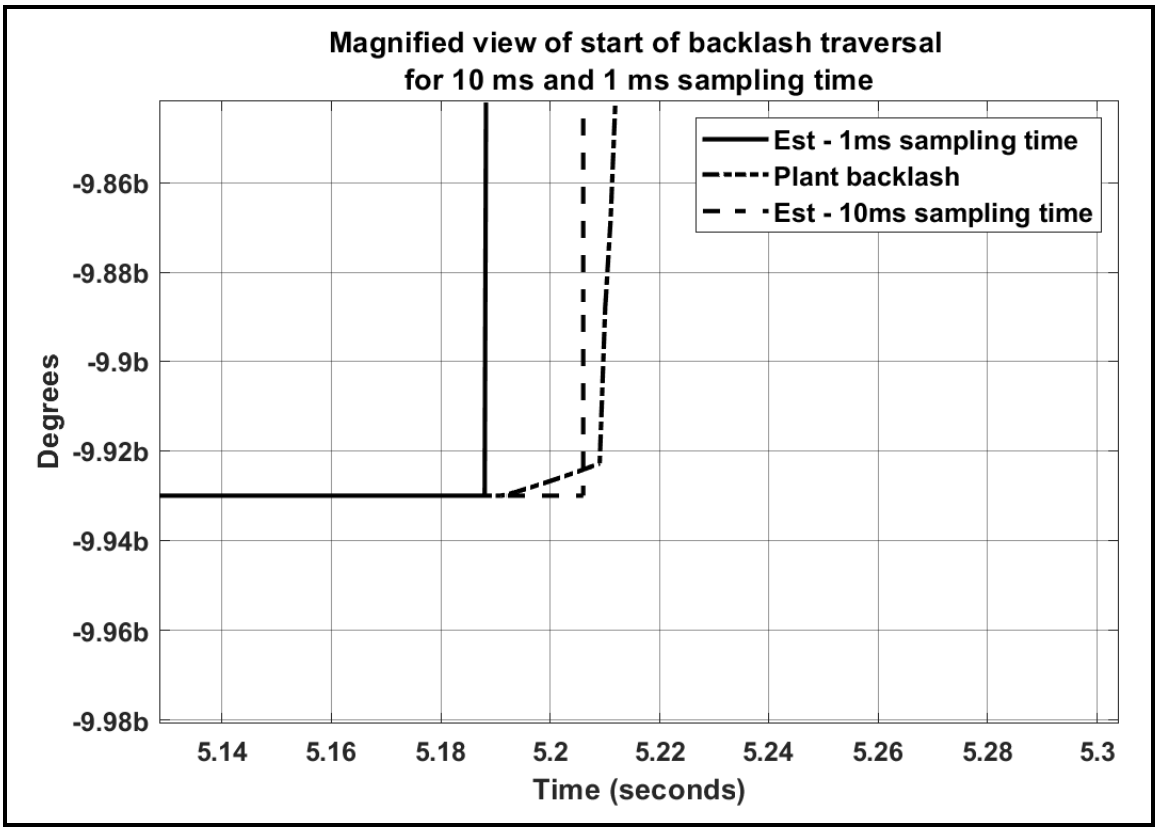

Figure 3.7: Comparison of start of backlash traversal for the FOM and the DSKSE

Table 3.4
Comparison of errors in the estimates with 10 ms and 1 ms sampling discretization times

Description	% Error - 10 ms	% Error - 1 ms
Engine speed estimate	2.50E-08	5.00E-09
Wheel speed estimate	1.00E-05	5.00E-06
Lash traversal time	14.29	5.59

from 14.3% to 5.6% via a change in sampling time from 10 ms to 1 ms.

3.3 Robustness analysis - DSKSE

The validation of the estimator discussed in the previous section has only been done for a fixed torque ramp rate and in an ideal simulation environment. But, the DSKSE should be able to estimate the states of the system for varying input torque rates, torque magnitudes, delays in the measurement inputs and the jitter in the CAN/-clock signals with a considerable amount of accuracy. This section thus discusses the robustness of the DSKSE to all those varying parameters which will lead to the assessment of limitations of the DSKSE.

3.3.1 Robustness to varying step torque inputs

As a first analysis, the robustness of the state estimator to varying magnitude of step input torque is done. These scenarios are representative of very sharp torque transients that can take place in the driveline. Figure 3.8 (a) shows the different step torque inputs to the estimator. These step torque inputs have a first order behavior due to the engine dynamics. Figure 3.8 (b) shows the variation in the lash estimation error with varying magnitudes of step inputs and at different sampling times.

A few important observations that can be made with the results of varying step inputs

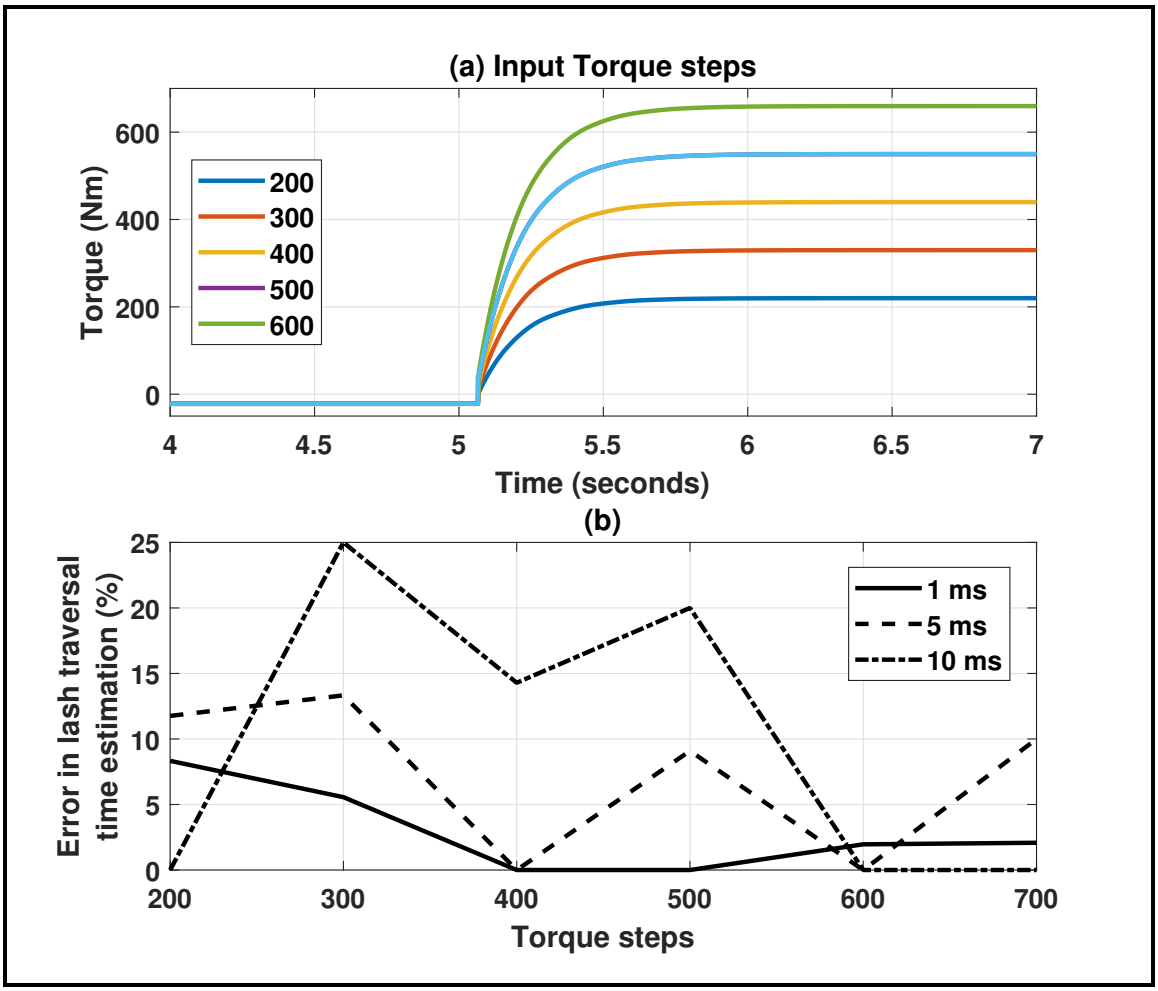

Figure 3.8: Error in the estimation of lash traversal time for different step torque inputs and sampling times

are listed below:

† The error in the lash traversal time estimate decreases with a decrease in sampling time of the engine and the wheel speed measurement inputs and the sampling time of the estimator.

† There is no general trend on the basis of increasing the magnitude of the step

torque inputs with respect to the resulting errors in the lash traversal time estimates.

3.3.2 Robustness to varying torque ramp rates

Figure 3.9 (a) shows the various torque ramp rates that have been used to estimate the backlash traversal. Figure 3.9 (b) shows the variation of the percentage error in the estimated lash traversal time with a change in torque ramp rates for different sampling times. Below are the observations that can be made -

† The DSKSE is sensitive to a very low torque input ramp rate of 200 Nm/s where the maximum error is observed for all sampling times.

† For torque ramp rates with 10 ms sampling time, the estimation errors, in general, increases with an increase in torque ramp rates. This is because, as the torque ramp rate increases the lash traversal time decreases and the impact of each sample time becomes more prominent.

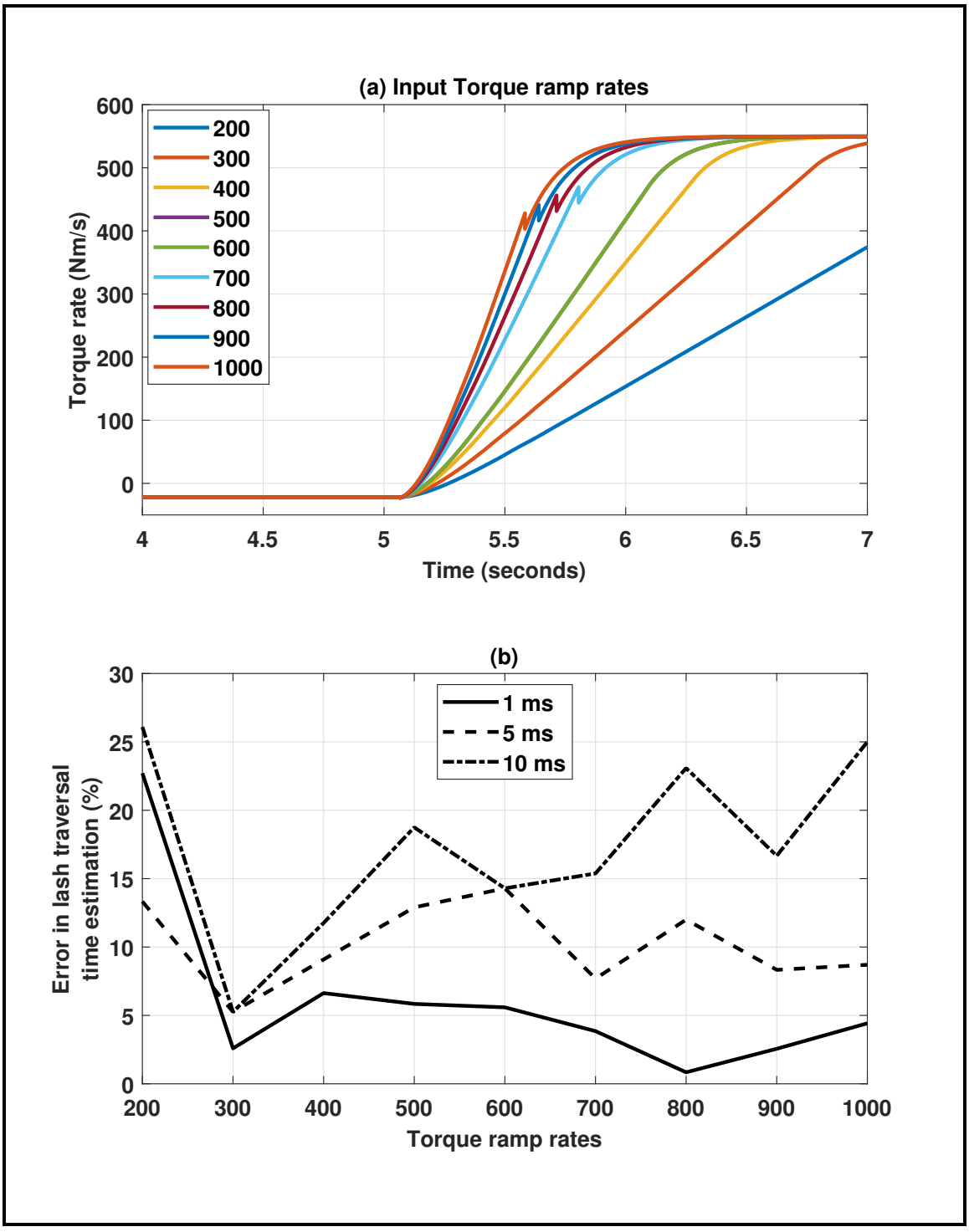

Figure 3.9: Error in the estimation of lash traversal time for different torque ramp rates and sampling speeds

3.3.3 Robustness to constant measurement delay

The DSKSE assumes that the measurements from the plant, i.e. FOM are available a without any delay. But in the vehicle application, the sensor signal needs to be sent to the ECU over CAN which can cause a delay in the signal when it is received by the estimator. Additionally, in case of wheel speed sensors, the speeds are first received by the ABS-ECU and then broadcasted to the powertrain ECU. This can also cause a constant delay in the signal when it is received by the estimator. To simulate this situation, a constant delay was added to the engine speed measurement input and the wheel speed measurement input to understand the effect on the DSKSE's estimates.

3.3.3.1 Effect of constant delay in engine speed

Figure 3.10 shows the comparison of estimates of the DSKSE with and without delay in the engine speed measurement input when sampling time is 10 ms. From 3.10 (b), the delay in the input engine speed can be seen. This causes a delay of 10 ms (1 sample time) in the estimate of start and end time of the lash traversal. This can be seen more clearly in Figure 3.11 were the backlash traversal ends after one sample time.

It is important to note here that the engine speed is one of the signals with the highest

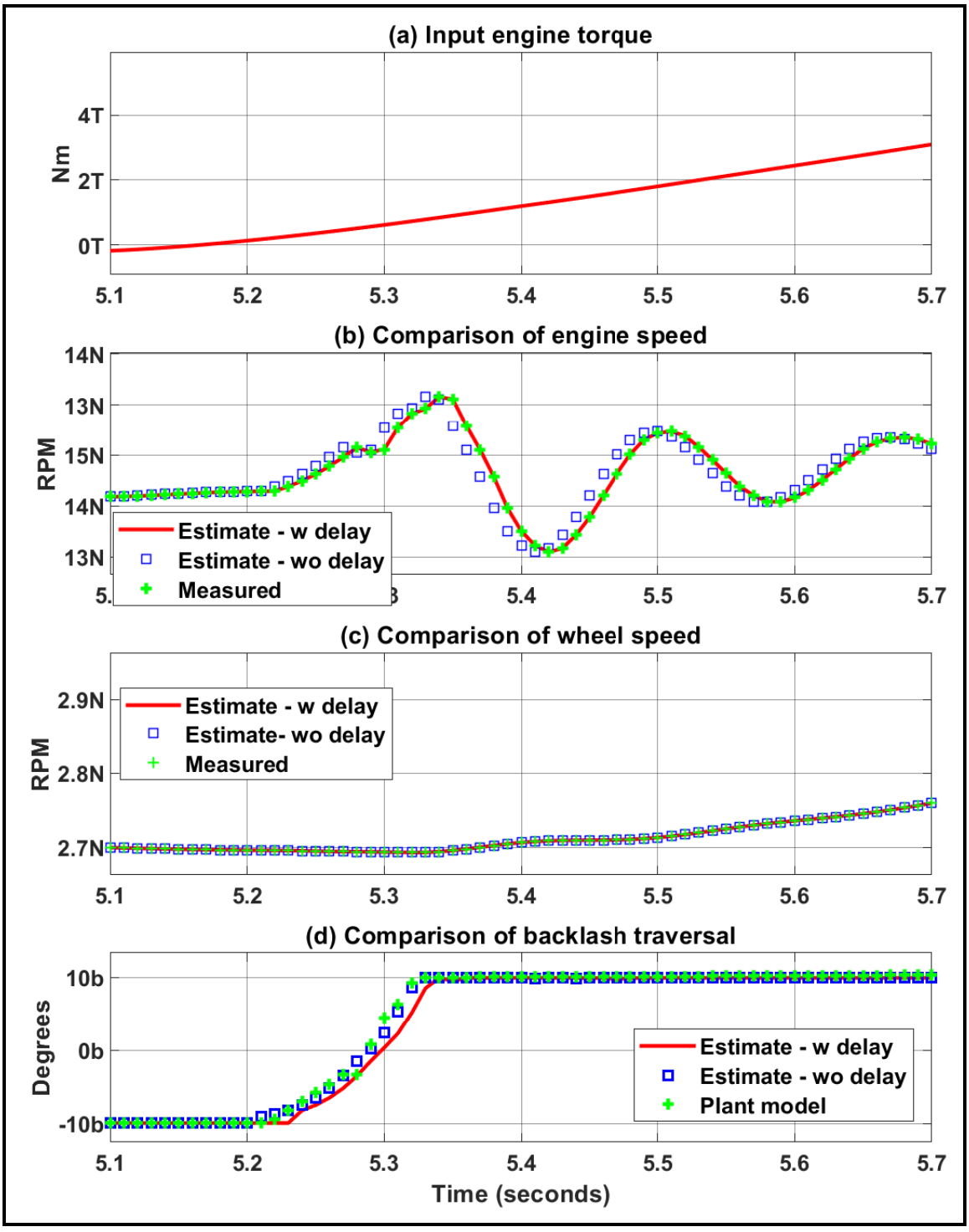

Figure 3.10: Effect of constant delay of 10 ms in engine speed measurement input on backlash position estimate

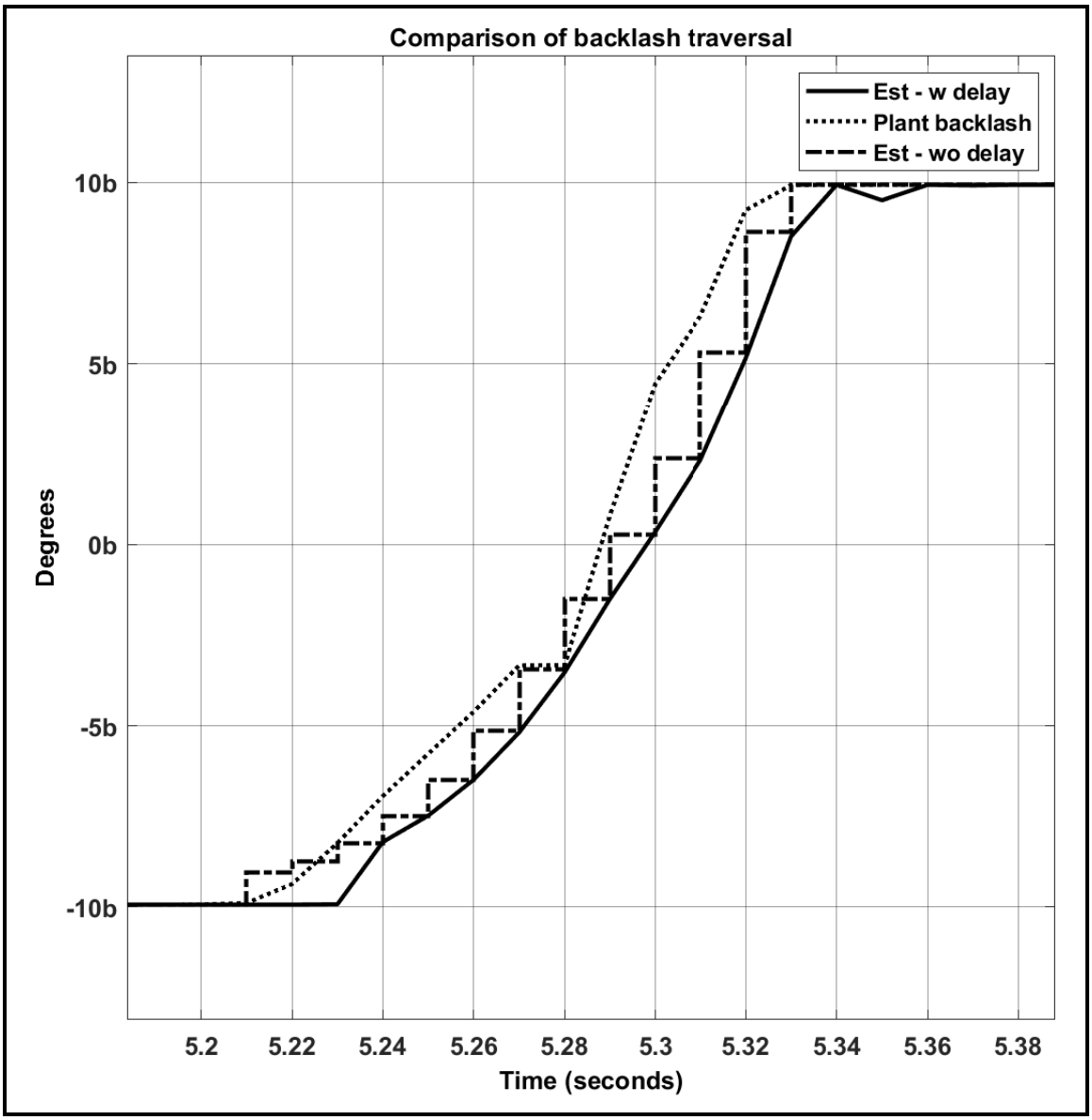

Figure 3.11: Effect of constant delay of 10 ms in engine speed measurement input on backlash position estimate

priority on the CAN bus. Furthermore, the engine speed is directly broadcasted to the Powertrain CAN. Because of these two reasons the constant delay in the engine speed can be assumed to be less than 10 ms.

3.3.3.2 Effect of constant delay in wheel speed

As compared to a constant delay in the engine speed, a constant delay in wheel speed is more likely. One of the major reasons for this is the multiple ECUs involved in the broadcast of wheel speed signals to the powertrain ECU. During a discussion with the sponsor organization, it was suggested that a constant delay of 30 ms is observed in the wheel speeds. Thus, the effect of a constant delay of 30 ms was checked on the estimator. From Figure 3.12 (c), it can be seen that the wheel speed estimate with delay is shifted with respect to the input wheel speed measurement as well as the wheel speed estimate without any delay. Even with this delay, the estimator is able to estimate the position of backlash without any change in traversal time or the traversal start and end time. This can be seen in Figure 3.13 where the backlash position estimate with and without delay has the same lash traversal time as well as the start and the end times.

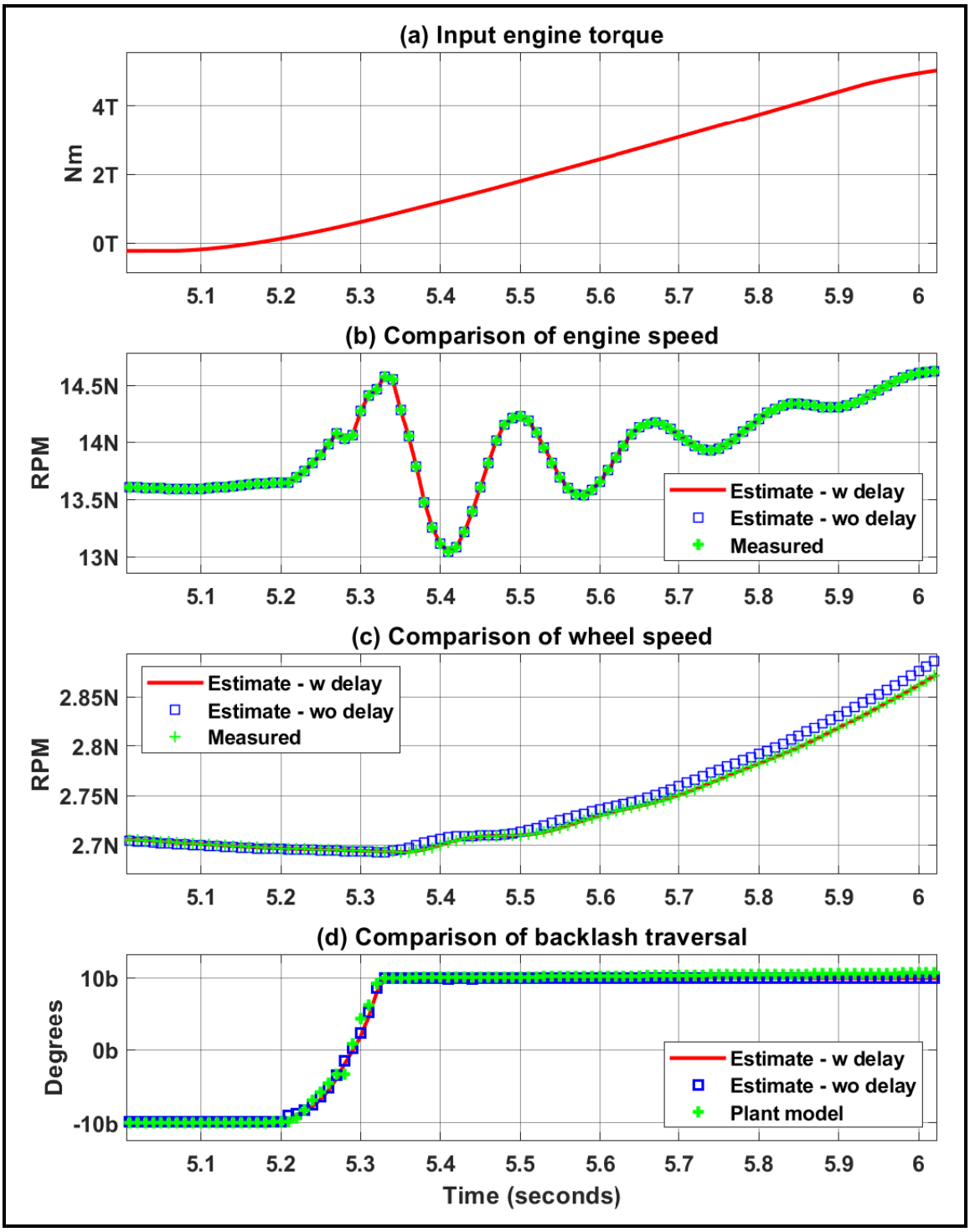

Figure 3.12: Effect of constant delay of 30 ms in wheel speed measurement input on backlash position estimate

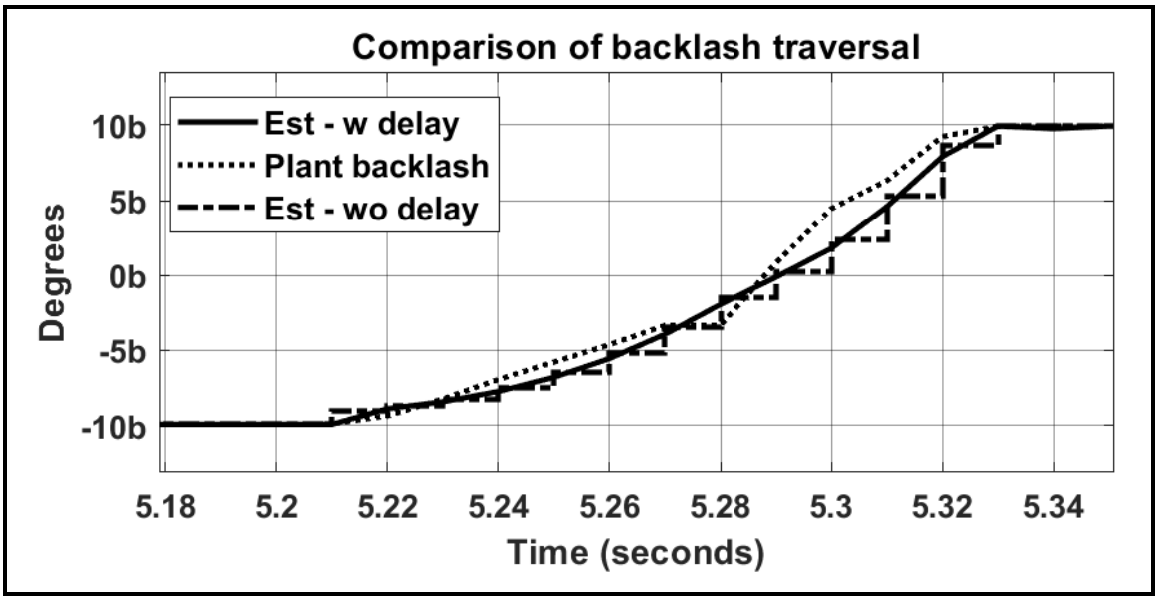

Figure 3.13: Effect of constant delay of 30 ms in wheel speed measurement input on backlash position estimate

3.3.4 Effect of combined delay in engine and wheel speed

The effect of combining the engine and wheel speed delays of 10 ms and 30 ms respectively leads to a delay of 1 sample time in the estimated end of backlash position. This is because the engine speed delay of 10 ms leads to a delay of 1 sample time in the estimated end of backlash position as discussed in Section 3.3.3.1 while the wheel speed delay of 30 ms does not affect the estimated end of backlash position, Section 3.3.3.2.

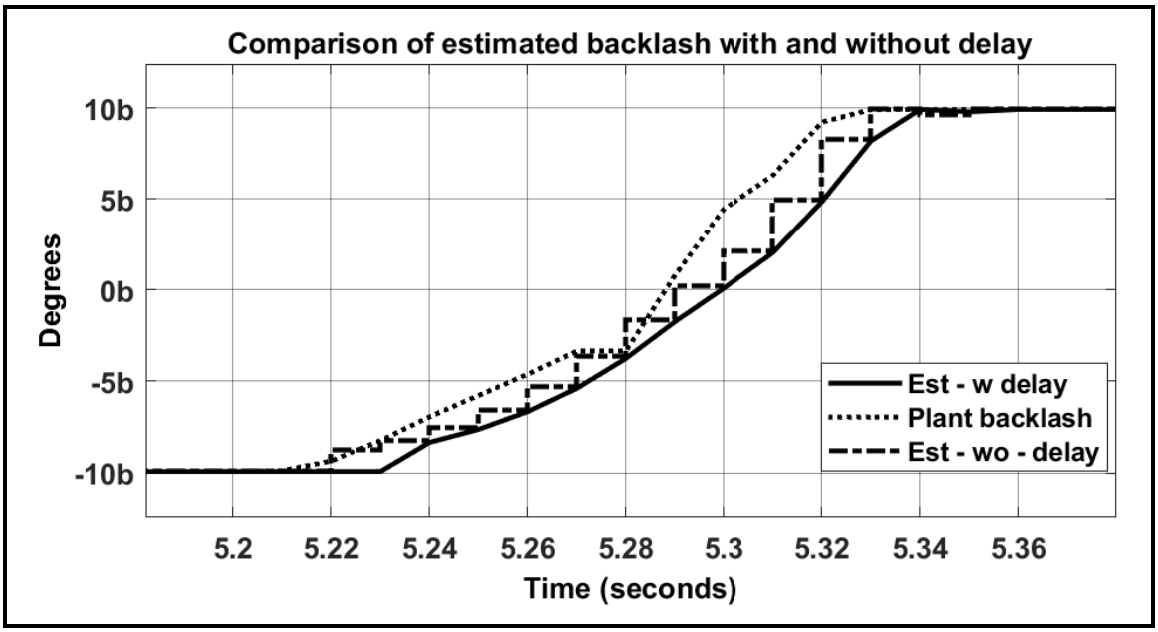

Figure 3.14: Effect of combined constant delay of 10 ms in engine speed and 30 ms in wheel speed measurement inputs on backlash position estimate

3.3.5 Effect of CAN jitter in engine and wheel speed measurements

To collect more data on the actual vehicle's behavior during tip-in and tip-out scenarios, the sponsor organization had shared a production vehicle with Michigan Tech. This was done so that the hardware team at MTU can instrument the vehicle and perform different tests to quantify clunk and shuffle. From the measurements taken by the hardware team, when the measurements of engine and wheel speeds of the vehicle were analyzed, it was found that the CAN updates in the engine and wheel

speeds had variations with respect to the ideal sampling time. This implies that the updates in speeds arrived in advance to or delayed with respect to the ideal sampling time. The distribution of this variation of the measurement updates in engine and the wheel speeds are plotted in Figure 3.15 and 3.16 respectively. Since the current DSKSE validation was carried out assuming that the measured data updates were received as per the ideal sampling time, the effect of this jitter in measurement updates and on the performance of the DSKSE needs to be checked and is discussed in this section of the robustness analysis.

Figures 3.15 and 3.16 (a), (b) and (c) represent the different measurement data sets taken by the hardware team. These data sets are named as "Data set 2", "Data set 3" and "Data set 4". The name "Data set 1" is used for the ideal sampling time data i.e. "No delay". This naming convention is used for both the engine and the wheel speeds. The positive values of time on the x-axis of this plot represent the delay in the update of the new measured sample data with respect to ideal time, while the negative values represent that the data are received in advance of the ideal sampling time. The "Measured data" bars on the histogram represent the distribution of the jitter in the measured data. It can be seen that the distribution of the jitter for all 3 data sets are different and are not normally distributed. As a result, a "Kernel Probability Density Function" was calculated and plotted for each of the measured data set. This kernel probability density function was used to generate jitter data that can be injected into the FOM outputs, of engine and wheel speeds, to understand the

performance of the DSKSE. This is represented as the "Generated data" bars on the histogram. The subplot (d) of 3.15 and 3.16 shows the comparison of the probability density functions of different data sets.

From Figures 3.15 and 3.16 it can be seen that the maximum amplitude of the jitter in engine and wheel speeds are 5ms. The Simulink®- AMESIM® plant model is operating in the continuous domain, thus the output engine and wheel speeds are also in the continuous domain. In order to analyze the response of the DSKSE to the engine and wheel speed CAN jitter for a sampling time of 10 ms, the measured engine and wheel speeds were sampled twice. From Figure 3.17 it can be seen that the continuous speed outputs of the plant are sampled first at 1ms. This makes it possible to add subtle variations due to the CAN jitter. After the jitter has been added to the measurements, they are sampled again at various sampling times (10 ms, 5 ms, and 1 ms) to assess the performance of the controller at those sampling times.

Figures 3.18 and 3.19 shows the results of delay in the estimation of lash traversal when the DSKSE is subjected to the jitter in the engine and the wheel speeds. The major observations from the plots are discussed below:

† For sampling time of 10 ms, there is no delay in the estimated lash traversal time. This can be explained by the fact that the maximum delay in the jitter

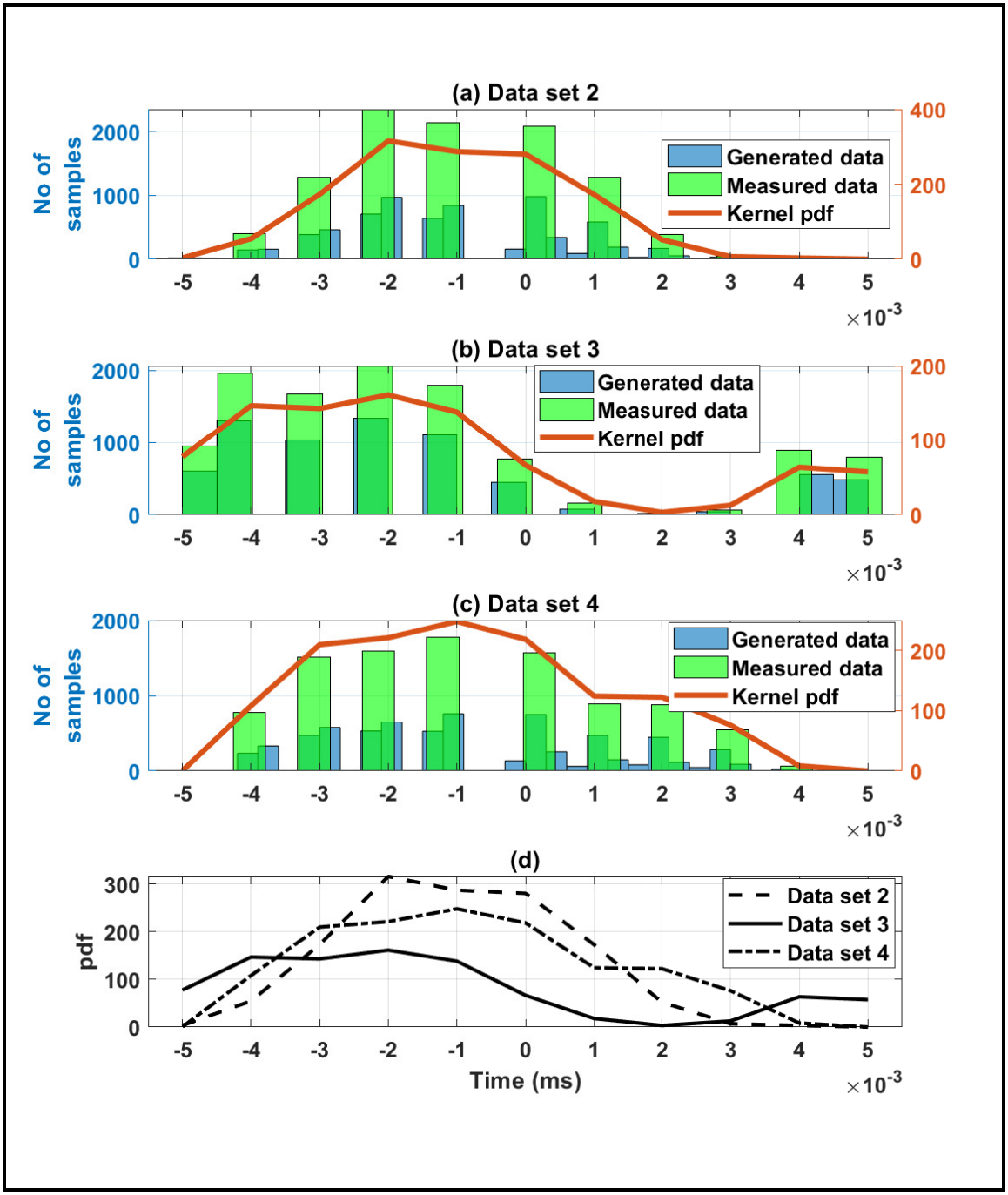

Figure 3.15: Distribution of CAN jitter in engine speed for different measured data set

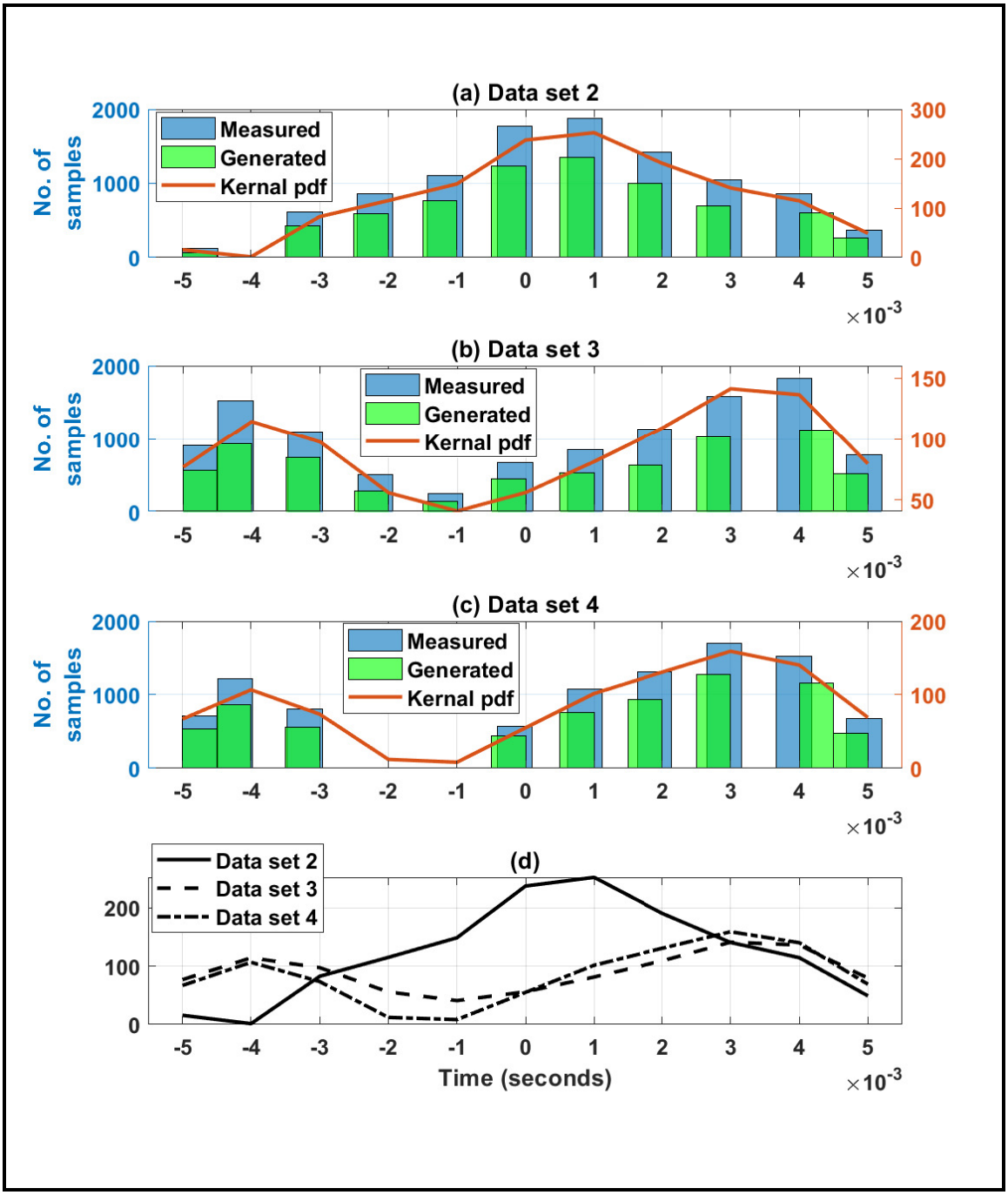

Figure 3.16: Distribution of CAN jitter in wheel speed for different measured data set

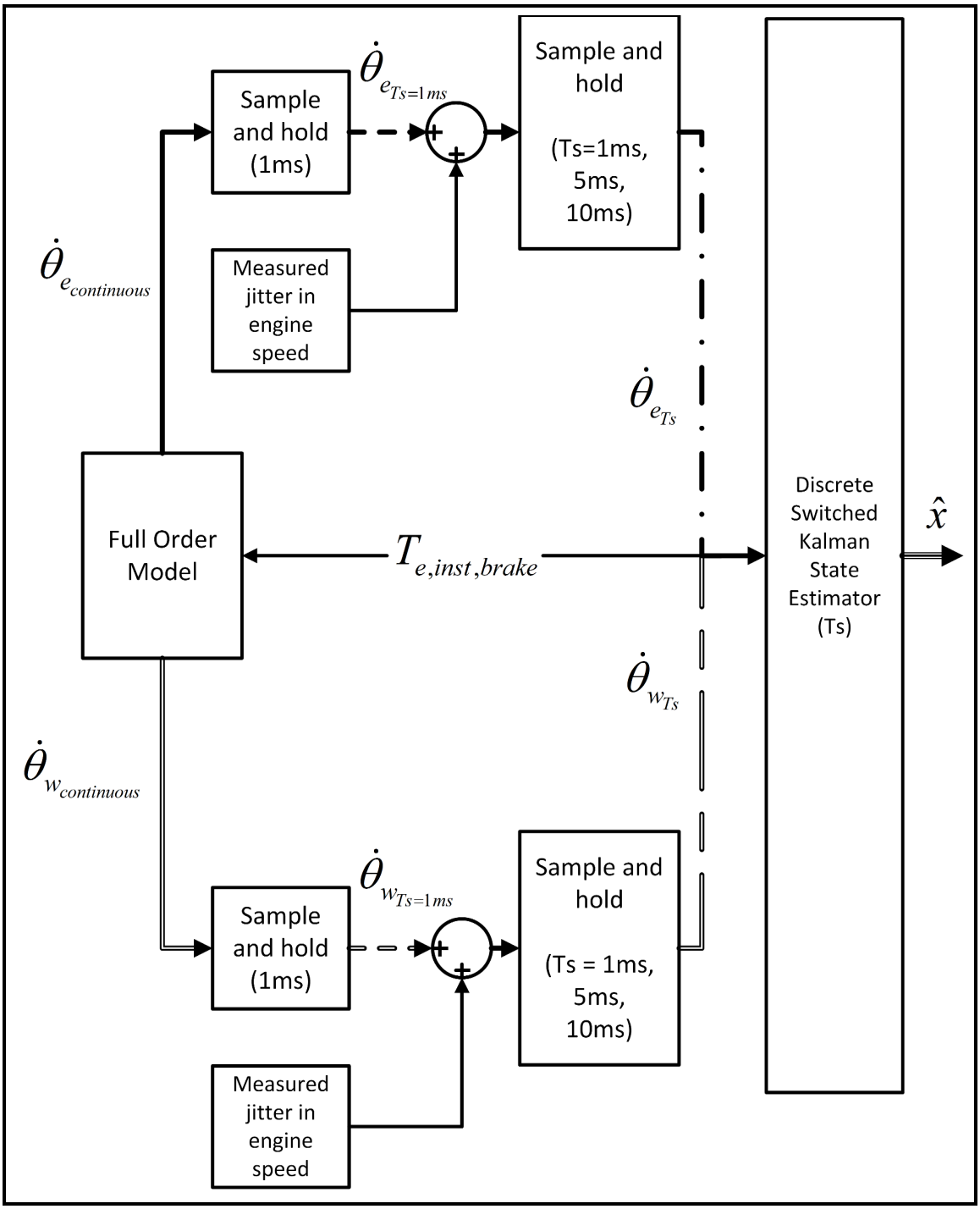

Figure 3.17: Layout for implementing CAN jitter in engine and wheel speeds

is of the order 5ms. With this delay and 10 ms sampling of engine and wheel speeds, the effect of delay would average out significantly over the simulation duration. Furthermore, the effect of 5ms delay on lash traversal would be maximum if it is encountered during the lash traversal, which can vary because of the probabilistic nature of the distribution.

† The data set 3 of the engine jitter has a bi-modol distribution with one peak around 5 ms, Figure 3.15. For sampling speed of 5 ms and 1 ms, this distribution causes a delay of 1 sample time, i.e. 5 ms and 1 ms respectively with all wheel jitter data sets.

† With wheel data set 4, 1 sample time delay (5 ms) is found for with and without the engine jitter, Figure 3.19 for DSKSE's sampling time of 5 ms. A closer inspection of the Figure 3.16 reveals that although the nature of distribution for data set 3 and 4 are similar, the number of samples in case of data set 4, with delay around 4-5 ms, are more than that in case of data set 3. This can also be seen in Figure 3.16 (d) where the area under the curve for data set 4 is more than that for data set 3 for the positive side of the delays.

To summarize, DSKSE with 10 ms sampling time is not able to identify the change in the engine and wheel speed signals because of the jitter, while the DSKSE with 5 ms sampling time is very sensitive to the jitter in engine and wheel speed and the DSKSE with 1 ms is most robust to the engine and wheel CAN jitters.

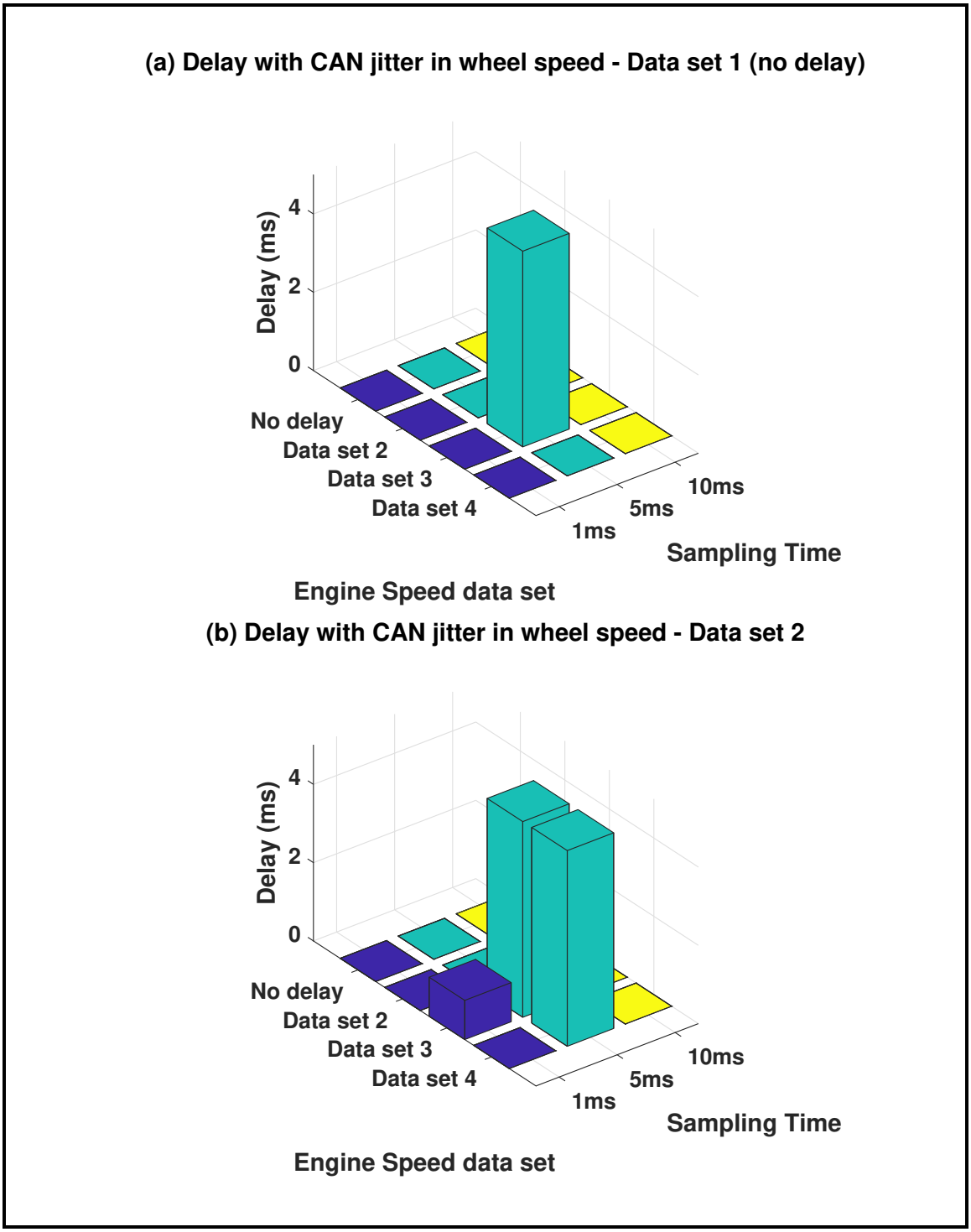

Figure 3.18: Effect of CAN jitter in engine and wheel speed - I

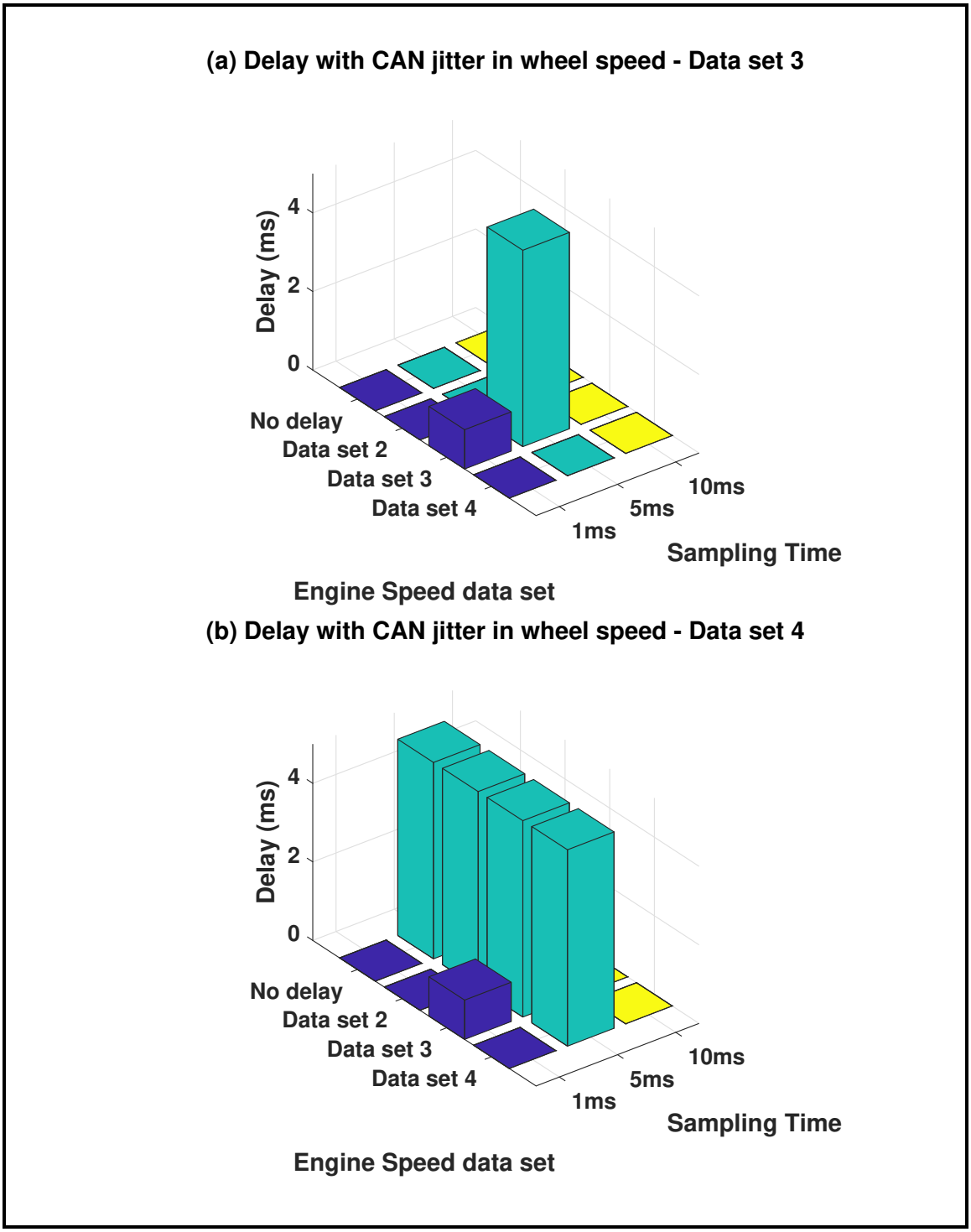

Figure 3.19: Effect of CAN jitter in engine and wheel speed - II

3.3.6 Effect of sampling time

Figure 3.20 shows a box plot of errors in the lash traversal time for various torque inputs (step as well as a ramp) to the DSKSE. The observations that can be made with the help of this figure are -

† With the decrease in the sampling time and estimator's time of discretization, the error in the lash traversal time (mean and mode) decreases.

† For a sampling time of 10ms, the distribution of the error in lash traversal is wide as compared to that with 5 ms and 1 ms.

† The average and the mode error in the lash traversal time estimation with 10 ms sampling time is around 15%.

† With 5 ms sampling time, the maximum error in lash traversal time estimate is less than the average or the mode error with 10 ms sampling time. Thus, 5 ms sampling time provides a significant improvement in the estimates. Furthermore, with 5 ms sampling time, the average and the mode of error in lash traversal time estimation is about 9%.

† A sampling time of 1 ms provides the best result in the lash traversal time estimation with maximum error being 8% and mode around 4%.

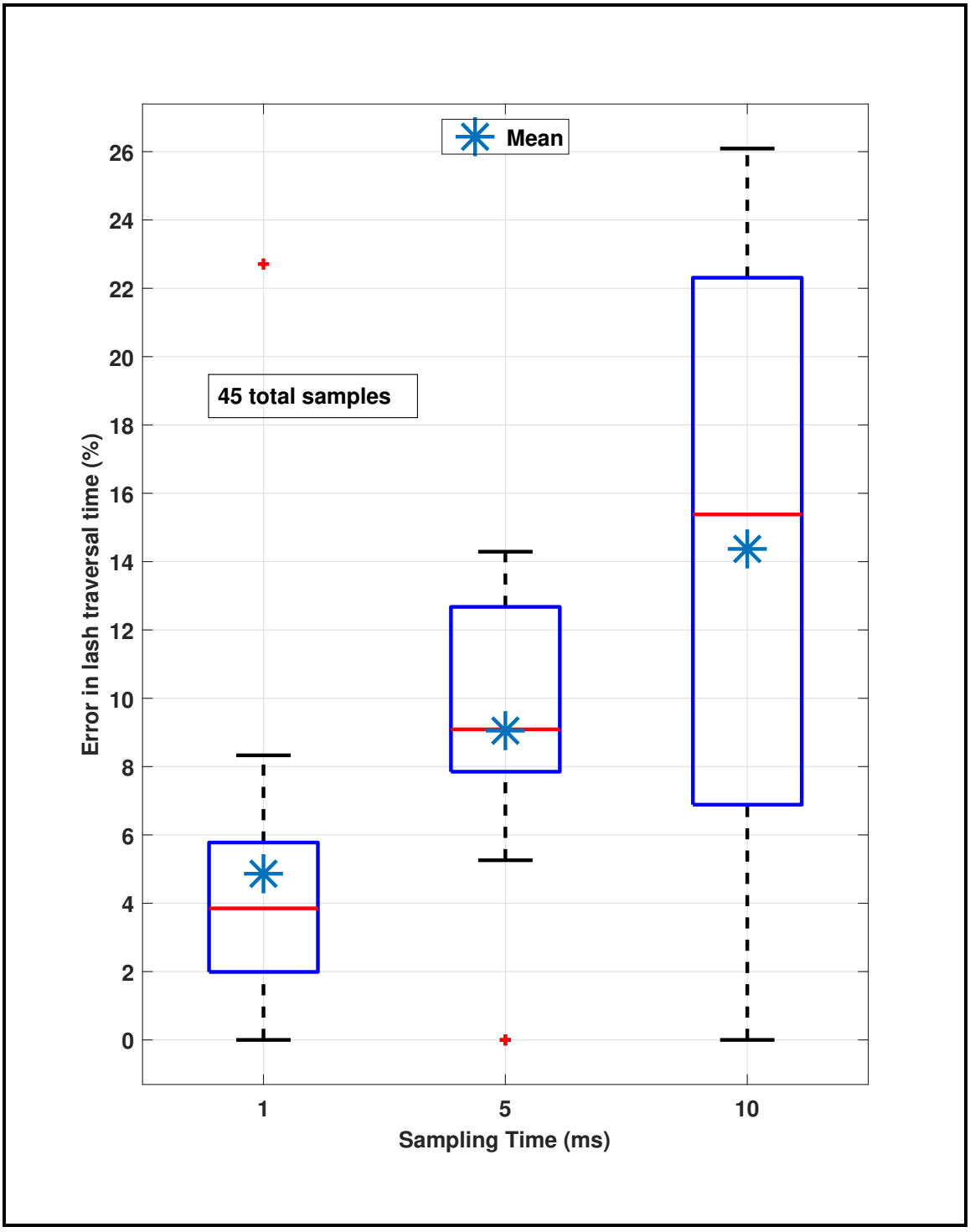

Figure 3.20: Box plot for error in lash traversal time with sampling time

† As the sampling time and the estimator's discretization time decreases, the range of error in the lash traversal time also decreases, barring an outlier for the 1 ms sampling time at 23%

Along with the effect of estimator's discretization time and sensor's sampling time on the accuracy of lash traversal time, other factors also need to be taken into account to decide the sampling time for the estimator. This includes the hardware to be used in the actual vehicle as well as the design of the controller. For instance, if the controller is robust to errors in lash estimation time then a larger sampling time can be used with less cost of the hardware.

To summarize, table 3.5 shows the various robustness analysis done for the backlash state estimator. All these robustness assessments provide an effective data summary of the performance and limitations of the estimator and finishes the development of the Discrete Switched Kalman State estimator.

Table 3.5
Summary of Discrete Switched Kalman State Estimator robustness analysis

Description	Status
Effect of varying torque step inputs	✓
Effect of varying torque ramp rates	✓
Effect of constant delay	
- Engine speed	✓
- Wheel speed	
- Combined engine and wheel speed	
Effect of CAN jitter in	
- Engine speed	✓
- Wheel speed	
- Combined engine and wheel speed	
Effect of sampling time	✓

This finishes the Discrete Switched Kalman State Estimator's model development, validation and robustness analysis.

3.4 Sensitivity analysis for DSKSE

3.4.1 Sensitivity to varying estimator model parameters

The parameters of the model that have been used to estimate the states of the driveline during tip-in and tip-out events can change due to (i) the part to part variation of the components of the driveline and (ii) the usage of the vehicle. For example, the mass of the vehicle varies with the number of passengers sitting in the vehicle as well as based on the luggage in the vehicle. Thus, the parameters of the model are varied to evaluate the performance of the estimator. The parameters that have been changed are listed below:

† Mass of the vehicle (M)

† Engine lumped inertia (J_1)

† Propeller shaft lumped stiffness (k_s)

† Wheel lumped stiffness (k_w)

† Propeller shaft lumped damping (c_s)

† Wheel lumped damping (c_w)

† Wheel lumped inertia (J_3)

These parameters are increased by 1.2, 1.3, and 1.5 times the baseline parameters and the error in lash traversal time as well as the delay in the start of lash traversal with respect to the baseline estimator outputs are shown in Figure 3.21 and Figure 3.22 respectively. An assumption has been made to consider a deviation of 1% in estimated value of lash, to be acceptable. This assumption is made to ignore very small value of error in the estimated backlash. The observations from the variation of error in lash traversal time in Figure 3.21 are discussed below:

† It is evident from Figure 3.21 (a), (b), and (c) for different increase in the values of baseline parameters that the estimator is most sensitive to the lumped propeller shaft stiffness. The error in the lash traversal is up to 40% for the three cases which occurs at 500 Nm/s of input torque ramp rate.

† The second most sensitive parameter is the mass of the vehicle with error ranging up to 18% in cases for torque ramp rates more than 500 Nm/s.

† For other parameters the error in lash traversal time is less than 10% even with an increase of up to 30% from the baseline value of the parameter.

† For wheel lumped stiffness and the wheel lumped damping, with an increase of 50% from the baseline values, the error increases to 18% as compared to 9% for 30% increase in the value from baseline values.

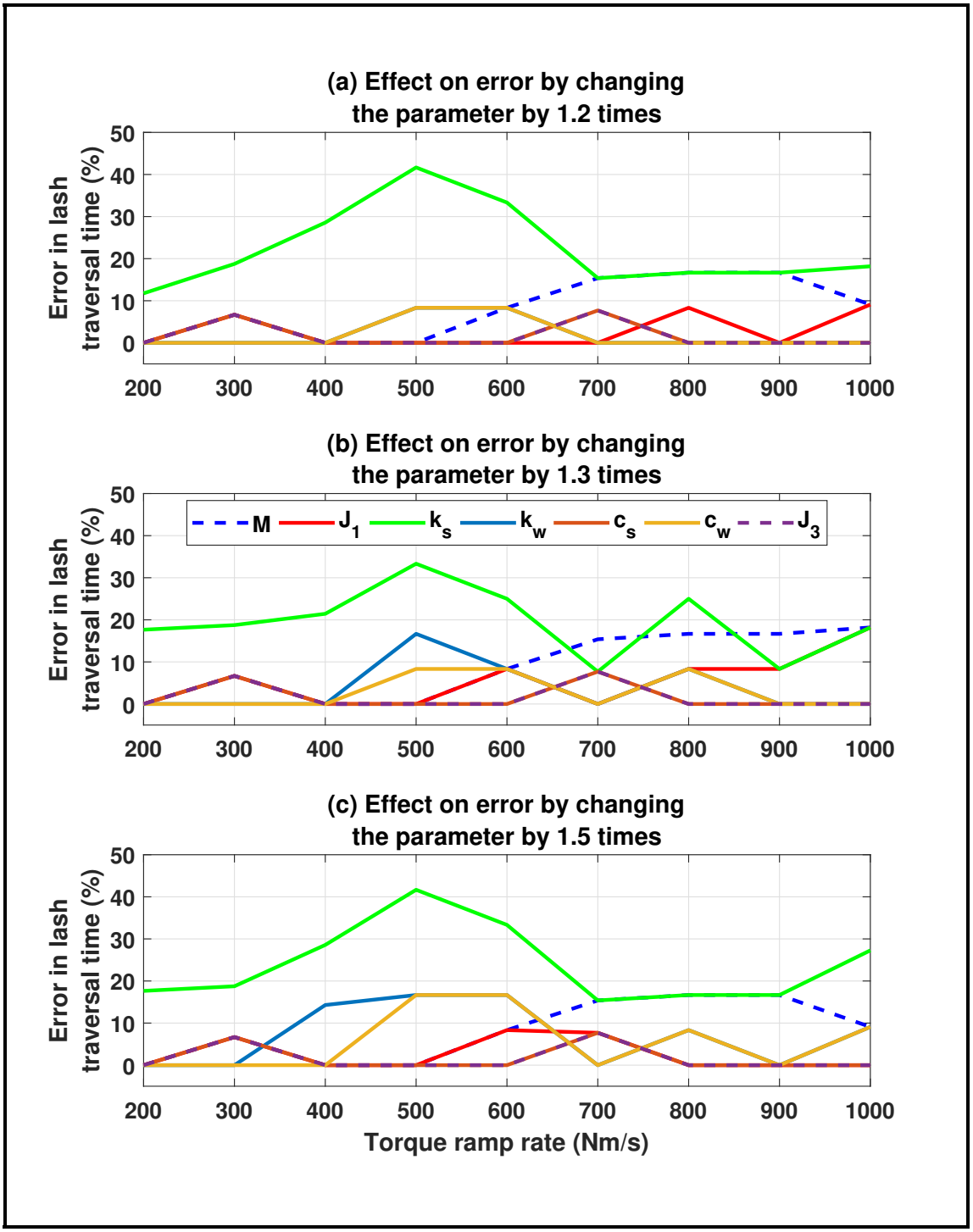

Figure 3.21: Plot showing the variation of error in lash traversal time with changing the estimator baseline parameters by 1.2, 1.3, and 1.5 times on the error for different input torque ramp rates at 10 ms sampling time

It was observed that the end of lash traversal time was same for all the scenarios, thus the error in the lash traversal time is because of the error in the start of lash traversal. This is shown in Figure 3.22 for varying different parameters of the estimator. The additional information Figure 3.22 provides with respect to observations made from the results of Figure 3.21 is, whether the lash traversal time increases or decreases when a particular parameter is changed. A positive value of delay suggests that the lash traversal time increases, while a negative value of delay suggests that the lash traversal time decreases. Thus, increasing the propeller shaft stiffness and mass of the vehicle increases the lash traversal time. This can be seen in Figure 3.23 which shows the comparison of estimated backlash position with baseline and 50% increased lumped propeller shaft stiffness. It can be seen for the torque ramp rates such as 200 Nm/s and 300 Nm/s that the estimated backlash position with modified propeller shaft stiffness slowly starts to traverse before the estimated backlash with ideal (baseline) propeller shaft stiffness. This causes the increase in error of the lash traversal time with changing the stiffness of the propeller shaft.

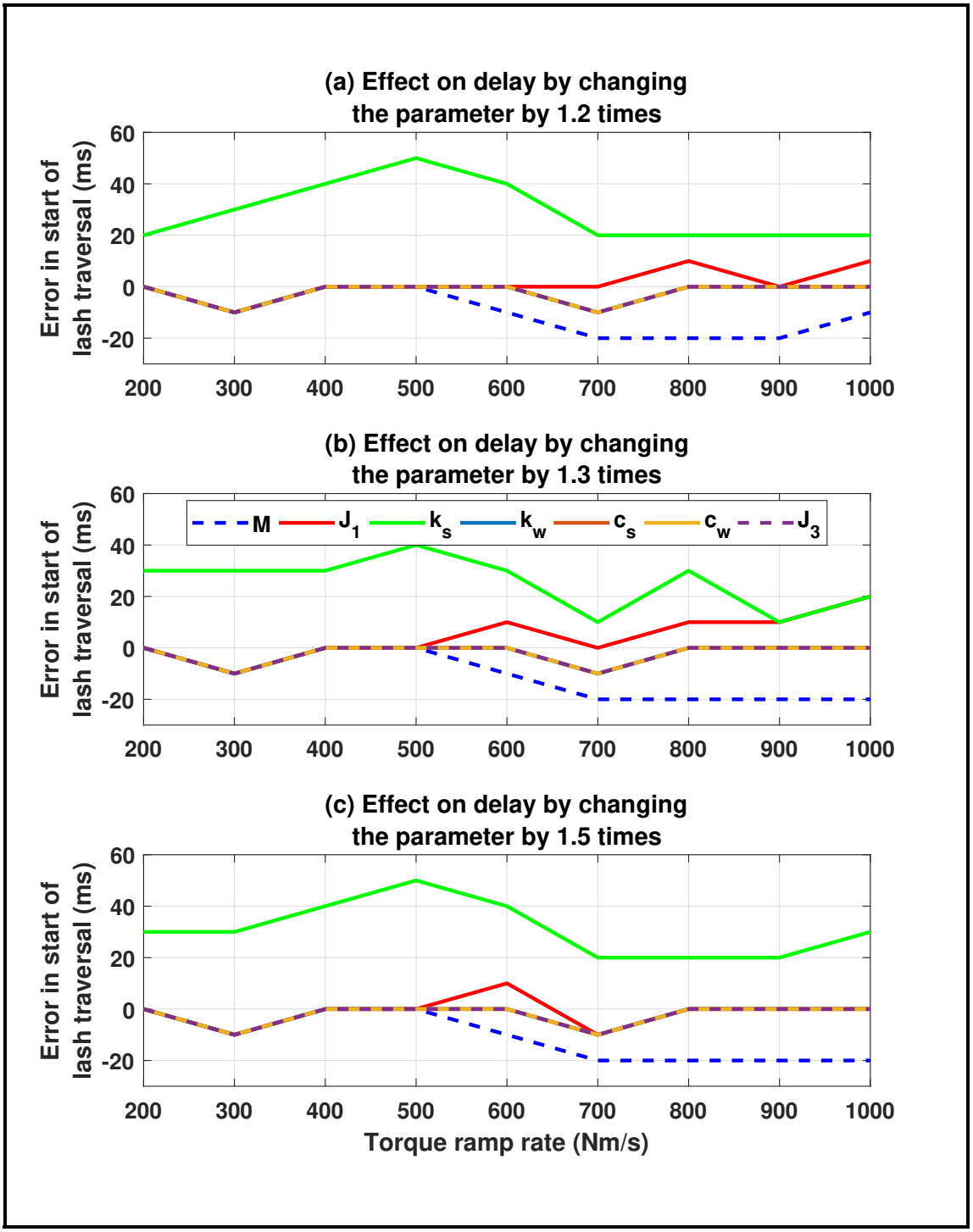

Figure 3.22: Plot showing the variation of error in start of lash traversal with changing estimator baseline parameters by 1.2, 1.3, and 1.5 times on the error for different input torque ramp rates at 10 ms sampling time

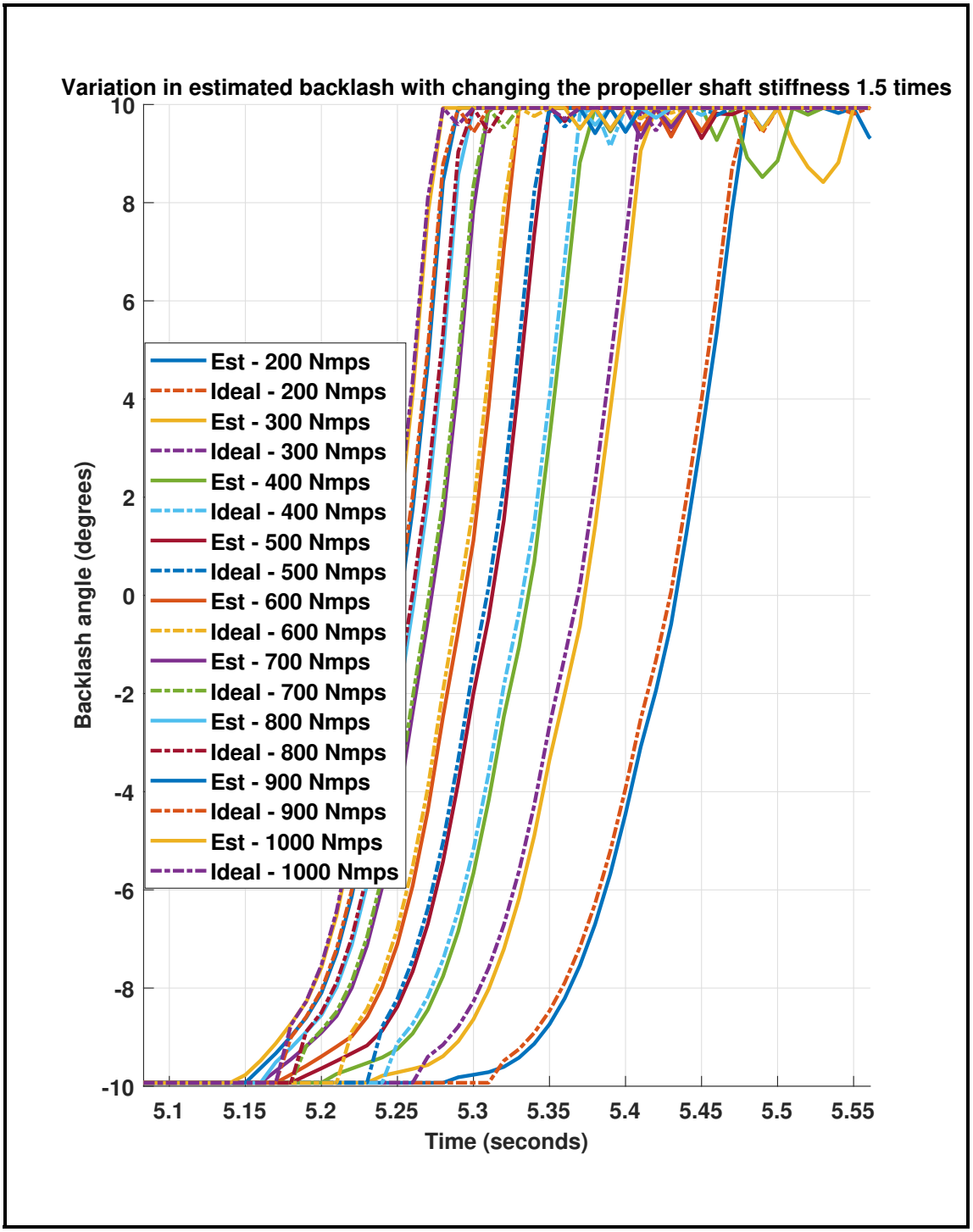

Figure 3.23: Comparison of estimated backlash traversal with baseline and 50% increased propeller shaft lumped stiffness for different input torque ramp rates at 10 ms sampling time

3.4.2 Sensitivity to different operating gear

To understand the performance of DSKSE to operating gear other than 5^{th}, an analysis was carried out in 6^{th} gear and result is shown in Figure 3.24. It can seen that the start and end of lash traversal for different ramp rate are similar to the simulated via the full order plant model. The modifications made to the estimator to adapt to 6^{th} condition are:

† The lumped engine inertia is changed (J_1) as it consists of the engine as well as the transmission inertia.

† The transmission gear ratio (i_{tr}) is changed to a value of 6^{th} gear.

† As the value of lumped backlash is dependent on the transmission gear ratio, the backlash angle was also modified.

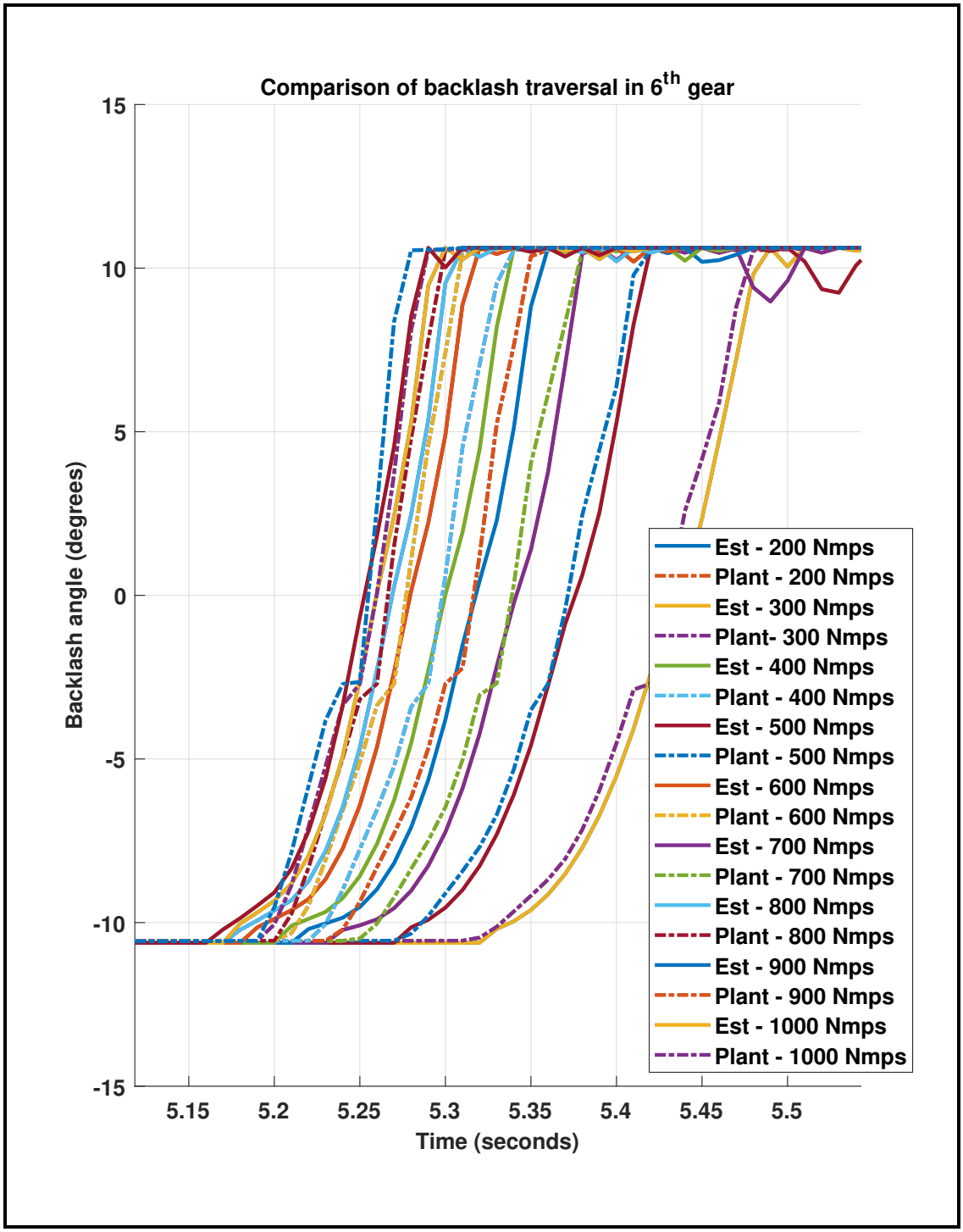

Figure 3.24: Comparison of estimated backlash traversal with plant backlash traversal in 6^{th} at 10 ms sampling time for different input torque ramp rates

Chapter 4

Backlash Size Estimator

The previous chapter discussed the estimation of backlash position when the size of the backlash is known. As discussed, the backlash size of the driveline is cumulative of individual backlashes distributed at various gear and spline mesh interfaces. Over the life the vehicle, there will be plastic deformation of the components of the driveline due to various loads the driveline is subjected to. This include the deformation of the gear and the spline geometries which will increase the size of the backlash over the life of the vehicle. In this scenario, where the backlash size is increased, if the backlash position estimator (DSKSE) estimates the position of backlash on the basis of an old value of the lash size, it can significantly hamper the performance of the anti-jerk controller. Thus, in order to have a sustained performance of the anti-jerk controller over the life of the vehicle, it is necessary that the size of the backlash can also be

estimated. This estimated lash size will update the lash size used by the DSKSE, ensuring that the backlash position estimate from the DSKSE to the controller is representative of the vehicle lash size.

This chapter discusses the development of a backlash size estimator using the state space model of the driveline model that has been developed for this work (refer Section 3.1.1.2). Post the development of the size estimator, the validation of the size estimator is discussed along with its capability to estimate the size of backlash for varying plant backlash sizes. Finally, this chapter discusses the robustness analysis of the developed size estimator to various scenarios.

4.1 Estimator model development

The size estimator development section of this chapter is subdivided into three sections. The first section discusses the rationale that has been used to develop the size estimator. The second section discusses the Kalman filter estimator approach and the layout of the estimator used to estimate the backlash size. The third section discusses the results of the size estimator and the final section discusses the modification that has been made to the representation of estimated lash size.

4.1.1 P for size estimator

Let the vehicle driveline be represented by only the contact mode dynamics of the driveline (Equations 3.13, 3.16 and 3.17) and let a Kalman filter is designed to estimate the states of the driveline with only contact mode dynamics. Now if the driveline is in contact mode, i.e. no change in the position of the lash, the lash estimate using contact mode dynamics should not change. But if the driveline is traversing through the lash, i.e. backlash mode, the estimator will accumulate some error in the lash position and would start estimating the lash angle. Finally, when the driveline has reached contact mode again, there will be no further change in the lash angle estimate and a steady offset in the lash angle would be achieved. This steady value will be the size of the driveline backlash.

4.1.2 Kalman backlash size estimator

Based on the rationale discussed in Section 4.1.1, a Triggered Kalman Backlash Size Estimator is designed (TKBSE) to estimate the size of the backlash while the driveline traverses from the negative contact to positive contact. The trigger to estimate the size of backlash is based on the commanded torque value by the engine ($T_{e,inst,brake}$).

If the engine commanded torque is greater than zero and the change in engine commanded torque is more than a small calibration value (6 Nm/s), this implies that the driveline is being forced to traverse backlash and achieve positive contact. This scenario provides important information to the estimator to estimate the backlash size.

Based on the above discussion, modified state variables for the size estimator can be given by:

$$\hat{\mathbf{x}} = \begin{bmatrix} \frac{\hat{\theta}_e}{i_{tr}} - \hat{\theta}_{fdr} i_{fdr} & \hat{\dot{\theta}}_e & \hat{\theta}_{fdr} - \hat{\theta}_w & \hat{\dot{\theta}}_{fdr} & \hat{\dot{\theta}}_w & 2\hat{\alpha} \end{bmatrix} \tag{4.1}$$

Here $2\hat{\alpha}$ represents the backlash size estimate. The **A**, **B** and **C** matrices for the size estimator are given by Equation 3.13, Equation 3.16 and Equation 3.17 respectively. If the Kalman gain is given by K_{cm}, then the estimates can be given by:

$$\hat{\dot{\mathbf{x}}} = \mathbf{A}_{cm}\hat{\mathbf{x}} + \mathbf{B}_{cm}\mathbf{u} + \mathbf{K}_{cm}[\mathbf{Z} - \mathbf{C}_{cm}\hat{\mathbf{x}}] \tag{4.2}$$

where, **Z** represents the measurement inputs to the Kalman estimator.

Fixed Kalman gains were calculated for the above state space model using a process noise co-variance (**Q**), a measurement noise co-variance (**R**) in Matlab®. The values of the measurement noise co-variance have been kept the same as the one used in the DSKSE as they depend on the accuracy of the sensors used to measure the engine and the wheel speeds. The process noise co-variance matrix was used as a calibration

to reduce the error between the estimated and actual backlash size.

Figure 4.1 shows the layout of TKBSE. A torque command, $T_{e,inst,brake}$ is sent to the vehicle model and the TKBSE. The resulting engine and wheel speeds from the vehicle model are sent to the estimator through a sample and hold block to discretize the continuous plant outputs. The vehicle road load is also calculated based on the measured wheel speed and sent to the TKBSE as an input. The torque command to the TKBSE is also sent to the trigger block. This block checks if the derivative of the torque is more than a calibration value (6 Nm/s) and compares the torque to a set value (0 Nm, in this case). If both the conditions are met, a trigger is sent to the TKBSE to start the lash size estimation. The trigger block also sends the initial conditions of the engine and wheel speeds based on the current measurements each time the TKBSE is triggered. The outputs of the TKBSE are the twist angles, speeds, and the size estimate.

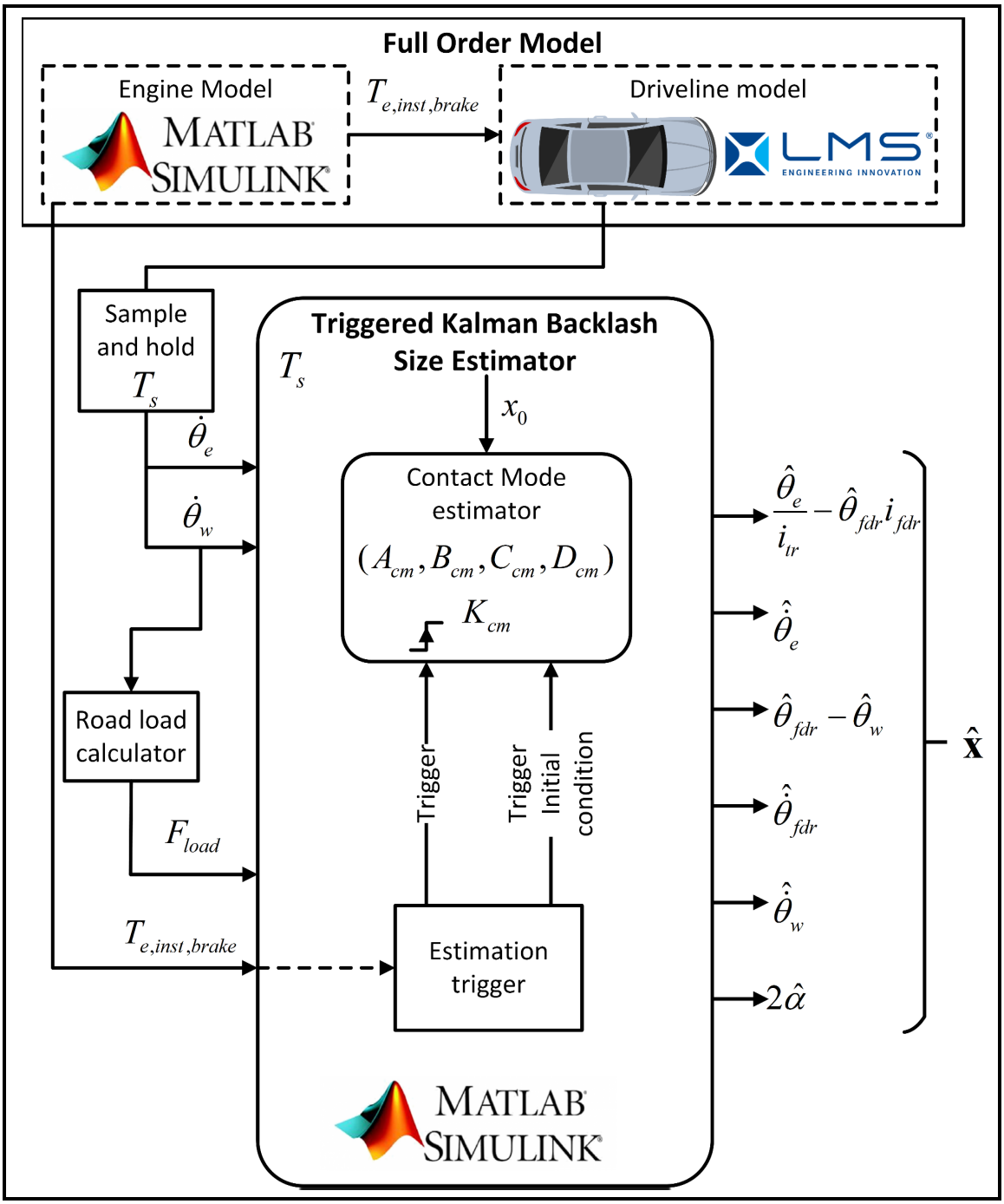

Figure 4.1: Layout of Triggered Kalman Backlash Size Estimator

4.1.3 TKBSE outputs

Figure 4.2 shows the output of the TKBSE. Figure 4.2 (a) shows the engine torque input to the estimator for two consecutive tip-ins and tip-outs. Figure 4.2 (b) shows the triggers which are used to trigger the size estimation. The solid line shows the trigger that the driveline torque is positive and the dashed line shows that the torque is increasing which implies a tip-in event. The size estimation is triggered when both the triggers are active. Figure 4.2 (c) shows the comparison of input and estimated engine and wheel speeds in the engine domain. It can be seen that the engine and wheel speeds are estimated only when both the triggers are active and the estimates are held constant to the last estimated value otherwise, indicating that the size estimator is not triggered anymore and thus not updating the size. Figure 4.2 (d) shows the size estimate which starts at zero and when the estimator is triggered for the first time, it experiences a transient to estimate the backlash size based on the error in the engine and the wheel speeds and then finally arrives at a value of size estimate which becomes constant when the estimator is triggered off. For the second tip-in, the size estimate re-corrects itself and again arrives at a value of the backlash size. The current analysis is done when the engine and wheel speeds are sampled at every 10 ms.

Figure 4.3 shows the size estimate of the TKBSE for multiple tip-in scenarios. Figure

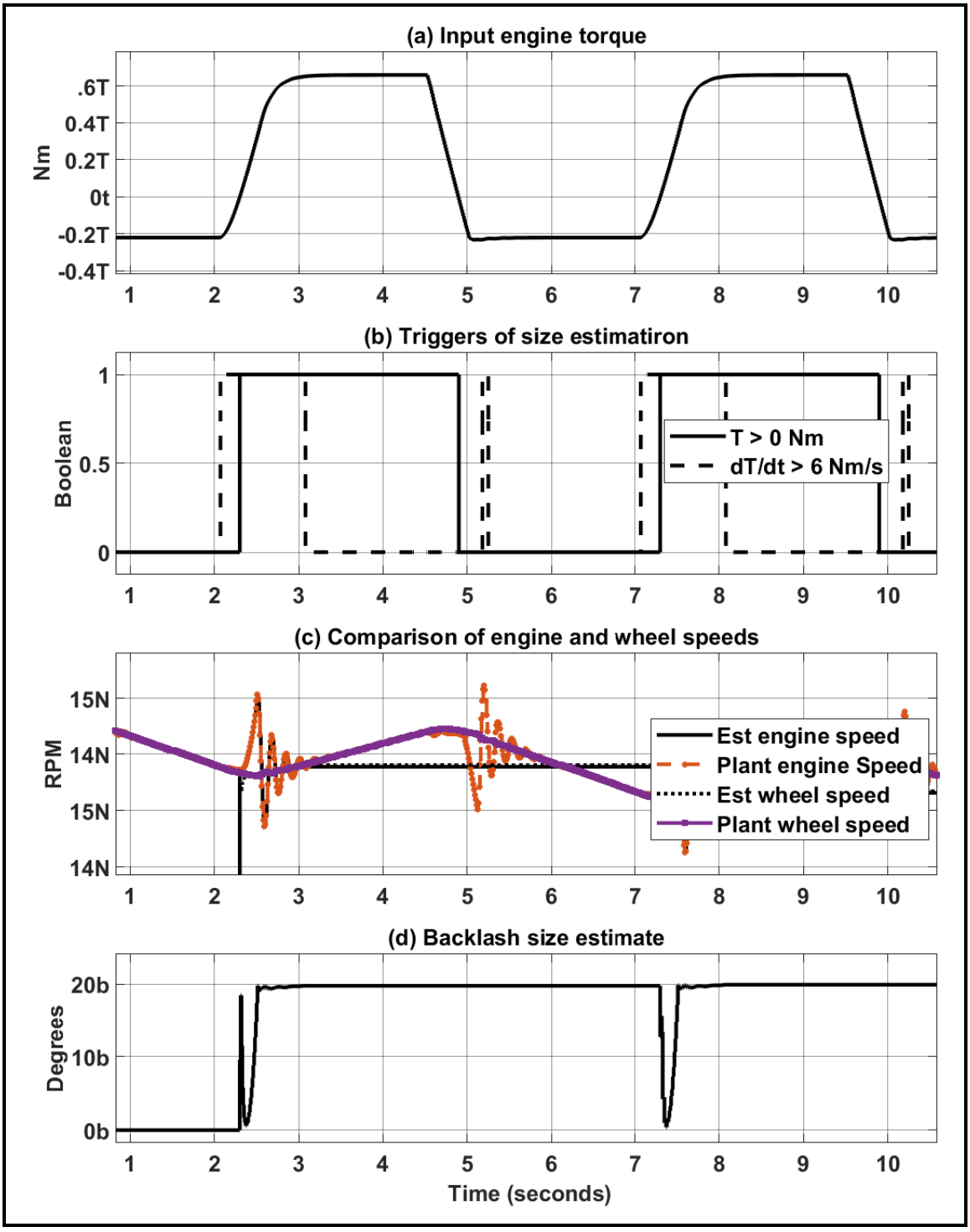

Figure 4.2: TKBSE outputs with input engine torque and triggers

4.3 (a) shows the input torque profile to the estimator. The only difference with respect to the analysis of Figure 4.2 is this analysis is done for a longer time duration. Figure 4.3 (b) shows the comparison of the estimated and the plant engine speeds. It can be seen that the estimator is triggered only during the tip-in scenarios where the backlash of the driveline is traversing. Rest of the time, the estimates are held constant while the plant engine speed varies. This can also be seen in Figure 4.3 (c) which shows the comparison of the estimated and plant wheel speeds where the estimated wheel speed deviates from the plant wheel speed (estimated speed is constant while the plant speed increases) when the estimator is not triggered. Figure 4.3 (d) shows the backlash size estimate with the transients during the start of each trisgger and the estimate converging to a final value of the lash size as the trigger continuous and eventually holding the last estimate until a new tip-in cycle starts.

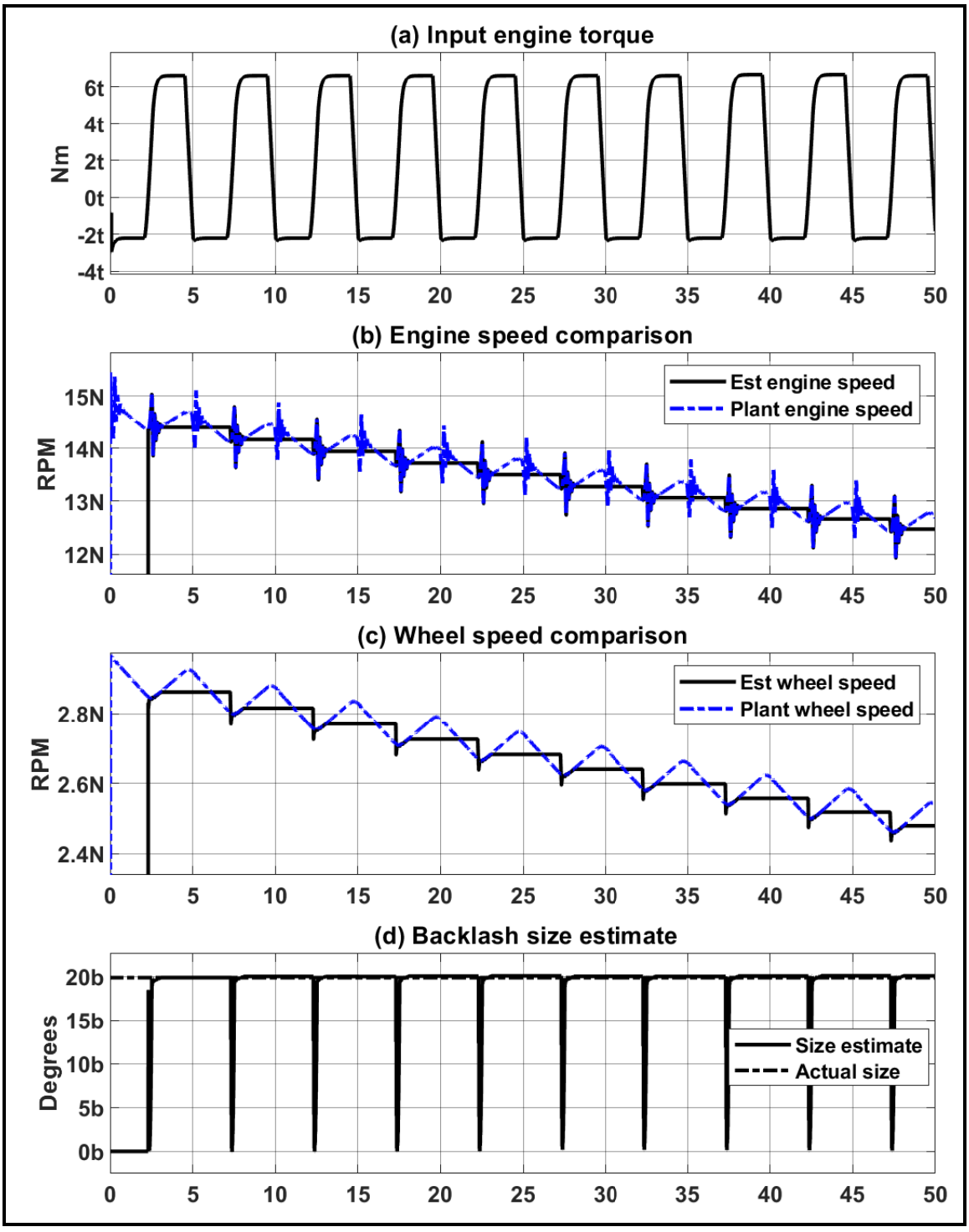

Figure 4.3: Comparison of TKBSE size estimate and actual backlash size for multiple tip-in events

4.1.4 Modified backlash size estimate for TKBSE

It can be seen from Figure 4.2 and Figure 4.3 that the backlash size estimate has an initial transient each time the estimator is triggered which settles down after some time to a final value. This final value represents the size of the backlash. Thus, the representation of the size estimate can be modified to show the final value of the estimate as shown in Figure 4.4 (d), where the modified lash signal takes the final value of the size estimate after each trigger cycle or when there is no change in the lash size estimate.

This representation for the backlash size will be used from here on to represent the estimated backlash size of the driveline.

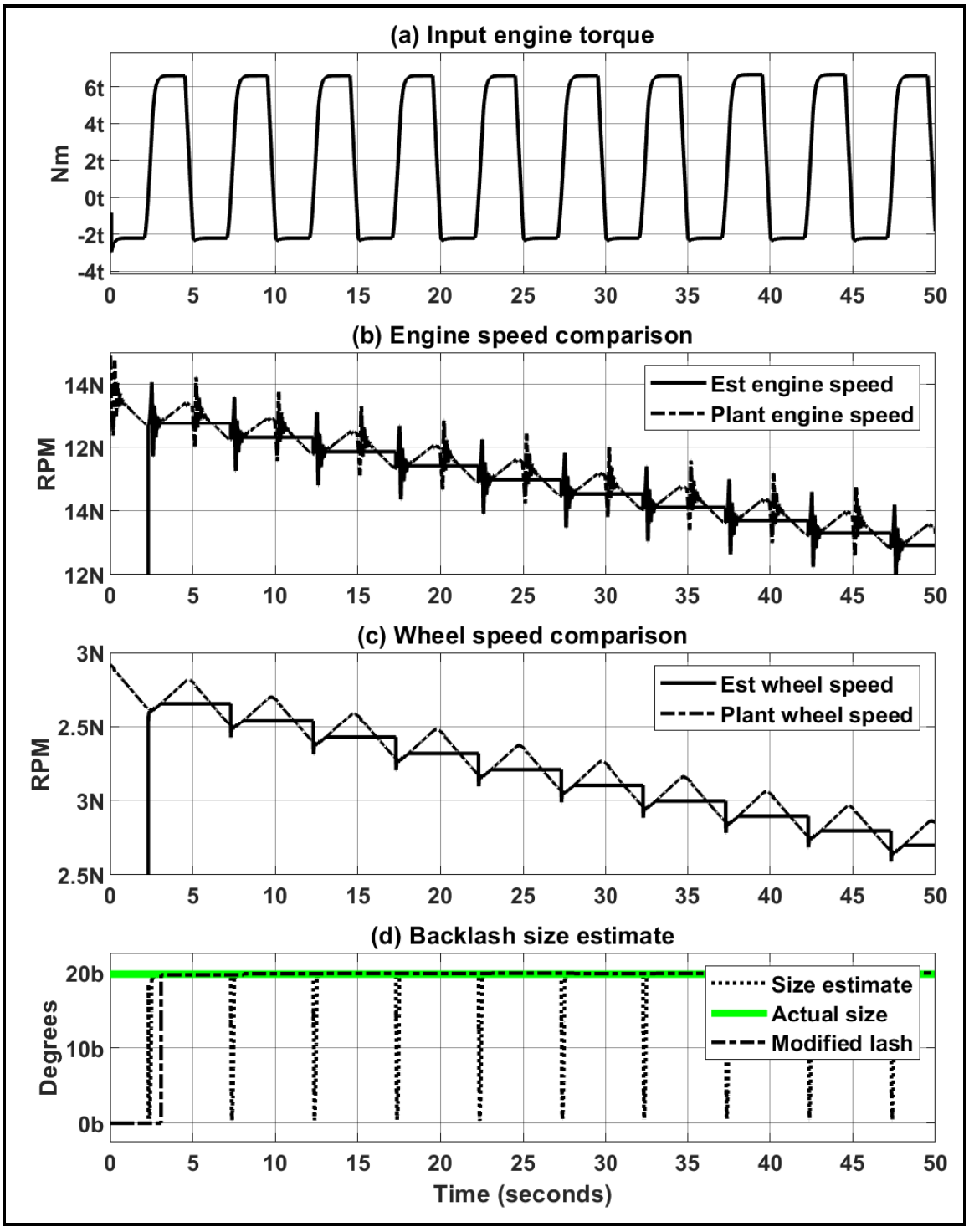

Figure 4.4: TKBSE outputs with modified representation of the backlash size

4.2 Validation of TKBSE

In order to validate the TKBSE, a torque profile is selected as an input to the plant model for different backlash sizes of the plant. Three backlash sizes have been chosen. Given the half backlash size is represented by α, the three chosen plant backlash sizes are represented as $2\alpha, 4\alpha$, and 6α. The torque input and the outputs of plant model, i.e. the engine and wheel speeds, for different backlash sizes are then fed to the TKBSE to estimate the size of backlash based on the inputs and the measurements, refer Figure 4.1 for inputs, measurements and estimates of the TKBSE and for the interface between the plant model and the TKBSE.

Figure 4.4 shows the result of size estimate for the baseline driveline backlash size (2α) with engine and wheel speeds sampled every 10 ms. Table 4.1 shows the comparison of error in the estimated lash size for different plant lash angles for a fixed torque input shown in Figure 4.4 (a) and with engine and wheel speeds sampled every 10 ms. Below are observations from the error in the estimated lash size:

† The maximum error for this torque profile with ramp inputs is less than 1%.

† As the plant lash size increases, the error in the estimated lash size decreases. This is because, as the lash size increases, for a given value of torque ramp rate and the magnitude of torque, the lash traversal time increases. With the

Table 4.1
Variation in error in TKBSE's size estimate with change in plant backlash size and 10 ms sampling time for the estimator and speeds

Actual backlash size	**% Error in lash size estimate**
2α	0.81
4α	0.25
6α	0.23

increased lash traversal time and a given discretization time of the estimator, more data samples are available to estimate the size of the backlash, reducing the error in the estimates.

With these values of error in the lash estimates, it can be said that the TKBSE is validated for a given torque ramp rate. A more detailed analysis of the estimator's performance to varying torque inputs and delays is done in the next section.

4.3 Robustness analysis of TKBSE

Similar to robustness analysis of the Discrete Switched Kalman State Estimator, the robustness analysis of Triggered Kalman Backlash Size Estimator is also done to assess the performance of the estimator to various torque inputs, ramp rates, delays, and sampling times. This is done so that the limitations of the TKBSE can also be identified as well as certain hardware level decision can be made.

4.3.1 Robustness to varying step torque inputs

The most severe clunk and shuffle are observed in the driveline with step torque inputs. Figure 4.5 shows a set of three step inputs which have been used to estimate the lash size with varying plant backlash sizes. It is important to notice that there is a first order shape to the torque inputs. This is due to the first order dynamics of the engine and because the step input is given to the base and the instantaneous torque commands. Figure 4.6 shows the simulation result for "Step 1" torque profile with 2α plant backlash size and 10 ms sampling time. It can be clearly seen in Figure 4.6 (b) and (c) of engine and wheel speeds respectively that the size estimator is triggered for a limited time and holds the value at the end of trigger for the rest of the time. Figure 4.6 (d) also shows the size estimate with (w) and without (wo) constraint. The without constraint signal shows the settling of backlash size estimate while the with constraint signal takes the final value of each trigger cycle.

Figure 4.7 shows the results of error in size estimates for different torque step inputs with the change in the plant backlash size and the sampling time of the TKBSE. Below are the observations that can be made from the result of errors in size estimate.

† As the magnitude of step input torque increases ("Step 1" to "Step 3"), for each sampling time, the error in the size estimate also increases. This can be

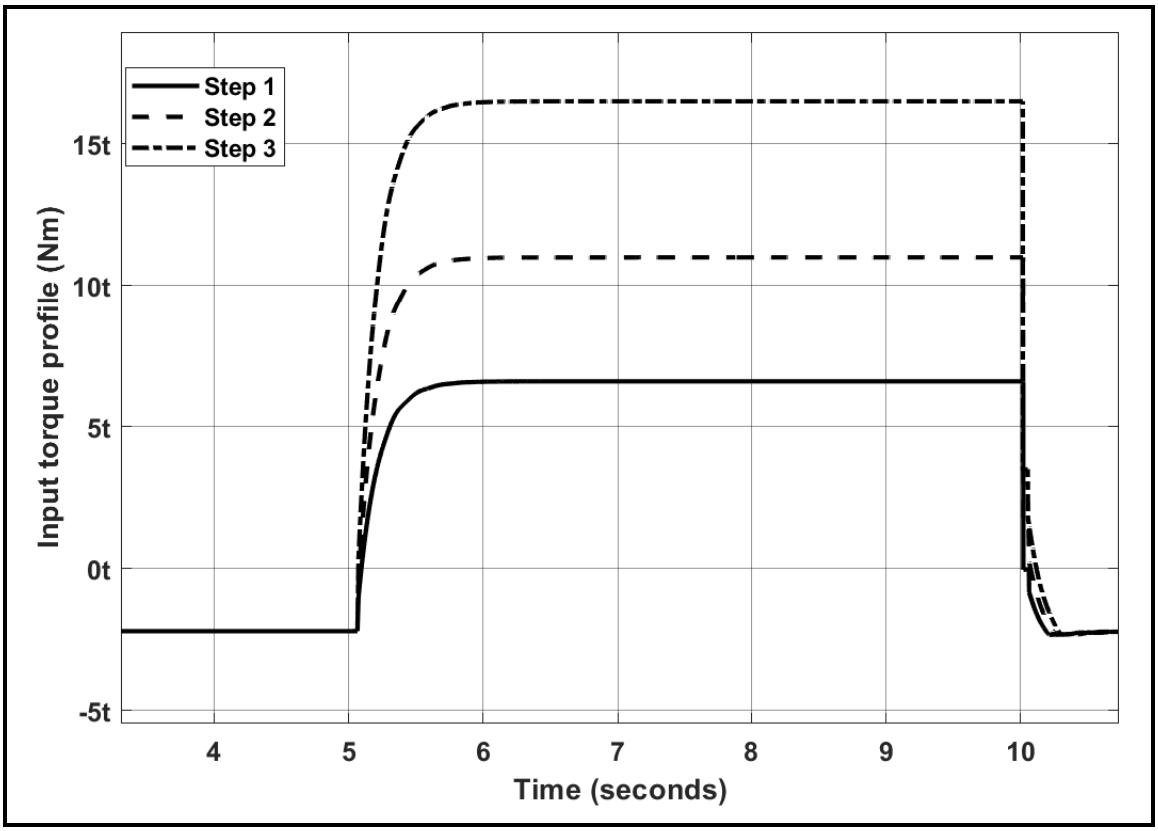

Figure 4.5: Step inputs used to assess the robustness of TKBSE

explained by two reasons, (i) the **Q** of the TKBSE is tuned for the torque "Step 1" leading to a lesser error in the lash estimates with torque "Step 1", (ii) with the increase in torque step from profile 1 to 3, the lash traversal time decreases because of the increasing final value of torque magnitude, thus the number of data samples available to the estimator are less, leading to increased error in the size estimate.

† For a given plant backlash size, as the sampling time decreases the error in the size estimate also decreases. This is because more data samples are available for a given lash traversal time for the estimator to estimate the backlash size

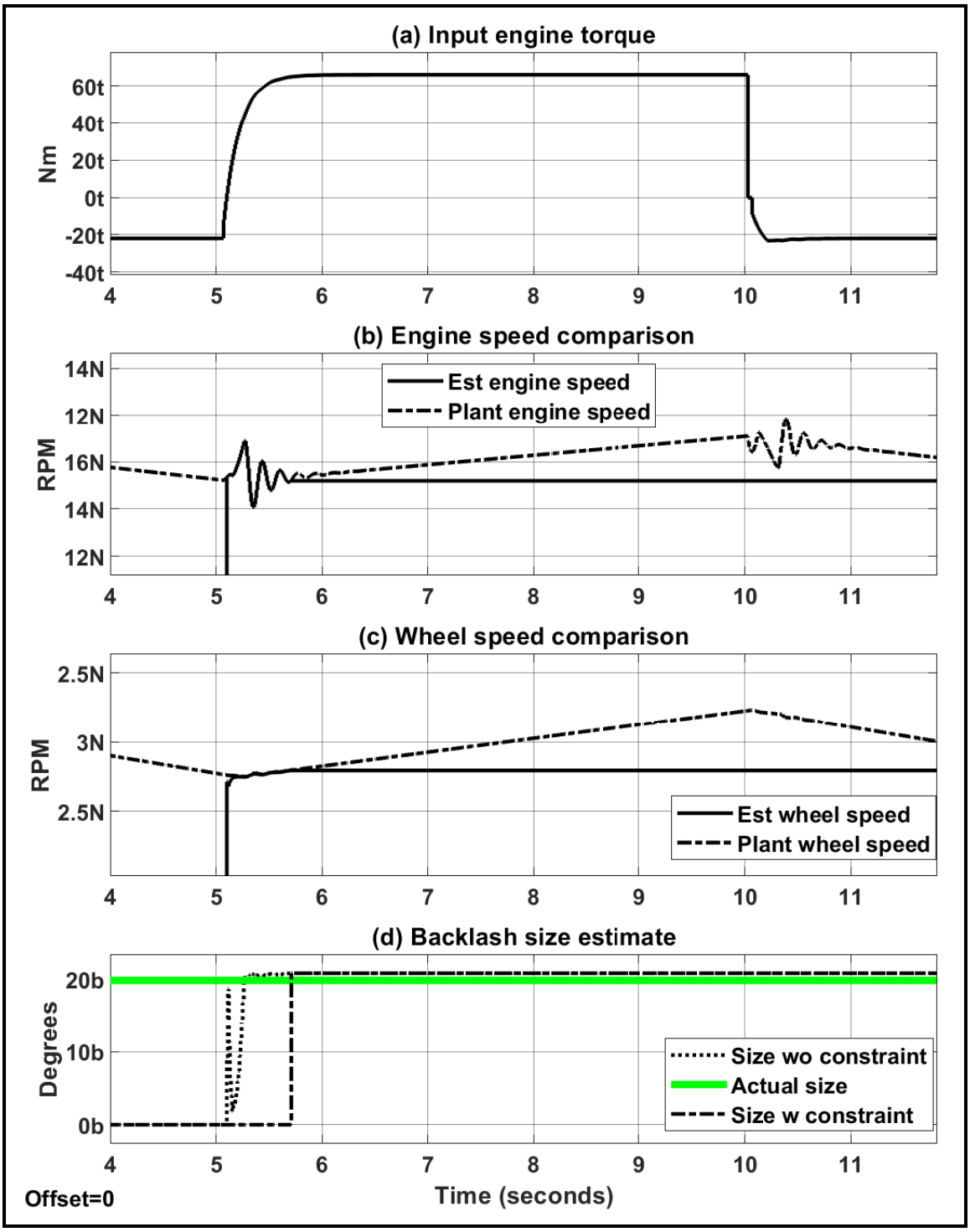

Figure 4.6: Simulation result for "Step 1" torque profile with 2α plant backlash size and 10 ms sampling time.

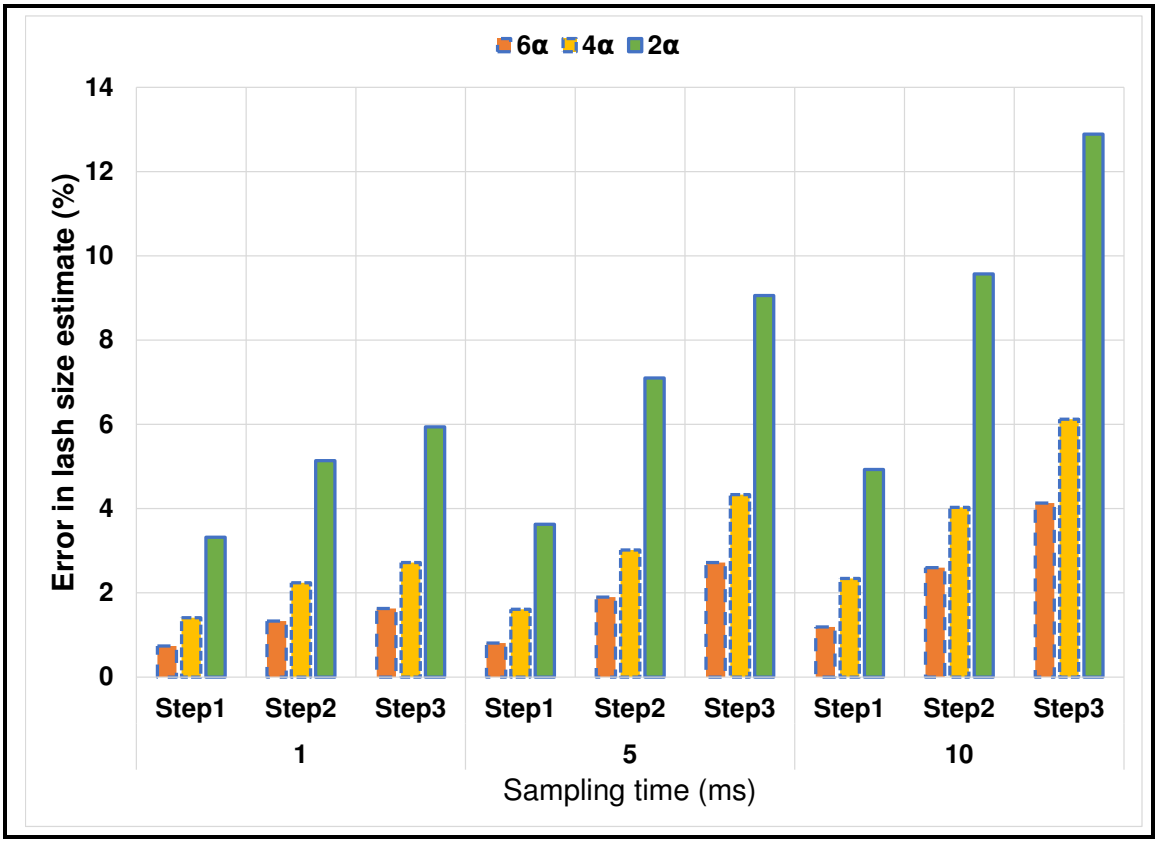

Figure 4.7: Variation of percentage error in size estimate for various step input torques at different sampling times and plant backlash sizes (2α, 4α and 6α).

resulting in a decrease in the error.

† For a given sampling time and torque step, as the plant backlash size increases, the error in the estimates of the backlash size decreases due to the longer backlash traversal time.

† For very large backlash size (6α) and for a given torque step input, the effect of sampling time on the error in the estimates decreases. This can be seen by comparing the error in lash estimation for plant lash size of 6α for torque "Step

1" and all sampling times.

4.3.2 Robustness to varying torque ramp rates

Post the analysis of the effect of various step torque inputs to the TKBSE, the effect of varying torque ramp rates were also studied. An intercept of the torque input (two tip-in and tip-out cycles out of a total 10 cycles) of varying ramp rates to the TKBSE is shown in Figure 4.8. A similar analysis, as done for the case of step input torque, was done and the results with "Ramp 1" torque ramp rate with 2α plant backlash size at 10 ms sampling time are shown in Figure 4.9. Figure 4.9 (d) of the simulation result shows that the actual and the estimated lash size are very close to each other. The quantitative summary of the error in lash size estimates with varying torque ramp rates, plant lash sizes and sampling times is shown in Figure 4.10

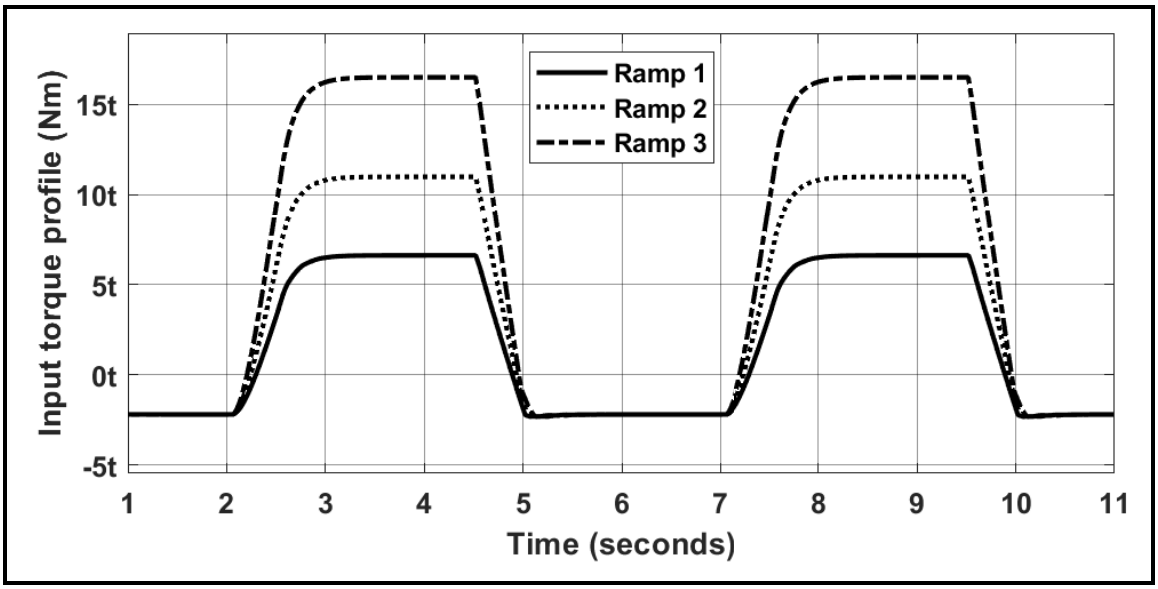

Figure 4.8: Ramp torque inputs used to assess the robustness of TKBSE

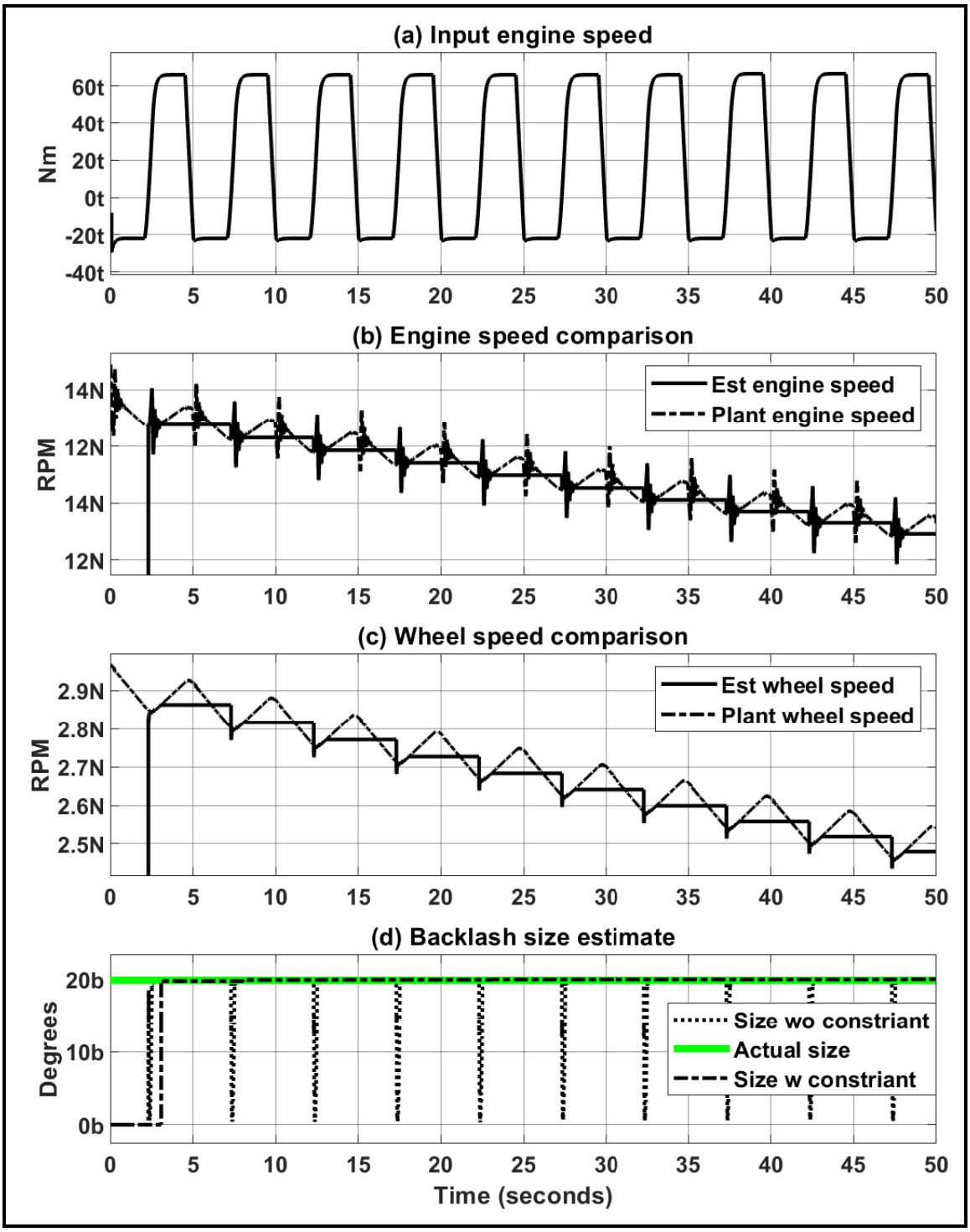

Figure 4.9: Simulation result for "Ramp 1" torque profile with 2α plant backlash size and 10 ms sampling time.

The key highlights of the variation of error with varying ramp rates are discussed below:

† As compared to the error in lash size estimation with step torque inputs, Figure 4.7, the error with ramp torque inputs has significantly reduced. This is due to increased lash traversal time with ramp torque inputs as compared to step torque inputs.

† As the magnitude of torque ramp rate increases, i.e. ramp converging to step, the error in the lash size estimate also increases. This is similar to the higher errors in the lash size estimates with ramp torque inputs as compared to step torque inputs.

† With decreasing the sampling time, the error in the lash size estimate decreases because more data samples are available to the estimator to estimate the lash size for a given lash traversal time.

† The decrease in error of lash size estimate with an increase in lash size is also evident throughout the different ramp rates as well as the sampling times.

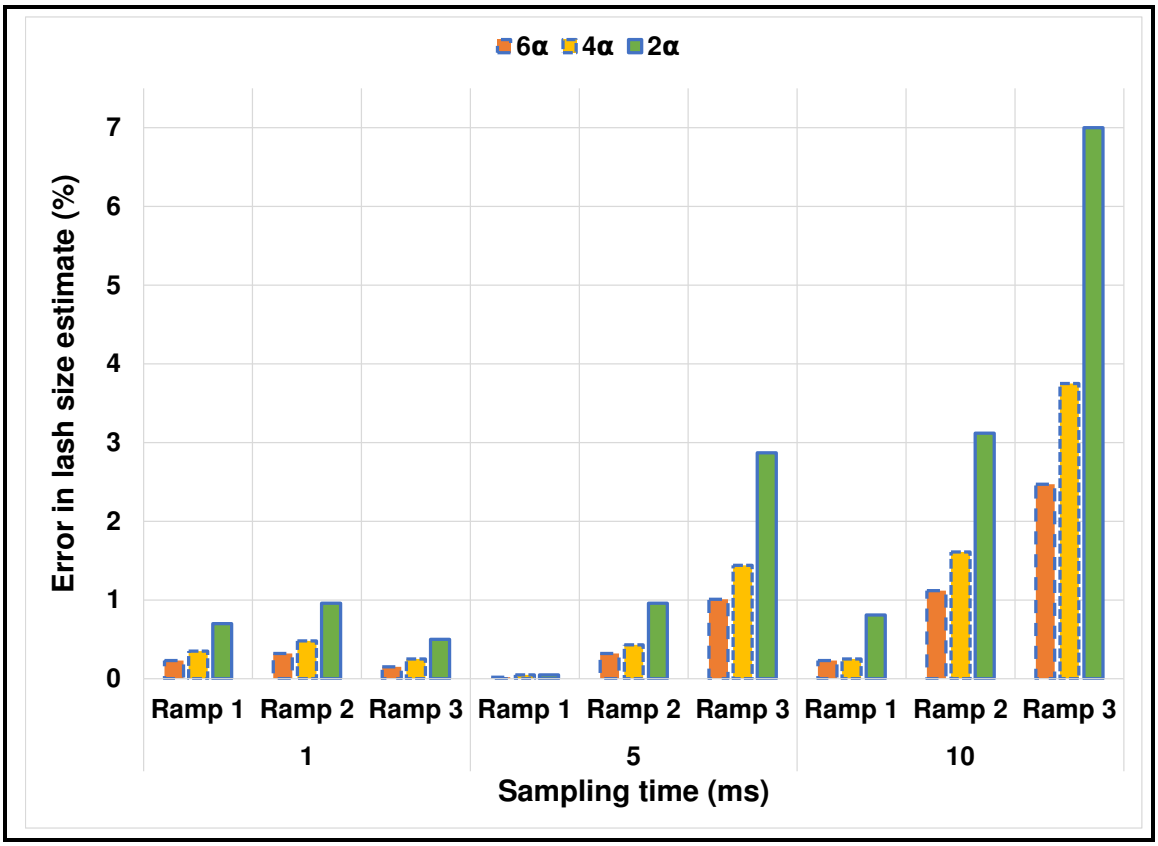

Figure 4.10: Variation of percentage error in size estimate for various ramp input torque rates at different sampling times and plant backlash size (2α, 4α and 6α).

4.3.3 Robustness to torque inputs with varying duty cycle and pulse width

For the discussions in Section 4.3.1 and Section 4.3.2, the duty cycle and pulse width of the torque inputs were constant even though the torque rates were different. In order to check whether the constant duty cycle and the pulse width are not causing

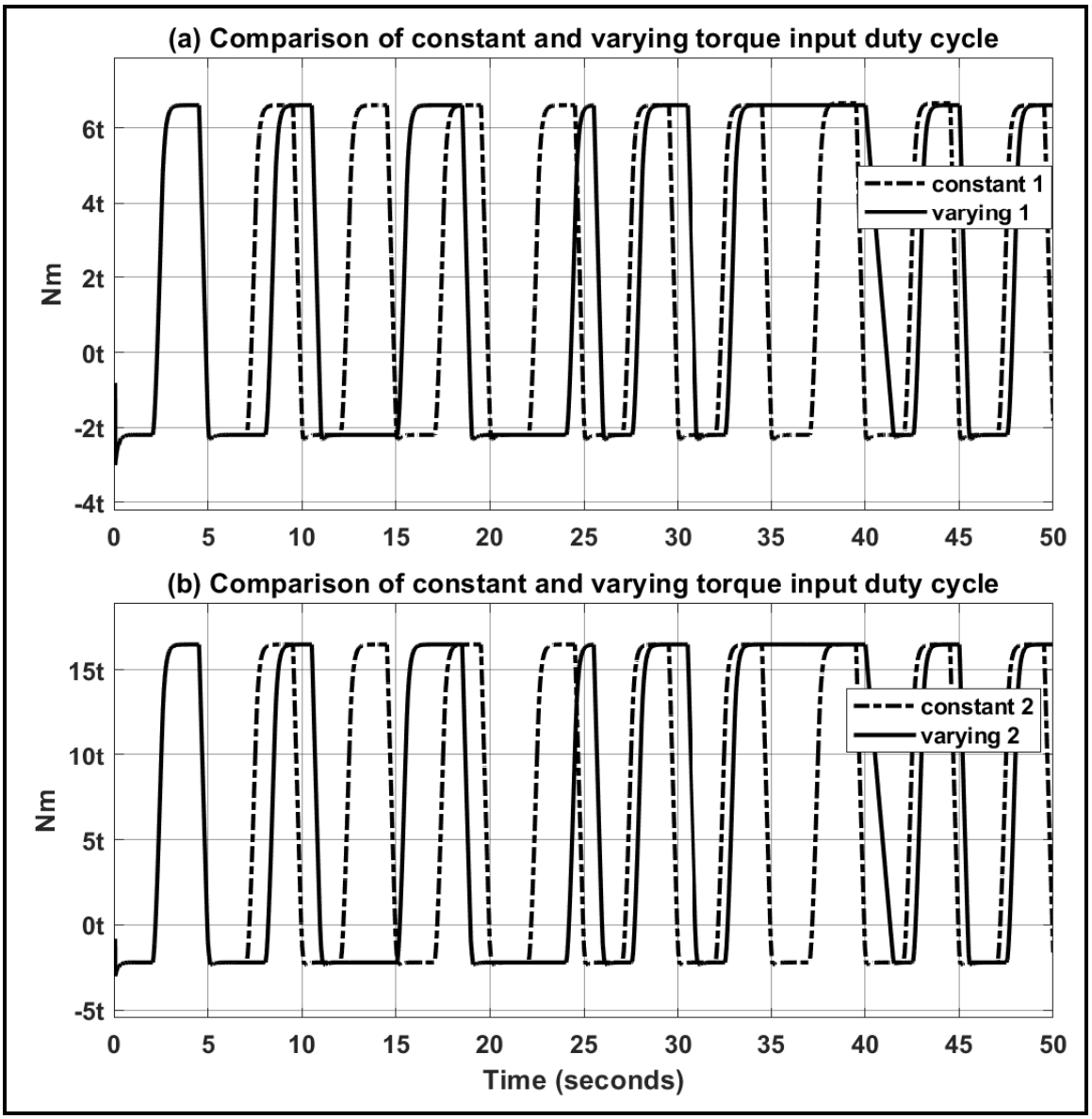

Figure 4.11: Comparison of varying duty cycle and pulse width torque input profiles with constant duty cycle and pulse width profiles

the size estimate to converge to a specific value, two torque input profiles with varying duty cycle and pulse width were also developed to check the error in the size estimate. A comparison of those varying duty cycle and pulse width torque inputs with constant duty cycle torque inputs is shown in Figure 4.11.

The result of the TKBSE for "Varying 1" torque profile, a plant backlash size of 2α and the sampling time of 10 ms is shown in Figure 4.12. Figure 4.12 (d) shows a good correlation between the estimated lash size and the actual plant backlash size.

Figure 4.13 shows the summary of variation of lash size estimate with the two varying duty cycle and pulse width torque input profiles for different lash sizes and sampling times. The observations are very similar to the previous two cases. The average errors in size estimate with this case are similar to those with ramp torque inputs.

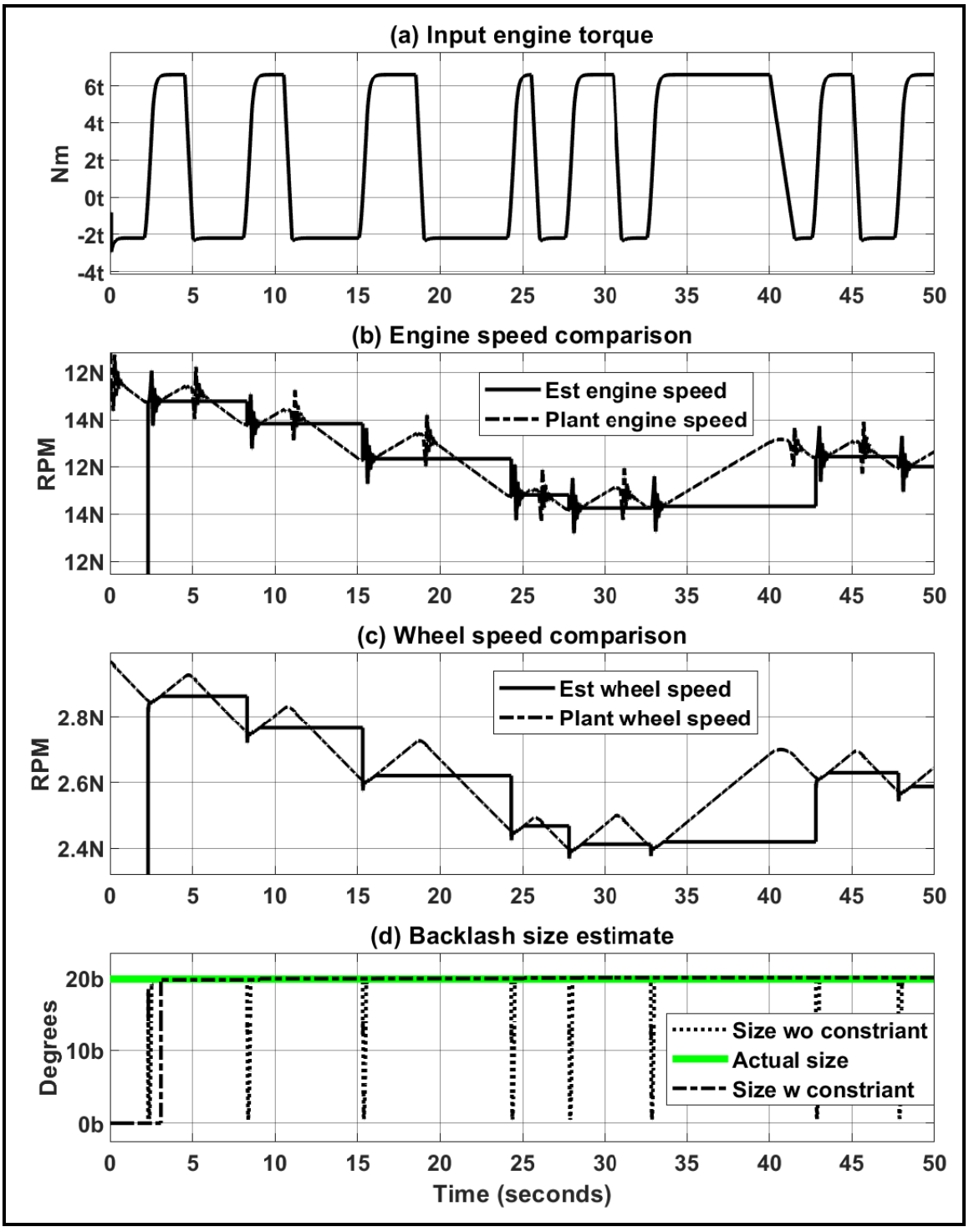

Figure 4.12: Simulation result for "Varying 1" torque profile with 2α plant backlash size and 10 ms sampling time.

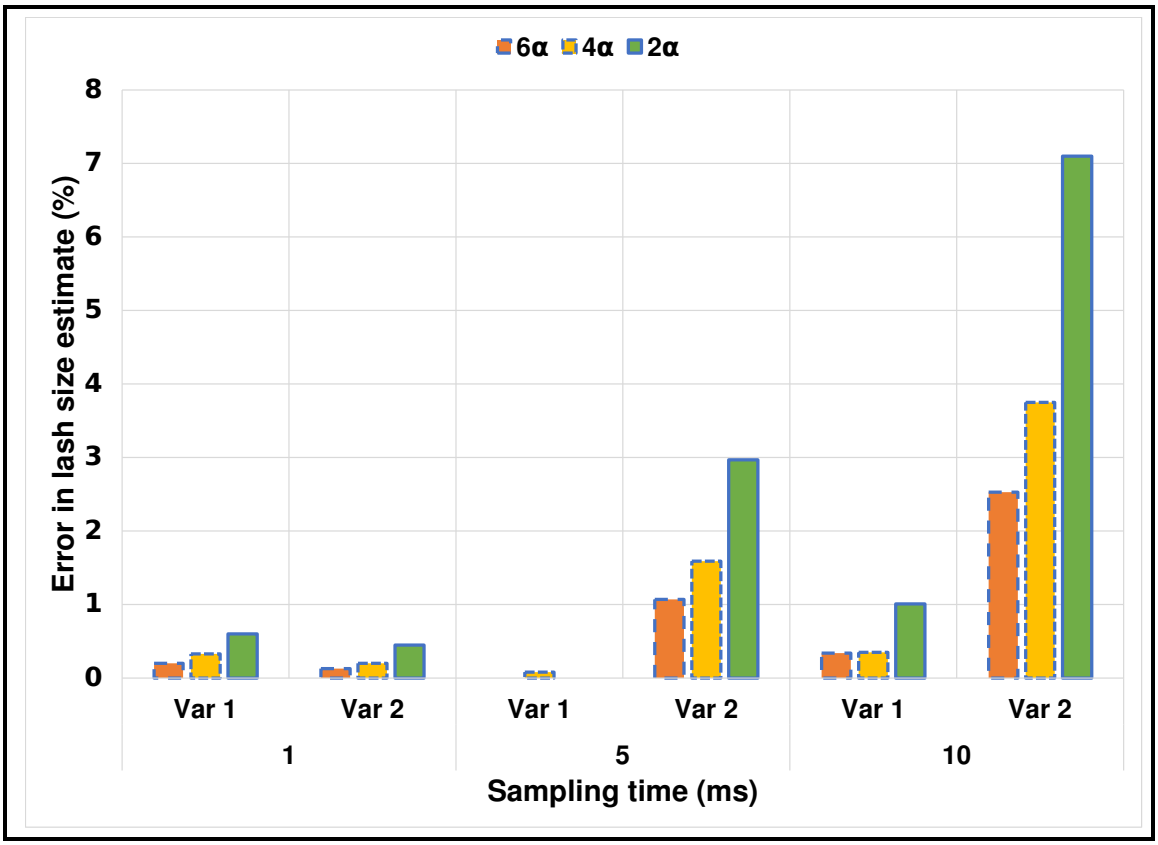

Figure 4.13: Variation of percentage error in size estimate for varying duty cycle input torque rates at different sampling times and plant backlash size (2α, 4α and 6α).

4.3.4 Robustness to variable torque input profile

Based on the results of the Section 4.3.1, Section 4.3.2 and 4.3.3, where one or the other parameter of the input torque was fixed, in this scenario, a random torque profile was generated to test the robustness of the size estimator. This is shown in Figure 4.14 (a) where the torque ramp rate, the magnitude of the final value as well as the duty cycle of the torque input, varies with time. The Figure 4.14 (b) and (c) shows the comparison of estimated and the measured engine and the wheel speeds. The estimates overlap with the measurements while the estimator is trigger ON and are held to a constant value when triggered OFF. Figure 4.14 (d) shows the comparison of the actual lash size, the estimated lash size without (wo) and with (w) constraint. It can be seen that the final value of the lash size is kept as the one for which the final torque value is maximum, i.e. the peak with 15t final value of torque.

Figure 4.15 shows the summary of variation in the error of lash size estimate for different plant backlash angles as well as the sampling times. The general observations from this plot are similar to previous robustness analyses. The order of error is similar to the error with variable duty cycle and ramp torque inputs with decreasing error in size estimate with increasing lash size as well as the sampling times.

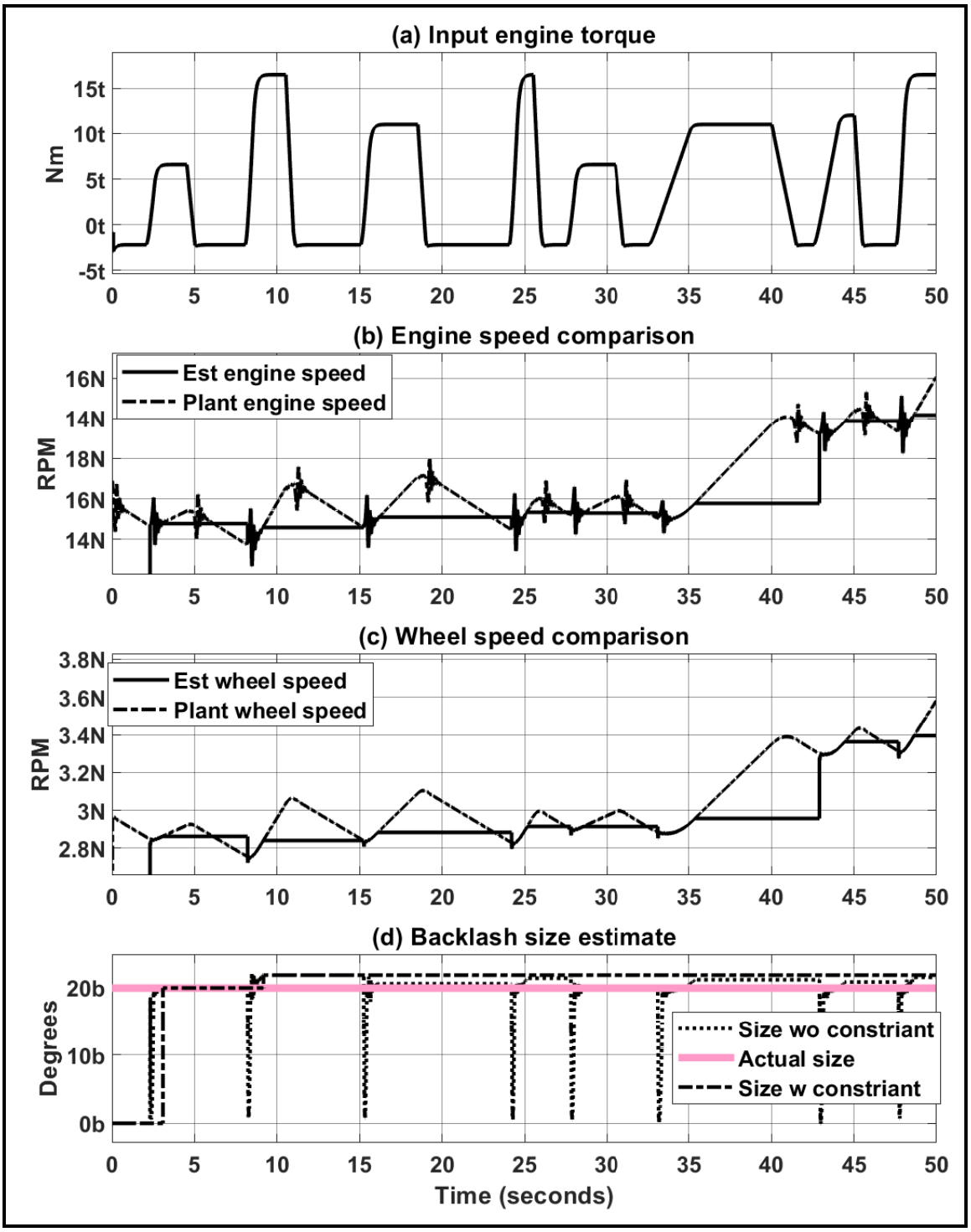

Figure 4.14: Simulation result for random torque profile with 2α plant backlash size and 10 ms sampling time.

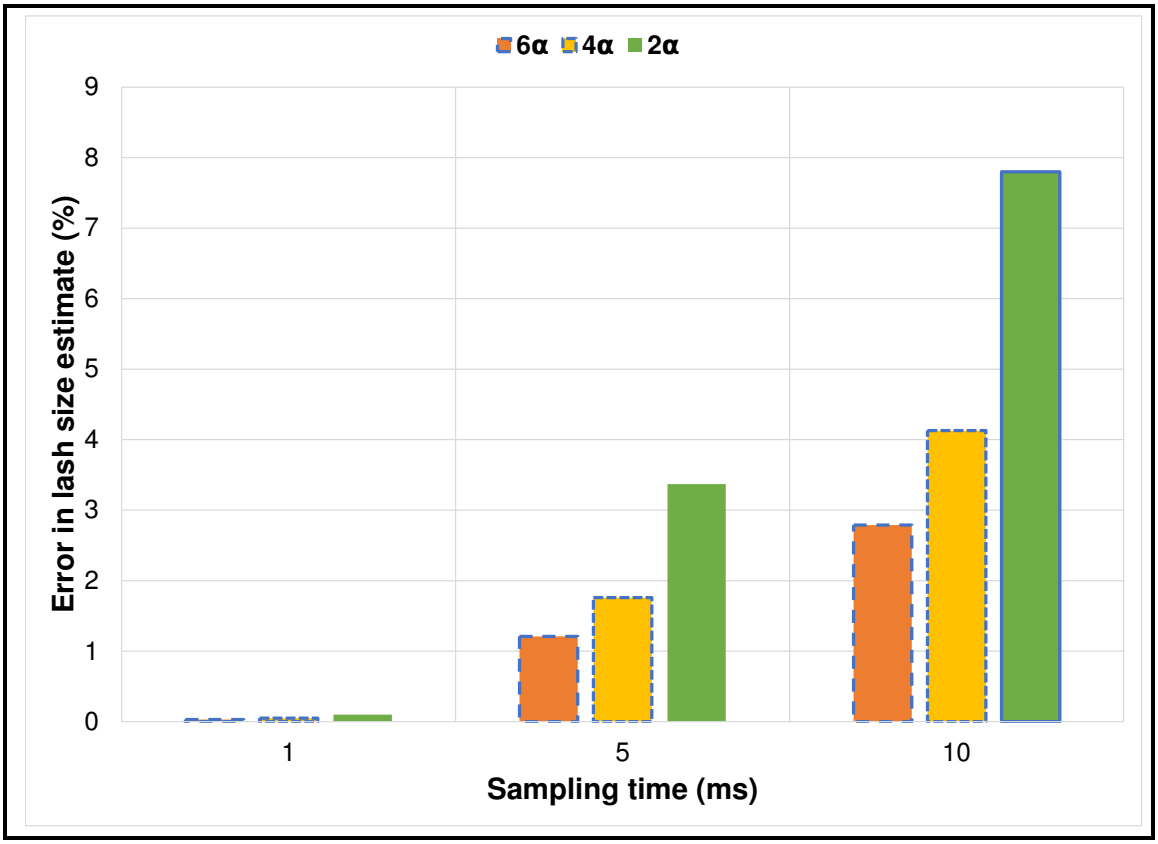

Figure 4.15: Variation of percentage error in size estimate for random input torque at different sampling times and plant backlash angles (2α, 4α and 6α).

4.3.5 Robustness to constant delay in engine speed

As discussed in the robustness analysis of the state estimator, the measurement input signals to the TKBSE can have a delay from the time it is measured at the crankshaft to the time it is received by the estimator. Normally, the engine speed signals are directly sent to the powertrain ECU and they have the highest priority in the CAN bus as compared to other signals. As a result, the delay in the engine speed signal should

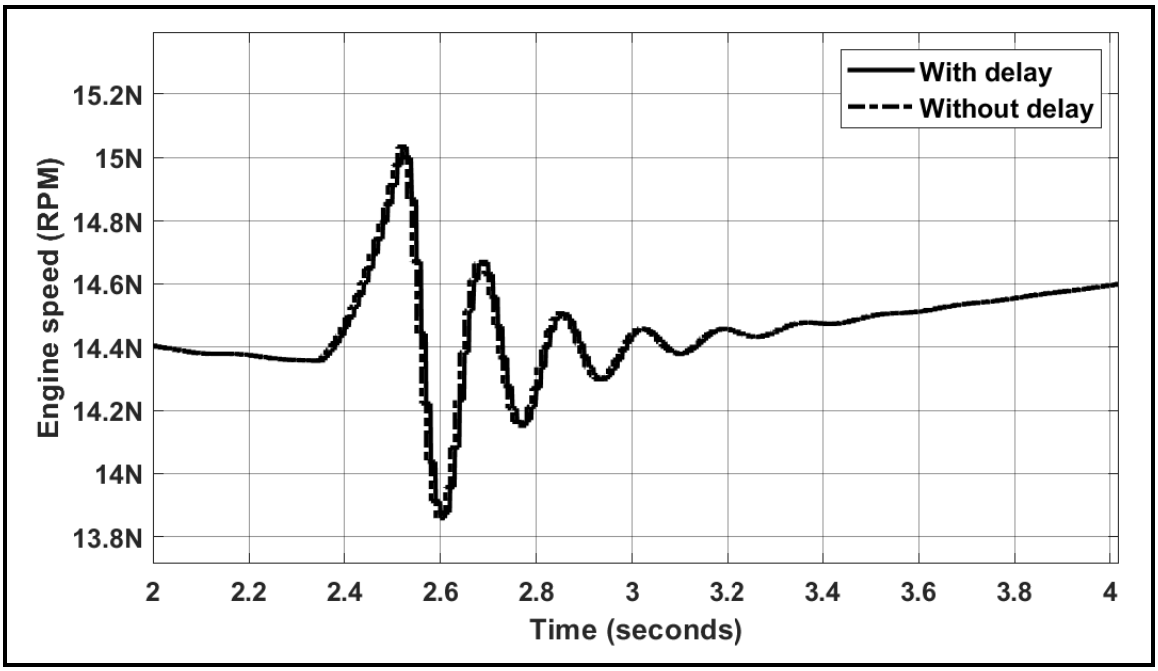

Figure 4.16: Comparison of input measured engine speed with and without delay.

be significantly less than other signals broadcasted over the CAN. An assumption is made that a delay of 10 ms is significant for the engine speed signal and accordingly simulation for delays of 5 ms,10 ms and 20 ms are done to understand the error in the size estimate. A comparison of engine speed with and without delay is shown in Figure 4.16 for engine speed sampled at 10 ms and with 10 ms of constant delay.

Figure 4.17 shows a plot of variation of error in size estimate with increasing constant delay in the engine speed for different sampling times. The observations that can be made from the distribution of error are:

† As the delay in the engine speed measurement increases, the error in the size

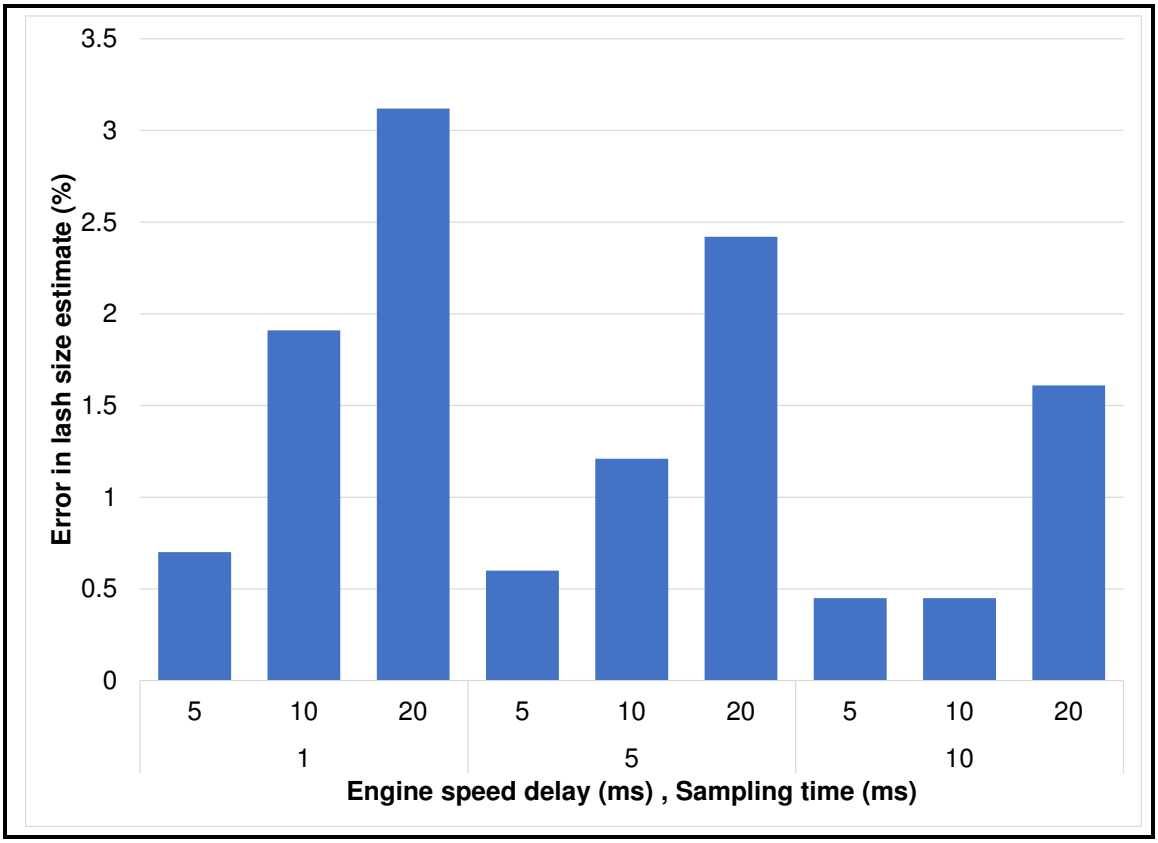

Figure 4.17: Variation of error in size estimate with variation in engine speed constant delay for different sampling times.

estimate also increases. This is because the trigger to estimate the lash size is active for a fixed period of time and is based on the engine torque input and its derivative values. As a result, a specific window of engine speeds measurement data is available to the estimator to estimate the size of the backlash. With the increasing delay in the engine speed measurement, the window of data with the knowledge of lash traversal is reduced consequently increasing the error in the lash size estimate.

† The variation of error also shows that as the sampling time decreases, the error

caused by the constant engine speed delay increases. This is contrary to the expected behavior where the error in size estimate decreases with a decrease in the sampling time.

4.3.6 Robustness to constant wheel speed delay

As compared to engine speed, the wheel speed data can have a higher delay and the discussions with the sponsor organization have indicated that a delay of maximum 30 ms is adequate. Accordingly, Figure 4.18 shows the comparison of input measured wheel speed with and without delay of 30 ms for sampling time of 10 ms. The summary of variation in size estimate is shown in Figure 4.19.

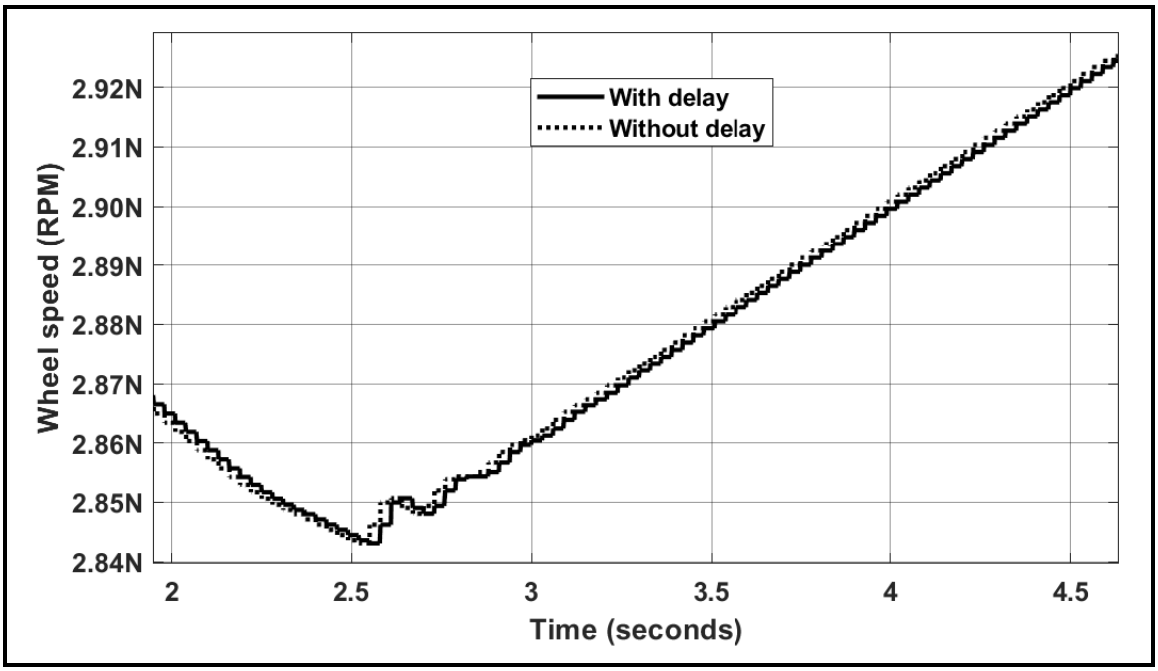

Figure 4.18: Comparison of input measured wheel speed with and without delay.

The observations from this analysis are listed below:

† Similar to the observation for variation of error in lash size estimate for a constant delay in engine speed, with a constant delay in wheel speed, the error also increases with an increase in the delay.

† On the contrary to the trend with a constant delay in engine speed, with a constant delay in wheel speed, as the sampling time decreases, the error in size estimate also decreases. This is more in line with observations that have been made with the rest of the robustness analysis.

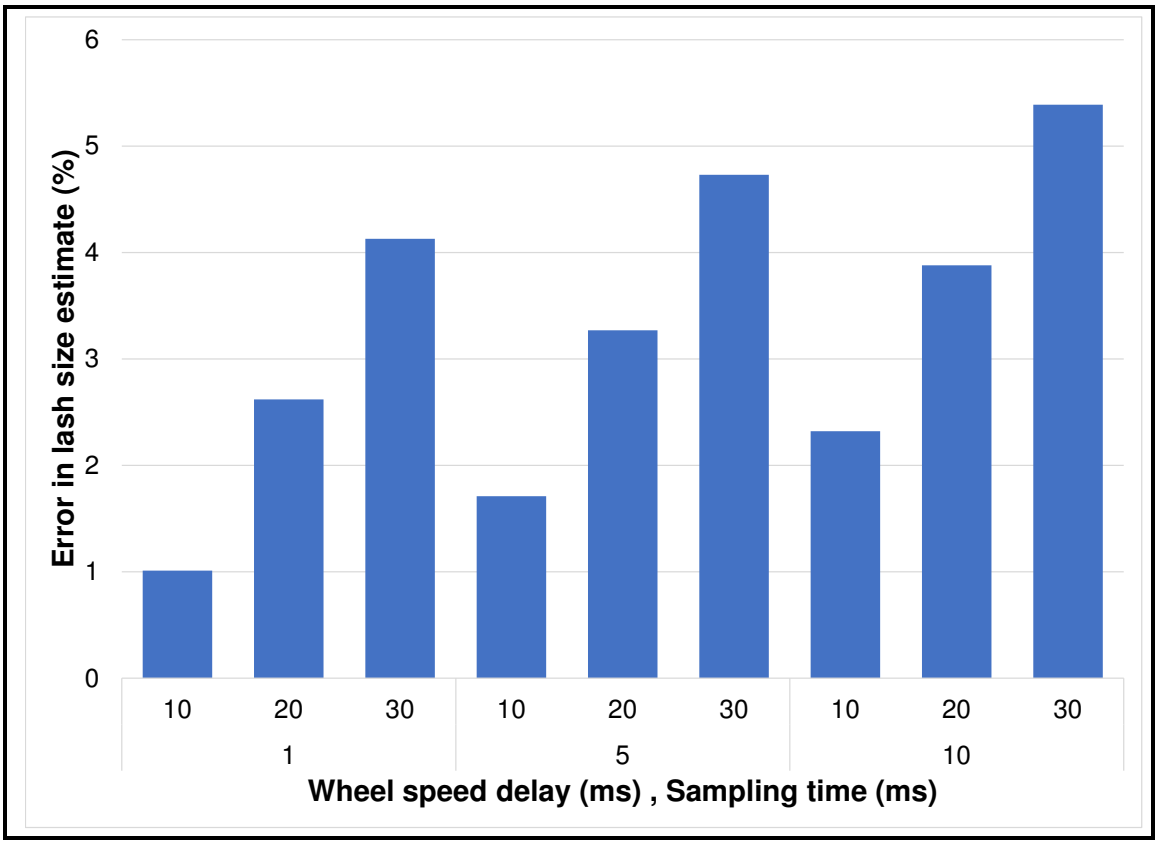

Figure 4.19: Variation of error in size estimate with variation in wheel speed constant delay for different sampling times.

4.3.7 Robustness to combined constant engine and wheel speed delays

As in the real world scenario, both the engine and wheel speed constant delay would be acting together, their combined effect on the lash size estimate for one backlash angle and different sampling times with 10 ms sampling delay in engine speed and 30 ms sampling delay in wheel speed is shown in this section of robustness analysis.

Figure 4.20 shows the TKBSE's output when the constant delays in the engine and wheel speeds for 10 ms sampling time are added. It is evident from Figure 4.20 (d) where the estimated size converges to the actual plant backlash size. The quantitative data for the analysis and the summary of the errors for different sampling times is shown in Figure 4.21. The maximum error of 4% is observed for 10 ms sampling with a decrease in error of lash size estimate with a decrease in sampling time.

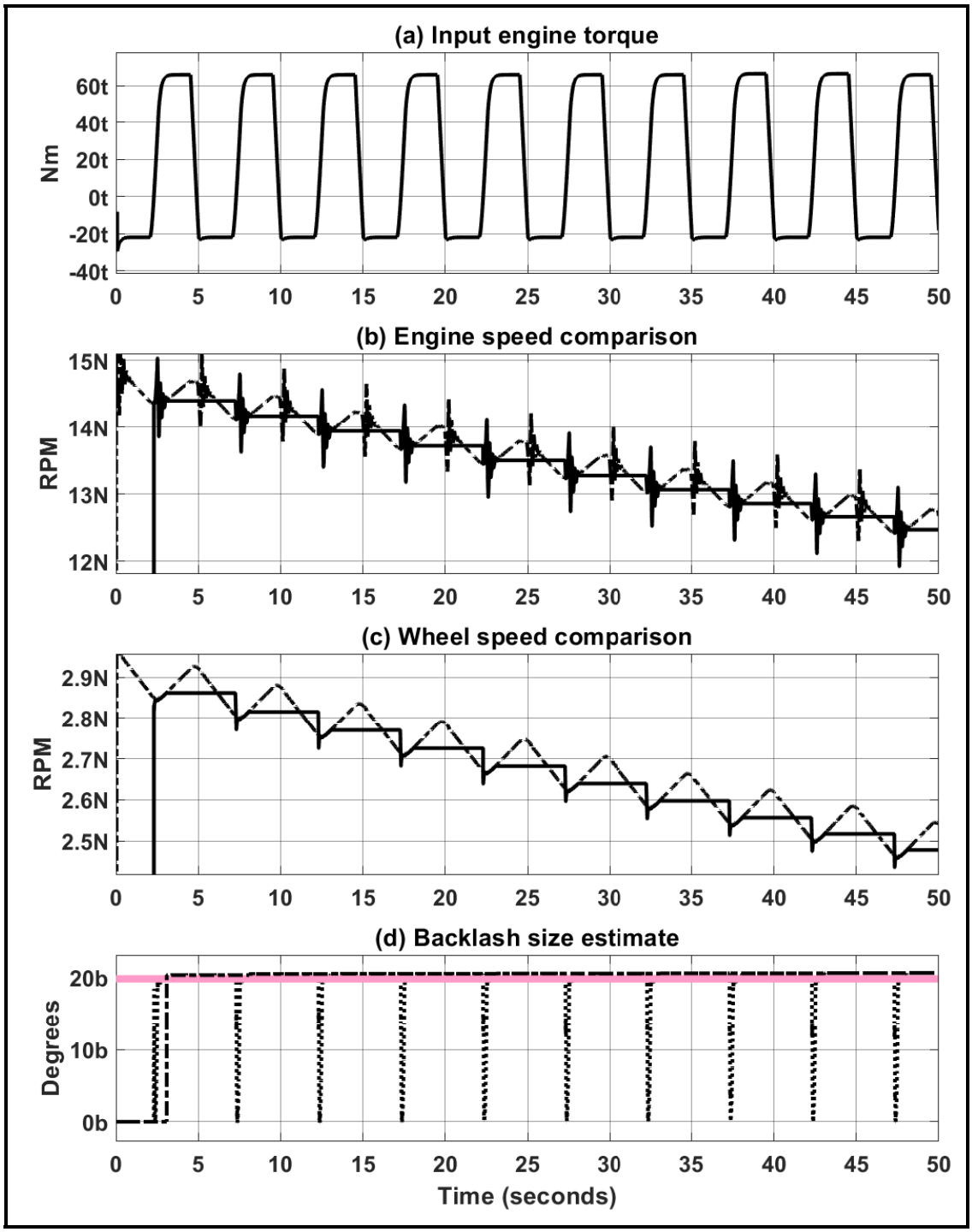

Figure 4.20: TKBSE's output for 10ms sampling of engine and wheel speed for 10 ms constant delay in the engine speed and 30 ms constant delay in wheel speed.

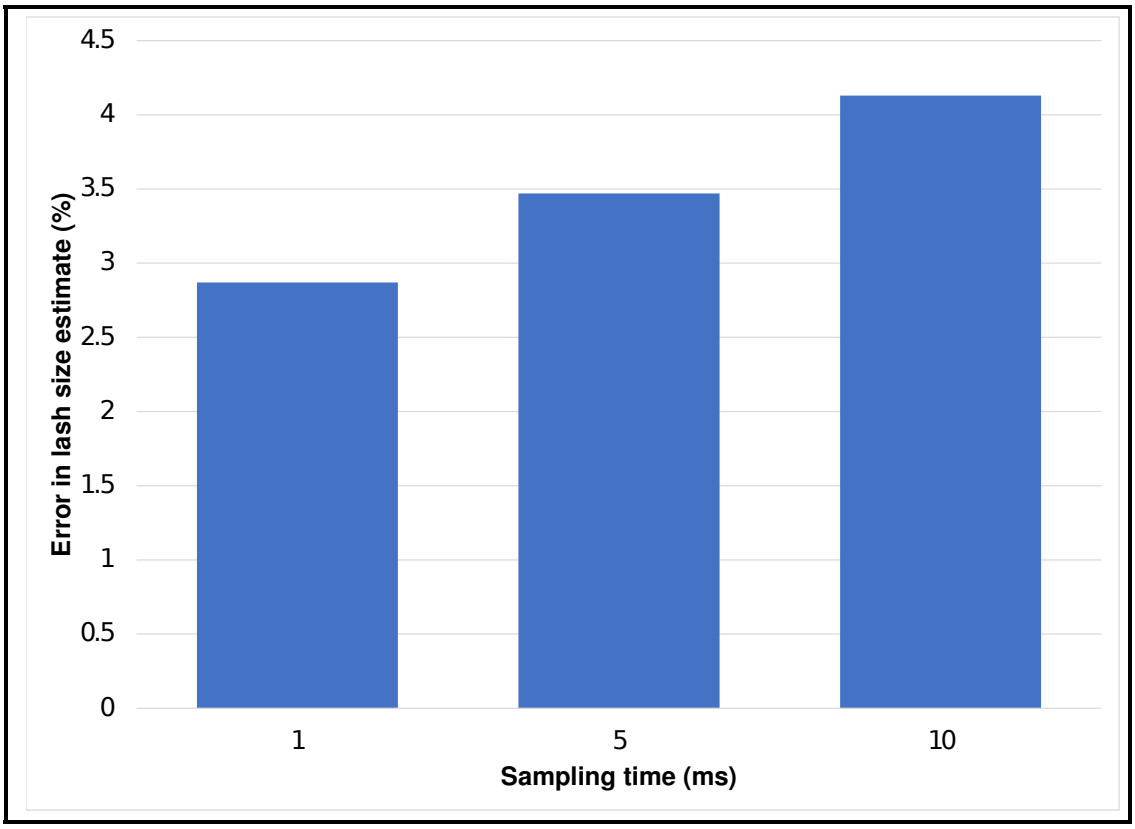

Figure 4.21: Summary of error in lash size estimate for different sampling times with 10 ms constant engine speed delay and 30 ms constant wheel speed delay.

4.3.8 Robustness to CAN jitter in engine and wheel speeds

Figure 3.15 and Figure 3.16 showed the distribution of jitter in the engine and the wheel speed signals and section 3.3.5 discussed the effect of jitter on the robustness of state estimator. The Kernel probability density functions derived for the engine and wheel measured data sets were used to generate sampling data to be used for robustness analysis of size estimator as well. As compared to the data generated for

state estimator's analysis, the number of samples were more for the analysis of size estimator as the simulation is run for 50 seconds as compared to 7 seconds for state estimator, leading to statistically close distribution of generated data. Furthermore, multiple tip-in scenarios are being considered for size estimator so the distribution of delay is also more uniform. The implementation of the jitter signal to the inputs of the engine and the wheel speed measurements is similar to the way it was implemented for the state estimator and can be seen in Figure 4.22. The summary of results with these jitter data set for different sampling times is shown in Figure 4.23.

Below are some of the major observations with respect to the error in size estimate with jitter in engine and wheel speed signals:

† The maximum error in the size estimate with combined engine and wheel speed jitters is less than 4%.

† The maximum error in size estimate occurs for engine speed distribution which has a high density at 4-5 ms delay for a 10 ms sampling time of the estimator and the engine and wheel speeds.

† The various distribution of wheel speed jitter data does not affect the error in lash size estimate for any given sampling time significantly. This is evident as the different peaks for given sampling time and engine data sets of jitter are of almost similar size.

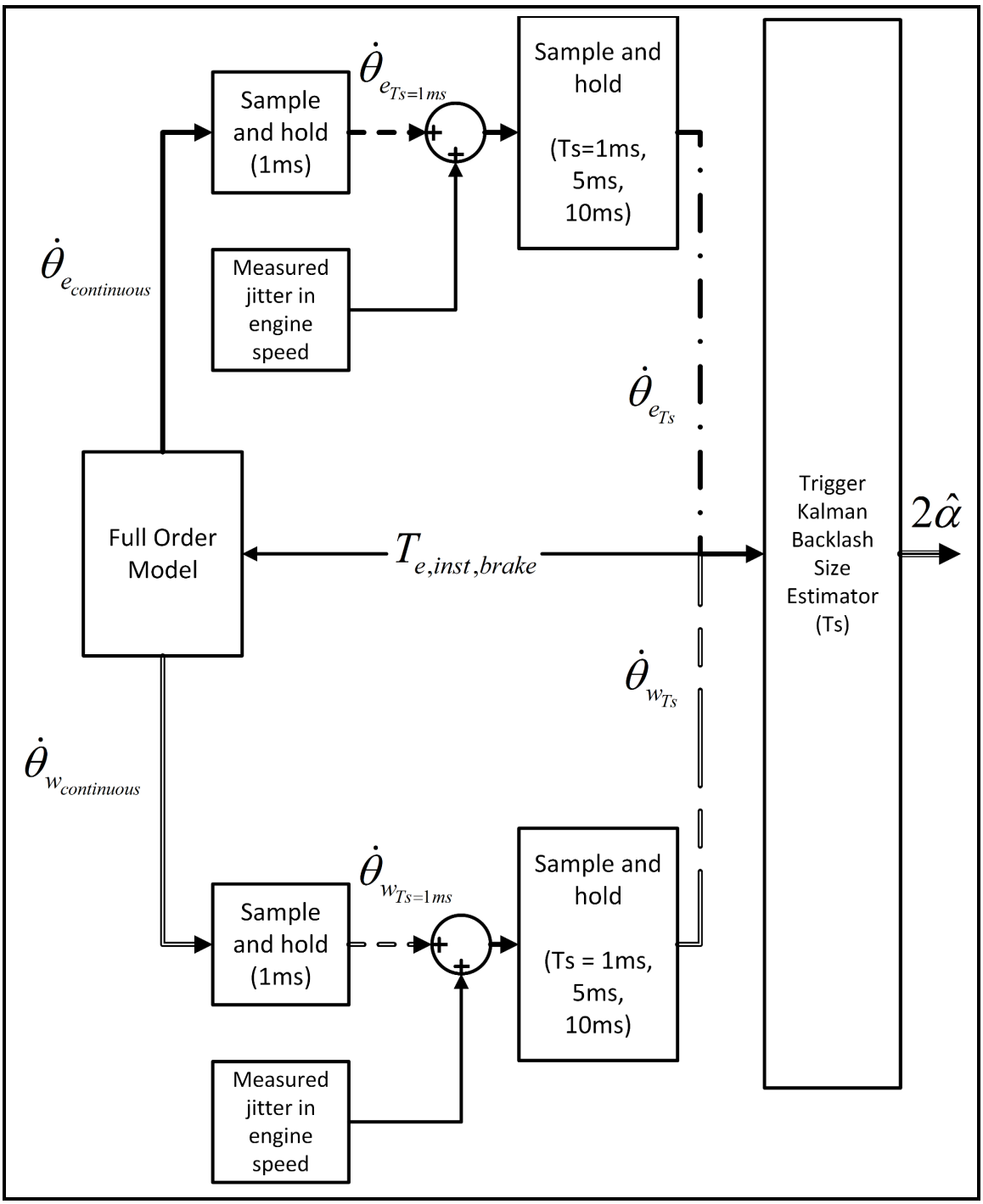

Figure 4.22: Implementation of CAN jitter delay in engine and wheel speed measurement data.

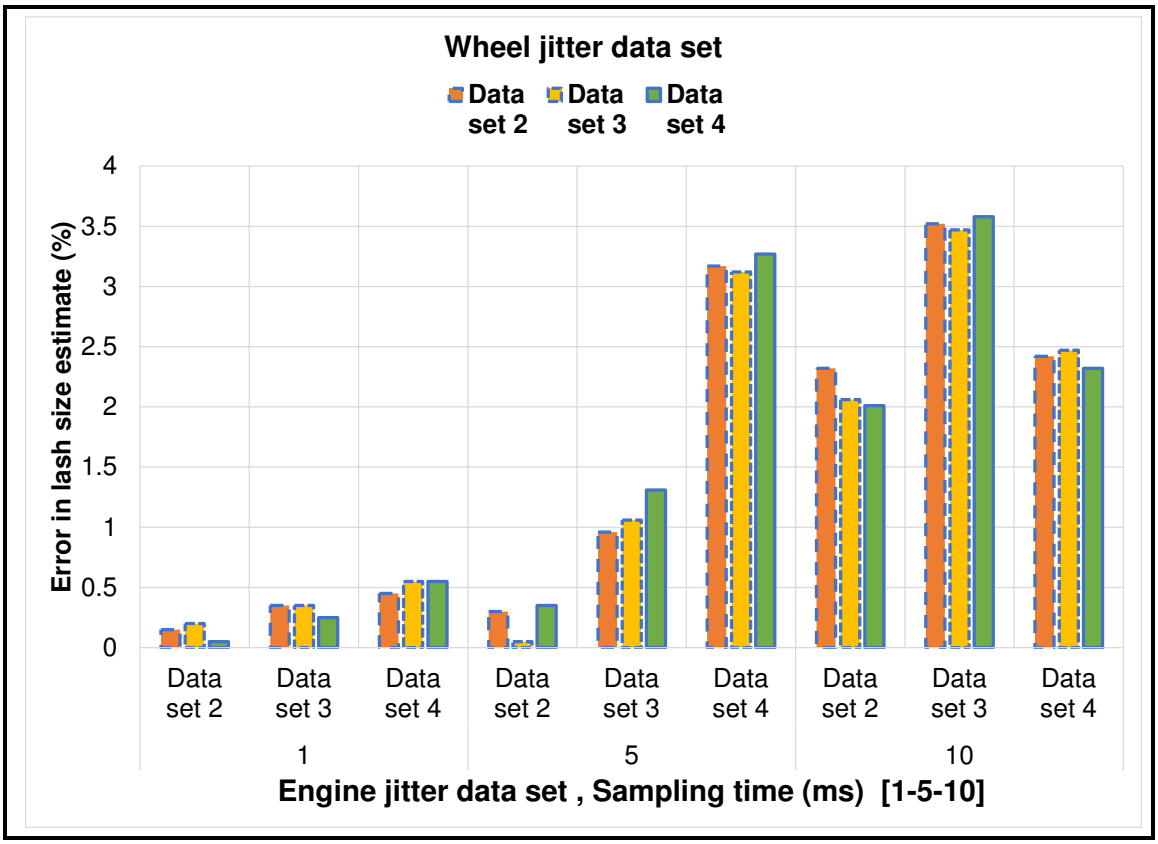

Figure 4.23: Summary of error in lash size estimate for different sampling times and CAN jitter in measured engine and wheel speed signals.

† Sampling time of 1 ms is most robust to the effect of jitter in engine and wheel speeds.

4.3.9 Robustness to sampling time

Even though the effect of sampling time has been a consistent parameter in all the robustness analysis so far, a cumulative plot for the error in lash size estimate for all the analysis with respect to sampling time is plotted in this section to evaluate the

overall performance of the TKBSE with different sampling times. Figure 4.24 shows a box plot with variation of percentage error in lash size for different sampling times.

Below are the observations from the box plot:

† For 10 ms sampling time, 50% of the data, quartile Q_1 to Q_3, lies between 1% to 4%. The mean and mode errors in the lash estimate are around 3%.

† For 5 ms sampling time, 50% of the data, quartile Q_1 to Q_3, lies between 0% to 3%. The mean and mode are around 2%.

† For 1 ms sampling time, 50% of the data, quartile Q_1 to Q_3, lies between 0% to 2%. The mean and mode are around 1.5%.

† With the decrease in sampling time, the span of distribution of error decreases.

† There are few outliers for all the sampling times.

As discussed in the state estimator chapter of this thesis, the decision to choose the sampling time for implementation in vehicle would further depend on the hardware available or to be used, cost of the hardware, and the allowable error in the size estimate from state estimator's point of view and its coupled effect on the control algorithm's performance, i.e. robustness of the controller to error in size estimate.

To summarize, Table 4.2 shows the various robustness analyses done for the backlash size estimator. All these robustness assessments provide an effective data summary

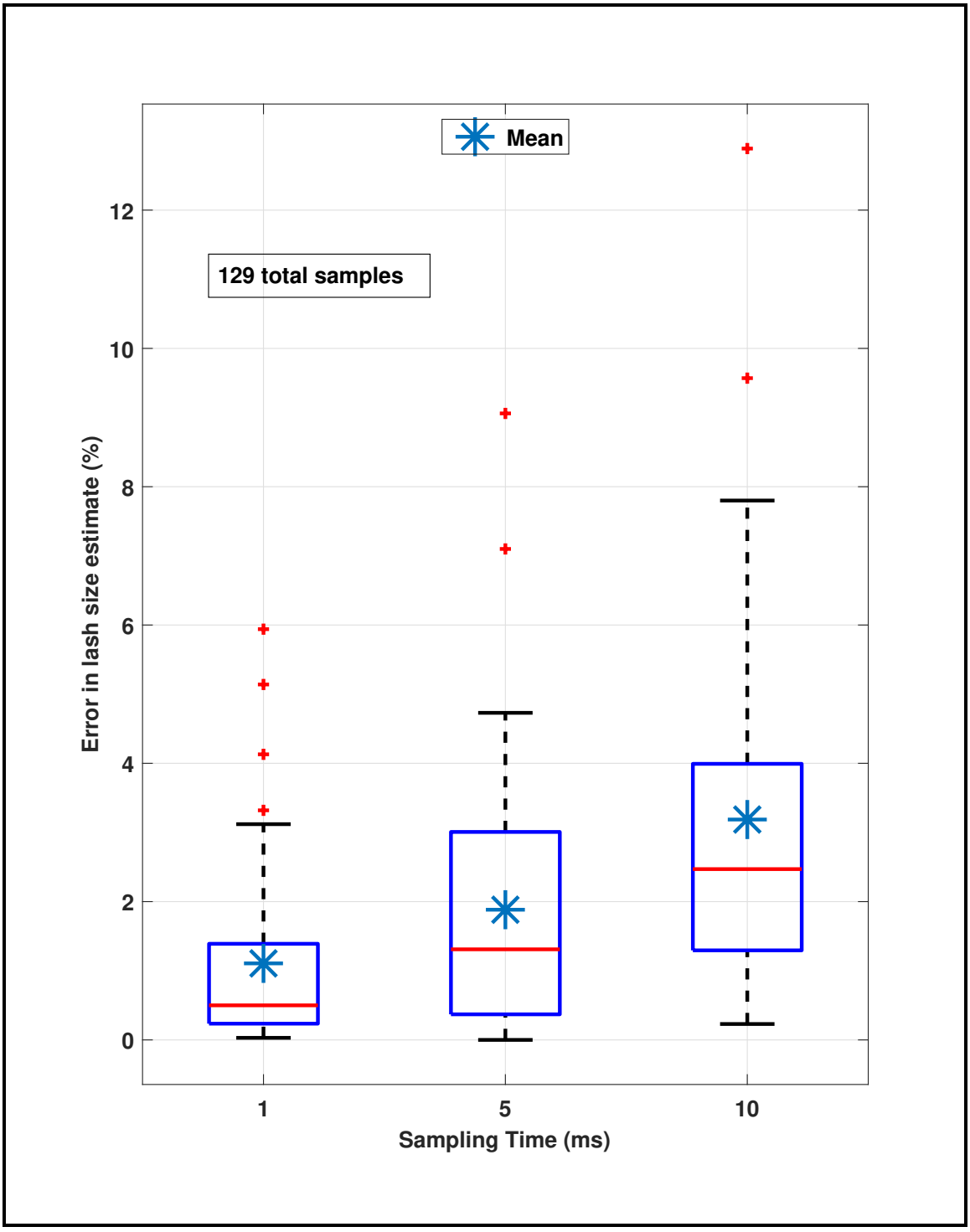

Figure 4.24: Box plot for error in lash size estimate with sampling time.

Table 4.2
Summary of robustness analysis for the size estimator

Description	Status
Effect of varying torque step inputs	✓
Effect of varying torque ramp rates	✓
Effect of varying duty cycle and pulse width of torque ramp inputs	✓
Effect of variable torque input profile	✓
Effect of constant delay in - Engine speed - Wheel speed - Combined engine and wheel speed delay	✓
Effect of CAN jitter in - Engine speed - Wheel speed - Combined engine and wheel speed	✓
Effect of sampling time	✓

of the performance and limitations of the estimator and finish the development of the Triggered Kalman Backlash Size estimator.

Chapter 5

Conclusion and Future Work

5.1 Conclusions

The conclusions of this work are categorized into three sections (*i*) the validation of the full order model and development of reduced order model, (*ii*) the backlash state estimator and (*iii*) the backlash size estimator and are discussed below -

† **Validation of full order model and development of reduced order model** -

– The full order vehicle model developed in [3] using Simulink® - AMESim® interface was validated for the case of locked torque converter and 5^{th}

gear operation. Validation was done using the vehicle measurement data provided by sponsor organization.

- The simulated frequency of shuffle oscillation of the validated model has less than 1% error with respect to vehicle measurement.
- In order to eliminate the phase lag between the measured and simulated values of propeller shaft torque, a low pass filter needs to be added to the model.
- A two mass reduced order model, generally used in literature to represent the automotive driveline with backlash, was not able to capture the dynamics of the full order model with sustained oscillations in simulated outputs.
- A three mass model with separate tire stiffness and damping was developed to simulate the driveline response which was able to capture the dynamics of the full order model.
- The start and end of lash traversal with lumped backlash reduced order model and split backlash reduced order model are same. Thus, the number of equations and states representing the reduced order model can be further reduced with lumping the backlash.
- The 3 degrees of freedom (3DOF) reduced order model simulated frequency of shuffle has less than 1% error with respect to vehicle measured frequency of oscillation.

- With the 3DOF reduced order model, the simulation time has decreased by 2.4 times and the number of states of the model has reduced from 47 to 10.

† **Backlash state estimator**

- Due to the backlash non-linearity, the driveline model needs to be divided into two linear models, one for the contact mode and other for backlash mode of operation.
- If the angular positions of the lumped inertia (engine, final drive and wheel) are considered as the states of the system, then using the engine and wheel speed as measurements, the system is not observable in the contact mode or the backlash mode.
- The contact mode model is observable with engine and wheel speeds measurements if the twist angles between the inertia are considered as the states of the system.
- As the driveline is not rigidly connected in the backlash mode, it is not observable with twist angles as the states of the system. Thus a reduced order backlash model is developed without the backlash position state and engine side twist angle. This reduced order backlash model is observable.
- The Kalman filter estimates all the positions in the contact mode, but only estimates 4 states in the backlash mode. The rest of the states in the

backlash mode are calculated/predicted using the state equations.

- The FOM developed for this work was used to validate the state estimator.
- Constant delays and CAN jitter delays in the engine and wheel speeds, used to assess the performance of the backlash state estimator, were derived from the measured data by the hardware group.
- The error in the estimated engine and wheel speeds is significantly less than the error in the lash traversal time. This is because the lash traversal time does not have the measurement based update during backlash traversal.
- The backlash state estimator's (DSKSE) estimated lash traversal time error reduces with reduction in the sampling time of the engine speed, wheel speed and the estimator.
- A delay of 1 step size in the estimation of end of lash traversal is seen for some of the torque inputs. The effect of this on the percentage error in lash traversal time changes with the sampling period.
- For a given constant delay in engine speed and wheel speed, the effect of delay in engine speed is more as compared to that of wheel speed.
- With 10 ms sampling time, the CAN jitter does not cause any delay in the end of lash traversal because the max delay due to jitter is 5 ms which the sample data is not be to perceive.
- Sampling time of 5ms is the most sensitive to the effect of CAN jitter in the engine and the wheel speeds.

- Sampling time of 1ms is most robust to the effect of CAN jitter in the engine and the wheel speeds.

† **Backlash size estimator**

- The validation of backlash size estimator was done using the FOM plant model developed for this work.
- Constant delays and CAN jitter based delays in the engine and wheel speeds, used to assess the performance of the backlash size estimator, were derived from the measured data by the hardware group.
- The error in lash size estimate is a function of the rate of torque input and the final value of the torque. This is because, both the rate and final value of torque input affect the number of data samples available to estimate the size of the backlash lash during lash traversal.
- As the sampling time of the engine speed, the wheel speed and the estimator decreases the error in size estimate also decreases because of the increased number of data samples available to estimate the size of the backlash.
- As the backlash size increases, the error in the lash size estimate also decreases. This is due to the increased lash traversal time which leads to increased number of sample data available to the size estimator to converge to the final value.

- A maximum error of 8% is observed in the estimated backlash size with 10 ms sampling time for estimator and the engine and wheel speed measurements.

- The measured CAN jitter causes a maximum error in size estimate of 3.5% for 10 ms sampling time.

5.2 Future Works

Below are some of the future work associated with this project -

† The full order plant model currently has been validated for 5^{th} gear only. Consequently, the reduced order model and the state and size estimators are also validated for 5^{th} condition. In order to implement the state and size estimator for vehicle application, it needs to be validated for the rest of the gears as well. This is because, the engine lumped inertia which contains the inertia of the transmission and the transmission gear ratio used in the state space model will change.

† Similarly, the model has been developed for only locked torque converter case. In case of slipping and open torque converter, the full order model will change

resulting in changes in the reduced order model and the state and size estimators.

† As the sensitivity analysis was done for the full order model in [3], a similar sensitivity analysis will also required to be done for the state and size estimator in order to understand the performance of the estimators to incorrect plant parameters.

† The estimator developed in this work have been validated in simulation environment, a test rig based validation of the estimator also needs to be done to understand the performance of the estimator in real vehicle environment.

† A control system needs to be developed which can shape the engine commanded torque such that at the point of impact, the torque can be reduced to reduce the clunk and shuffle.

References

[1] https://www.edmunds.com/car reviews/, Accessed on March 19th 2019. *Edmunds*. Edmunds, ONLINE.

[2] Study, G. A. C., 2014. *Exploring consumers' mobility choices and transportation decisions*. Deloitte.

[3] Reddy, P., 2018. "Control oriented modeling of an automotive drivetrain for anti-jerk control". Master's thesis, Michigan Technological University.

[4] P. Reddy, K. Darokar, D. R. M. S. J. B. M. R. M. F., and Doering, J., 2006. "Control oriented modeling of a vehicle drivetrain for shuffle and clunk". In 2006 IEEE International Conference on Mechatronics, Budapest, Hungary.

[5] Puhui Liu, T. Z., and Zhao, X., 2018. "Vehicle drivability evaluation and pedal-acceleration response analysis". Clean Energy Automotive Engineering Center, Tongji University, Shanghai.

[6] https://communityrising.kasasa.com/gen-x-gen-y-gen z/, Accessed on March 19th 2019. *KASASA*. KASASA, ONLINE.

[7] List, H. O., and Schoeggl, P., 1998. "Objective evaluation of vehicle drivability". SAE International, 980204.

[8] Everett, R. L., 1971. "Measuring vehicle driveability". SAE International, 710137.

[9] Dorey, R. E., and Holmes, C. B., 1999. "Vehicle driveability - its characterisation and measurement". SAE International, 1999-01-0949.

[10] Isa Yassir Arafat Machmudi Isa, M. A. Z. A., and Mansor, S., 2014. "Objective driveability: integration of vehicle behaviour and subjective feeling into objective assessments". *Journal of Mechanical Engineering and Sciences*, pp. 782–792. e-ISSN: 2231-8380; Volume 6.

[11] Griffin, M. J., 2012. *Handbook of human vibrations*. Academic Press.

[12] M. C. Tsangarides, W. E. T., and Heermann, C. R., 1985. "Interactive computer simulation of drivetrain dynamics". pp. 143–158. SAE Technical Paper 850978.

[13] Krenz, R., 1985. "Vehicle response to throttle tip-in/tip-out". pp. 45–52. SAE Technical Paper 850967.

[14] Lagerberg, A., 2001. "A literature survey on control of automotive powertrains with backlash". *Department of Signals and Systems, Chalmers University of Technology, Goteberg, Sweden*. R013/2001.

[15] Lagerberg, A., and Egardt, B., 2002. "Evaluation of control strategies for automotive powertrains with backlash". *Department of Signals and Systems, Chalmers University of Technology, Goteberg, Sweden*. R013/2001.

[16] Lagerberg, A., and Egardt, B., 2007. "Backlash estimation with applications to automotive powertrains". *IEEE Transactions on Control System Technology, Vol. 15, No. 3*, pp. 483–493.

[17] T. Karikomi, K. Itou, T. O., and Fujimoto, S., 2006. "Development of shaking vibration control for electric vehicles". *In 2006 SICE-ICASE International Joint Conference*. Busan, Korea.

[18] Templin, P., 2008. "Simultaneous estimation of driveline dynamics and backlash size for control design". *17th IEEE Transactions on Control Applications Part of 2008 IEEE Multi-Conference on Systems and Controls*, pp. 13–18. San Antonio, Texas, USA.

[19] Lagerberg, A., 2003. "Estimation of backlash with application to automotive powertrains". *Proceedings of 42nd IEEE Conference on Decision and Control*.

[20] Martin Grotjahn, L. Q., and Zemke, S., 2019. "Modeling and identification of car driveline dynamics for anti-jerk controller design". SAE International.

[21] Canova, M., Cristian Rostiti, Luca D'Avico, S. S. G. C. M. P., and Dourra, H., 2017. "Model based whee torque and backlash estimation for drivability control". SAE International, 2017-01-1111.

[22] Templing, P., and Egardt, B., 2011. "A powertrain lqr torque compensator with backlash handling". *Oil Gas Science and Technology - Rev. IFP Energies nouvelles*, pp. 645–654. Vol. 66, No. 4).

[23] Guido Ricardo Guercioni, Enrico Galvagno, A. T., and Vigliani, A., 2018. "Driveline backlash and half shaft torque estimation for electric powertrain controls". SAE International, 2018-01-1345.

[24] Julian Baumann, Dara D. Torkzadeh, A. R. U. K., and Schlegl, T., 2006. "Model based predictive anti jerk control". *Control Engineering Practice 14*, pp. 259–266.

[25] Lakhani, P., 2018. "Modeling and analysis for driveline jerk control". Master's thesis, Michigan Technological University.

[26] Stefano Di Cairano, Jeff Doering, I. V. K., and Hrovat, D., 2014. "Model predictive control of engine speed during vehicle deceleration". *IEEE Transactions of Control System Technology*, pp. 2205–2217. Vol. 22, No. 6.

[27] Gillespie, T. D. *Fundamentals of vehicle dynamics*. Society of Automotive Engineers, Inc.

[28] Barbir, F., 2012. *PEM Fuel Cells, 2nd Edition*. Academic Press.

[29] https://www.epa.gov/compliance-and-fuel-economy-data/data-cars-used-testing-fuel economy. *EPA Compliance and Fuel Economy Data*. EPA, The Internet.

[30] Wilhelmus H. A. Schilders, Henk A. van der Vorst, J. R., 2008. *Model order reduction: Theory, Research Aspects and Applications*. Springer.

[31] https://www.mathworks.com/help/control/ug/about-model-order reduction.html. *Simulink*. Matlab/Simulink, Online.

[32] M. Nordin, J. G., and Gutman, P., 1997. "New models for backlash and gear play". *International Journal of Adaptive Control and Signal Processing*, pp. 1:9–63.

[33] Nordin, M., and Gutman, P., 1995. "A robust linear design of an uncertain two-mass system with backlash". *Proceedings of 1st IFAC Workshops in Automotive Control*, pp. 183–188. Ascona, Schweiz.

[34] Kenan Ezal, P. V. K., and Tao, G., 199. "Optimal control of tracking systems with backlash and flexibility". *Proceedings of the 36th Conference on Decision and Control*, pp. 1749–1754. San Diego, California.

[35] Templin, P., 2009. "An lqr torque compensator for driveline oscillation damping". *18th IEEE International Conference on Control Applications Part of 2009 IEEE Multi-Conference on Systems and Controls*, pp. 352–356. Saint Petersberg,Russia.

[36] Donghao Hao, C. Z., and Huang, Y., 2018. "A reduced-order model for active suspension control of vehicle longitudinal low-frequency vibration". *Hindawi Shock and Vibration*. Volume 2018, Article ID 5731347.

[37] Orhan Atabay, M. O., and Ereke, I. M., 2005. "Model based predictive engine torque control for improved drivability". In Proceedings of IMechE Part D J Automobile Engineering,, Vol. 232(12), pp. 1654–1666.

[38] How, P. J. P., and Frazzoli, P. E., 2010. Lecture notes in 16.30 feedback controls system, Fall.

[39] Kalman, R. E., 1960. "A new approach to linear filtering and prediction problems". *Transactions of the ASME–Journal of Basic Engineering,* ***82***(Series D), pp. 35–45.

[40] Elbert Hendricks, O. J., and Sørensen, P. H. *Linear Systems Control, Deterministic and Stochastic Methods*. Springer.

[41] Antsaklis, P. J., and Michel, A. N., 2006. *Linear Systems*. Birkhäuser Boston.

[42] Rowell, D., and Takahashi, S., 2004. Lecture notes in 2.151 advance system dynamics and control, Fall.

[43] Ogata, K., 2010. *Modern Control Engineering*. Prentice Hall, Fifth Edition.

Appendix A

State Estimator Calibration

This section briefly discusses the calibration parameters that have been used to tune the DSKSE. Refer to Section 3.1.2.4 for more details. The process noise co-variance and the measurement noise co-variance coefficients that have been used for the DSKSE are shown below:

$$\mathbf{Q} = \begin{bmatrix} q_1 & 0 & 0 & 0 & 0 & 0 \\ 0 & q_2 & 0 & 0 & 0 & 0 \\ 0 & 0 & q_3 & 0 & 0 & 0 \\ 0 & 0 & 0 & q_4 & 0 & 0 \\ 0 & 0 & 0 & 0 & q_5 & 0 \\ 0 & 0 & 0 & 0 & 0 & q_6 \end{bmatrix} \tag{A.1}$$

where, the values of the coefficients used are:

$$\begin{aligned} q_1 &= 1e-2 \\ q_2 &= 1e3 \\ q_3 &= 5e-3 \\ q_4 &= 4e-3 \\ q_5 &= 1e-1 \\ q_6 &= 1e-3 \end{aligned} \tag{A.2}$$

$$\mathbf{R} = \begin{bmatrix} r_1 & 0 \\ 0 & r_2 \end{bmatrix} \tag{A.3}$$

where, the values of the coefficients used are:

$$\begin{aligned} r_1 &= 2e-5 \\ r_2 &= 3e-5 \end{aligned} \tag{A.4}$$

From the values of the **Q** and **R** shown in the Equation A.2 and A.4 respectively, it can be seen that the values of **R** matrix are smaller in magnitude as compared to the values of **Q**. This implies that the speed measurements (engine and wheel speeds) are trusted more, as compared to the model to estimate the states of the system.

To understand the effect of the individual process noise co-variance matrix coefficients on the estimate of the backlash position, these coefficients are varied and the results are shown Figure A.1 and Figure A.2. The observations made from the Figure A.1 and Figure A.2 are listed below:

† Changing the magnitudes of co-variances associated with the engine side twist angle state ($\frac{\theta_e}{i_{tr}} - \theta_{fdr} i_{fdr}$), the final drive speed state ($\dot{\theta}_{fdr}$), and the backlash position state (θ_b) does not significantly affect the backlash position estimate.

† During the backlash traversal, since there is no load acting on the engine inertia, the engine side shaft does not twist. As a result of this, changing the value of the error co-variance associated with respect to engine side twist angle does not significantly affect the estimated backlash traversal.

† Since one side of the final drive inertia is connected to the backlash element,

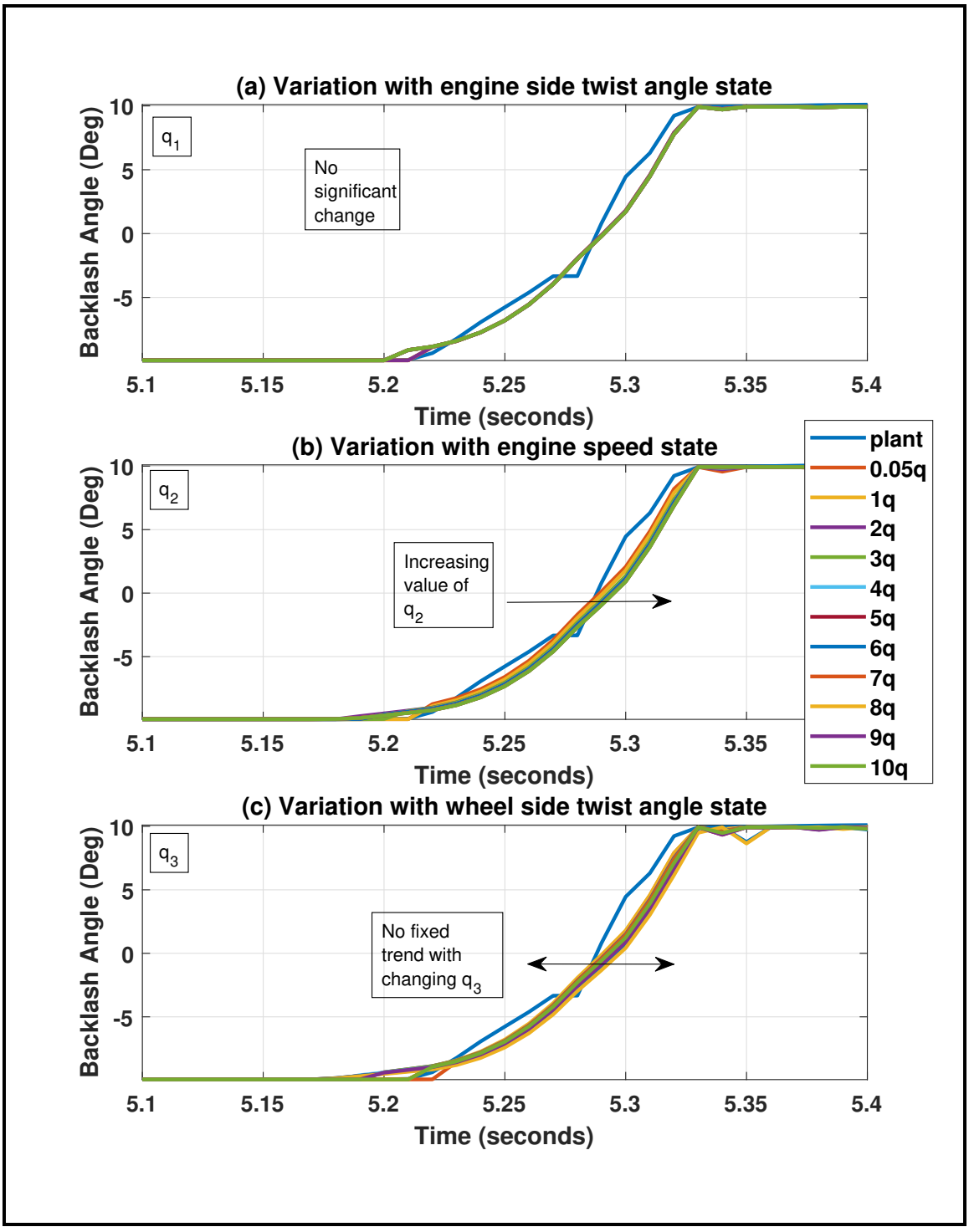

Figure A.1: Effect of varying the engine side twist angle state, engine speed state, and the wheel side twist angle state on the backlash position estimate

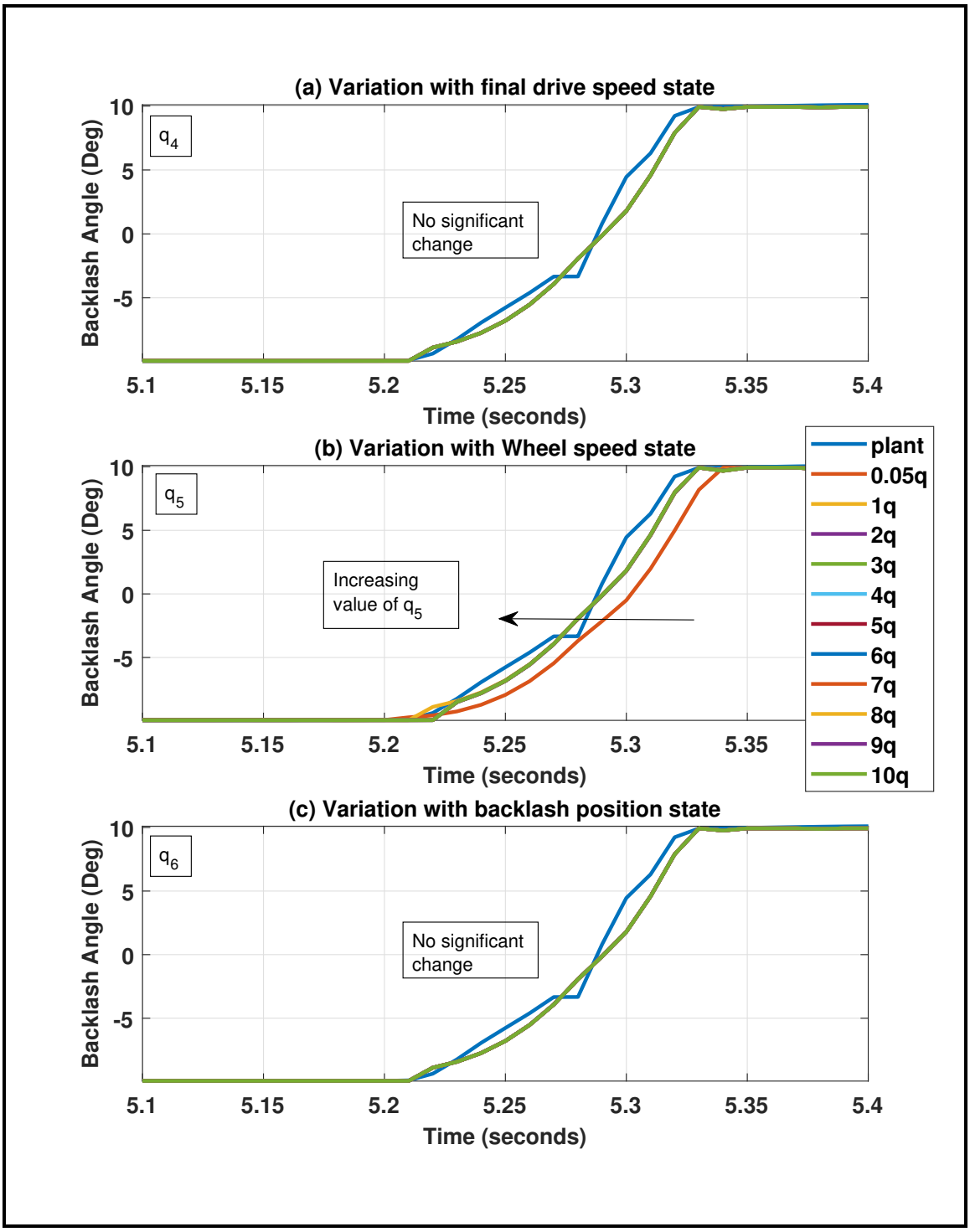

Figure A.2: Effect of varying the final drive speed state, wheel speed state, and the backlash position state on the backlash position estimate

the engine side torque does not affect the final drive speed during the backlash mode. This reduces the effect of changing the magnitude of error co-variance associated with final drive speed on the estimated backlash position.

† Figure A.1 (b) shows the variation of backlash position estimate with changing the engine speed measurement error co-variance. It can be seen that as the error co-variance increases the deviation of estimated backlash traversal from the plant backlash traversal increases. This happens because engine speed is one of the primary source of information for the estimates and increasing its error co-variance leads to reducing the trust on the engine speed estimate from the driveline dynamics model. This increases the error in the backlash position estimate.

† Changing the error co-variance associated with the wheel side twist angle does not have any fixed impact on the estimated backlash position. This can be seen from Figure A.1 (c).

† When the error co-variance associated with the wheel speed is increased for a fixed value of the error co-variance associated the engine speed, it implies that more trust is given to the engine speed as compared to the previous scenario. This leads to decreasing the error in deviation of lash traversal with respect to the plant lash traversal. This can also be seen in Figure A.2 (b).

Appendix B

Publications from this thesis

B.1 Conference Paper

B.1.1 Published Conference Paper

1. P. Reddy, K. Darokar, D. Robinette, M. Shahbakhti, J. Blough, M. Ravichandran, M. Farmer and J. Doering, "Control-Oriented Modeling of a Vehicle Drivetrain Modeling for Shuffle and Clunk Mitigation", SAE International WCX - 2019.

B.2 Ford Internal Publication

1. M. Ravichandran, J. Doering, R. Johri, P. Reddy, K. Darokar, D. Robinette and M. Shahbakhti, "Introductory description of AJC feature and its performance evaluation in MHT, Report No. SRR-2019-0024.

Appendix C

Program and Data File Summary

Tables in this section lists the figures, model files, script files and data files that were used to generate the results shown in this work.

C.1 Chapter 1

Table C.1
Chapter 1 figure files

File Name	File description
Fig_1_1.pdf	Figure 1.1
Fig_1_2.pdf	Figure 1.2
Fig_1_3.pdf	Figure 1.3
Fig_1_4.pdf	Figure 1.4
Fig_1_5.pdf	Figure 1.5
Fig_1_6.vsdx	Figure 1.6
Fig_1_7.vsdx	Figure 1.7
Fig_1_8.vsdx	Figure 1.8
Fig_1_9.vsdx	Figure 1.9
Fig_1_10.vsdx	Figure 1.10

C.2 Chapter 2

Table C.2
Chapter 2 figure files

File name	File description
Fig_2_1.pdf	Figure 2.1
Fig_2_2.pdf	Figure 2.2
Fig_2_3.vsdx	Figure 2.3
Fig_2_4.fig	Figure 2.4
Fig_2_5.fig	Figure 2.5
Fig_2_6.fig	Figure 2.6
Fig_2_7.jpg	Figure 2.7
Fig_2_8.vsdx	Figure 2.8
Fig_2_9.fig	Figure 2.9
Fig_2_10.vsdx	Figure 2.10
Fig_2_11.fig	Figure 2.11
Fig_2_12.fig	Figure 2.12
Fig_2_13.fig	Figure 2.13
Fig_2_14.vsdx	Figure 2.14
Fig_2_15.fig	Figure 2.15

Table C.3
Chapter 2 Simulink® and AMESim® model files

File name	File description
ROM_cosim_Jul20_2DOF.ame	2DOF AMESim ROM model
ROM_cosim_Jul20_3DOF_modified.ame	3DOF lumped backlash AMESim ROM model
ROM_cosim_Jul20_3DOF_modified_2backlash.ame	3DOF Split backlash AMESim ROM model
Vehicle_Model_trials_mod.ame	Full order AMESim model
AJC_Torque_Shaping_TCC_July23_new.slx	Simulink model file to run all AMESim models

Table C.4
Chapter 2 data files required to run the Simulink® and AMESim® models

File name	File description
wheel_slip.data	AMESim model data file
5th_gear_losses.data	AMESim model data file
crankshaft_torque_locked_5th_gear_translosses_removed.data	AMESim model data file
Engine.torque.data	AMESim model data file
Engine.torque.limits.data	AMESim model data file

Table C.4 continued from previous page

File name	File description
engine_speed_50%load.data	AMESim model data file
lockedtcc.validation.data.gear.table.data	AMESim model data file
opentcc.validation.gearshift.data	AMESim model data file
ROM_cosim_Jul20_3DOF_modified_.data	AMESim model data file
Torque.converter.data	AMESim model data file
Torque.converter.kfactor.data	AMESim model data file
Torque.converter.kfactordaNm.data	AMESim model data file
Torque.converter.kfactordaNm.lbfconverted.data	AMESim model data file
Torque.converter.kfactorNm.data	AMESim model data file

Table C.4 continued from previous page

File name	File description
Vehicle_Model_with_tyre_dynamics_2_.data	AMESim model data file
18-03-07_160337_P552_35_mfarmer5_lockedpressoverride_400.mat	Vehicle measured data Mary Farmer - locked TCC

C.3 Chapter 3

Table C.5
Chapter 3 figure files

File name	File description
Fig_3_1.vsdx	Figure 3.1
Fig_3_2.vsdx	Figure 3.2
Fig_3_3.fig	Figure 3.3
Fig_3_4.fig	Figure 3.4
Fig_3_5.fig	Figure 3.5
Fig_3_6.fig	Figure 3.6
Fig_3_7.fig	Figure 3.7

Table C.5 continued from previous page

File name	File description
Fig_3_8.fig	Figure 3.8
Fig_3_9.fig	Figure 3.9
Fig_3_10.fig	Figure 3.10
Fig_3_11.eps	Figure 3.11
Fig_3_12.fig	Figure 3.12
Fig_3_13.fig	Figure 3.13
Fig_3_14.fig	Figure 3.14
Fig_3_15.fig	Figure 3.15
Fig_3_16.vsdx	Figure 3.16
Fig_3_17.fig	Figure 3.17
Fig_3_18.fig	Figure 3.18
Fig_3_19.fig	Figure 3.19
Fig_3_20.fig	Figure 3.20
Fig_3_21.fig	Figure 3.21
Fig_3_22.fig	Figure 3.22
Fig_3_23.fig	Figure 3.23
Fig_3_24.fig	Figure 3.24

Table C.6
Chapter 3 Simulink® file for the estimator

File name	File description
new_estimator_kalman_inversion.slx	State Estimator new

Table C.7
Chapter 3 Matlab® script files

File name	File description
new_kalman_filter_script.m	Estimator initialization file
Robustness_analysis_plots.m	Plot file
wheel_speed_sampling_error_Jons_data.m	Plot file for CAN jitter wheel speed
data_dist_engine_speed_Jons_data.m	Plot file for CAN jitter engine speed

Table C.8
Chapter 3 data files required to run Simulink® model

File name	File description
Measured_FOM_for_state_estimator_inputs_step400Nm.mat	Step input plant data
Measured_FOM_for_state_estimator_inputs_step200Nm.mat	Step input plant data

Table C.8 continued from previous page

File name	File description
Measured_FOM_for_state_estimator_inputs_step300Nm.mat	Step input plant data
Measured_FOM_for_state_estimator_inputs_step700Nm.mat	Step input plant data
Measured_FOM_for_state_estimator_inputs_step600Nm.mat	Step input plant data
Measured_FOM_for_state_estimator_inputs_step500Nm.mat	Step input plant data
Measured_FOM_for_state_estimator_inputs_1000Nm.mat	Ramp input plant data
Measured_FOM_for_state_estimator_inputs_200Nm.mat	Ramp input plant data
Measured_FOM_for_state_estimator_inputs_300Nm.mat	Ramp input plant data
Measured_FOM_for_state_estimator_inputs_400Nm.mat	Ramp input plant data
Measured_FOM_for_state_estimator_inputs_500Nm.mat	Ramp input plant data

Table C.8 continued from previous page

File name	File description
Measured_FOM_for_state_estimator_inputs_600Nm.mat	Ramp input plant data
Measured_FOM_for_state_estimator_inputs_700Nm.mat	Ramp input plant data
Measured_FOM_for_state_estimator_inputs_800Nm.mat	Ramp input plant data
Measured_FOM_for_state_estimator_inputs_900Nm.mat	Ramp input plant data
r_state_estimator_wheel.mat	wheel jitter data
r_state_estimator.mat	engine jitter data
new_estimator_kalman_inversion.slx	State Estimator new
new_kalman_filter_script.m	intialization file state estimator
Robustness_analysis_plots.m	Plot file
wheel_speed_sampling_error_Jons_data.m	Plot file

Table C.8 continued from previous page

File name	File description
r_eng_and_wheel_speed_with_dataset_delay_state_estimator.mat	Plot file
data_dist_engine_speed_Jons_data.m	data can jitter

C.4 Chapter 4

Table C.9
Chapter 4 figure files

File name	File description
Fig_4_1.vsdx	Figure 4.1
Fig_4_2.fig	Figure 4.2
Fig_4_3.fig	Figure 4.3
Fig_4_4.fig	Figure 4.4
Fig_4_5.fig	Figure 4.5
Fig_4_6.fig	Figure 4.6
Fig_4_7.pdf	Figure 4.7
Fig_4_8.fig	Figure 4.8
Fig_4_9.fig	Figure 4.9
Fig_4_10.pdf	Figure 4.10

Table C.9 continued from previous page

File name	File description
Fig_4_11.fig	Figure 4.11
Fig_4_12.fig	Figure 4.12
Fig_4_13.pdf	Figure 4.13
Fig_4_14.fig	Figure 4.14
Fig_4_15.pdf	Figure 4.15
Fig_4_16.fig	Figure 4.16
Fig_4_17.pdf	Figure 4.17
Fig_4_18.fig	Figure 4.18
Fig_4_19.pdf	Figure 4.19
Fig_4_20.fig	Figure 4.20
Fig_4_21.pdf	Figure 4.21
Fig_4_22.vsdx	Figure 4.22
Fig_4_23.pdf	Figure 4.23
Fig_4_24.fig	Figure 4.25

Table C.10
Chapter 4 Simulink® estimator files

File name	File description
Onlysizeestimator_Amesim_inputs_discrete_thesis_correction.slx	Size Estimator simulink file

Table C.11
Chapter 4 Matlab® script file

File name	**File description**
ROM_based_size_estimator_discrete_thesis_correction.m	Size estimator initialization file

Table C.12
Chapter 4 data files

File name	**File description**
Size_est_uni.mat	Data files
size_est_input_step_minus20to60Nm_1backlash.mat	Data files
size_est_input_step_minus20to60Nm_2backlash.mat	Data files
size_est_input_step_minus20to60Nm_3backlash.mat	Data files
size_est_input_step_minus20to100Nm_1backlash.mat	Data files
size_est_input_step_minus20to100Nm_2backlash.mat	Data files
size_est_input_step_minus20to100Nm_3backlash.mat	Data files

Table C.12 continued from previous page

File name	File description
size_est_input_step_minus20to150Nm_1backlash.mat	Data files
size_est_input_step_minus20to150Nm_2backlash.mat	Data files
size_est_input_step_minus20to150Nm_3backlash.mat	Data files
size_est_inputs_1basebacklash_minus20to60Nm.mat	Data files
size_est_inputs_1basebacklash_minus20to60Nm_variable.mat	Data files
size_est_inputs_1basebacklash_minus20to100Nm.mat	Data files
size_est_inputs_1basebacklash_minus20to150Nm.mat	Data files
size_est_inputs_1basebacklash_minus20to150Nm_variable.mat	Data files
size_est_inputs_2basebacklash_minus20to60Nm.mat	Data files
size_est_inputs_2basebacklash_minus20to60Nm_variable.mat	Data files
size_est_inputs_2basebacklash_minus20to100Nm.mat	Data files
size_est_inputs_2basebacklash_minus20to150Nm.mat	Data files
size_est_inputs_2basebacklash_minus20to150Nm_variable.mat	Data files
size_est_inputs_3basebacklash_minus20to60Nm.mat	Data files
size_est_inputs_3basebacklash_minus20to60Nm_variable.mat	Data files
size_est_inputs_3basebacklash_minus20to100Nm.mat	Data files
size_est_inputs_3basebacklash_minus20to150Nm.mat	Data files
size_est_inputs_3basebacklash_minus20to150Nm_variable.mat	Data files

Table C.12 continued from previous page

File name	File description
Size_est_nor.mat	Data files
size_est_random_profile_1backlash.mat	Data files
size_est_random_profile_2backlash.mat	Data files
size_est_random_profile_3backlash.mat	Data files
r_size_estimator.mat	Data files
r_size_estimator_wheel.mat	Data files

C.5 Appendix A

Table C.13
Appendix A figure files

File name	File description
Fig_A_1.fig	Figure A.1
Fig_A_2.fig	Figure A.2